SANDIA REPORT

SAND2010-6531
Unlimited Release
Printed September 2010

High-Efficiency High-Energy Kα Source for the Critically-Required Maximum Illumination of X-Ray Optics on Z Using Z-Petawatt-Driven Laser-Breakout-Afterburner Accelerated Ultrarelativistic Electrons

LDRD 130805

Guy R. Bennett, Adam B. Sefkow

Prepared by
Sandia National Laboratories
Albuquerque, New Mexico 87185 and Livermore, California 94550

Sandia National Laboratories is a multi-program laboratory managed and operated by Sandia Corporation, a wholly owned subsidiary of Lockheed Martin Corporation, for the U.S. Department of Energy's National Nuclear Security Administration under contract DE-AC04-94AL85000.

Issued by Sandia National Laboratories, operated for the United States Department of Energy by Sandia Corporation.

Available to DOE and DOE contractors from
U.S. Department of Energy
Office of Scientific and Technical Information
P.O. Box 62
Oak Ridge, TN 37831

Telephone: (865) 576-8401
Facsimile: (865) 576-5728
E-Mail: reports@adonis.osti.gov
Online ordering: http://www.osti.gov/bridge

Available to the public from
U.S. Department of Commerce
National Technical Information Service
5285 Port Royal Rd.
Springfield, VA 22161

Telephone: (800) 553-6847
Facsimile: (703) 605-6900
E-Mail: orders@ntis.fedworld.gov
Online order: http://www.ntis.gov/help/ordermethods.asp?loc=7-4-0#online

SAND2010-6531
Unlimited Release
Printed September 2010

High-Efficiency High-Energy Kα Source for the Critically-Required Maximum Illumination of X-Ray Optics on Z Using Z-Petawatt-Driven Laser-Breakout-Afterburner Accelerated Ultrarelativistic Electrons

Guy R. Bennett (05711) & Adam B. Sefkow (01644)
Sandia National Laboratories
P.O. Box 5800
Albuquerque, New Mexico 87185-0406

Abstract

Under the auspices of the Science of Extreme Environments LDRD program, a <2 year theoretical- and computational-physics study was performed (LDRD Project 130805) by Guy R Bennett (formally in Center-01600) and Adam B. Sefkow (Center-01600): To investigate novel target designs by which a short-pulse, PW-class beam could create a brighter Kα x-ray source than by simple, direct-laser-irradiation of a flat foil; Direct-Foil-Irradiation (DFI). The computational studies – which are still ongoing at this writing – were performed primarily on the RedStorm supercomputer at Sandia National Laboratories Albuquerque site. The motivation for a higher efficiency Kα emitter was very clear: as the backlighter flux for any x-ray imaging technique on the Z accelerator increases, the signal-to-noise and signal-to-background ratios improve. This ultimately allows the imaging system to reach its full quantitative potential as a diagnostic. Depending on the particular application/experiment this would imply, for example, that the *system* would have reached its full design spatial resolution and thus the capability to see features that might otherwise be indiscernible with a traditional DFI-like x-ray source. This LDRD began FY09 and ended FY10.

ACKNOWLEDGMENTS

This work was supported by the Laboratory Directed Research and Development program at Sandia National Laboratories. Sandia is a multiprogram laboratory operated by Sandia Corporation, a Lockheed Martin Company, for the United States Department of Energy's National Nuclear Security Administration under Contract DE-AC04-94AL85000.

CONTENTS

FIGURES

Figure 1. Figure Caption: The electron and proton impact K-Shell ionization cross sections [barns] as a function of kinetic energy [MeV] for tin (Sn). In the case of Sn, the first 1s electron to be completely ionized requires 29.200 keV. It is important to notice the logarithmically increasing cross section for the electron impact case, compared to the single peak of a proton. Ion impact has a similar behavior to protons, except the cross section is higher, proportional to the square of the charge state.

Figure 2. Figure Caption: Sn $K\alpha_1$ production efficiency as a function of electron kinetic energy. This calculation takes into account: (a) the energy-dependent cross section (Fig. 1); (b) the energy-dependent stopping power of electrons in Sn; and (c) the probability of 1s vacancy leading to $K\alpha_1$ emission rather than $K\alpha_2$, $K\beta_1$, etc. or non-radiative Auger.

Figure 3. Figure Caption: Part of the setup for the computational model used to study Center-01600 DFI x-ray DFI data.

Figure 4. Figure Caption: The electric field (left) and electron temperature (right) at t=1000 fs for the Sn target depicted in Fig. 3.

Figure 5. Figure Caption: Two additional data points (55 and 98 J) that also indicate simulated ε within measurement error bars.

Figure 6. Figure Caption: Illustrative cartoon of the two-stage concept using a BOA-produced "superbeam" (electrons+ions+laser) to significantly increase the efficiency of a fixed amount of laser energy into $K\alpha$ x-rays.

Figure 7. Figure Caption: Simulation setup specifics of a Two-Stage target.

Figure 8(a). Figure Caption: At t=30 fs the laser is about to strike the fully-ionized carbon BOA foil.

Figure 8(b). Figure Caption: At t=380 fs the laser field is a little more than midway between the BOA foil and the Sn target. Notably the electron density has not necessarily dropped by a 660x factor, but rather the electrons have increased their mass relativistically to the extent that the plasma frequency has decreased in proportion to $\gamma^{-1/2}$.

Figure 8(c). Figure Caption: At t=470 fs an apparently coherent electron beam has reached and then passed through the 10-μm-thick Sn target. The carbon ion beam is now established but, being slower moving, it is mid way between the BOA foil and Sn target. Sn electrons are beginning to heat up, likely due to direct laser irradiation.

Figure 8(d). Figure Caption: At 560 fs Sn electrons within the Sn slab have heated to approximately 100 keV, and the temperature profile almost extends through the 10 μm target thickness (z-axis). The profile is tightly centered about the origin of the x-axis, because the heating is mostly due to the self-focused laser field.

Figure 8(e). Figure Caption: At 870 fs the ion beam has reached the Sn slab and passed through it. The beam has high density at z>45 μm, implying no refluxing. The BOA and Sn electrons on the other hand are recirculating. The BOA electrons within the Sn may have reached their peak "temperature" at this point, 13-25 MeV; which is above the 5-10 MeV *kinetic energy* corresponding to peak efficiency. Note 1: one cannot use $E_{ave,e}=(3/2)K_BT_e$ is this case because the normal Maxwell-Boltzmann distribution is relativistically skewed. Note 2: for comparison, the lower-irradiance, lower-laser-energy DFI case in Fig. 4 reaches a peak <0.4 MeV electron temperature.

Figure 8(f). Figure Caption: At 1050 fs the ion beam has widened in the x-direction but it is possibly losing energy. Bulk tin electrons are beginning to cool, as are the BOA-originating electrons. For the latter, a uniform temperature of 6-13 MeV appears to exist throughout the Sn volume. It may be the general case that recirculating BOA electrons within Sn are creating more x-rays than recirculating Sn-electrons.

Figure 9(a). Figure Caption: At t=0 ps there is of course no expansion.

Figure 9(b). Figure Caption: At t=10.5 ps only the highest irradiance prepulse, 1e+12, has increased in its normalized overdense thickness (right panel); by a factor of ~3.75x in fact. It is not yet known whether a 3.75x30=112.5 nm thick, 2.255/3.75 g/cc density foil will initiate the BOA mechanism.

Figure 9(c). Figure Caption: At t=27 ps both the 1e+12 and 1e+11 prepulses have led to 13x and 7.5x normalized overdense thicknesses. The other two lower irradiances however, 1e+09 and 1e+10, have yet to expand significantly.

Figure 9(d). Figure Caption: At t=100 ps only the 1e+09 irradiance case has not expanded significantly, because the specified intensity lacks the energy necessary to melt the thin foil (according to the QEOS model used for the carbon).

1. INTRODUCTION

Within the fields of Inertial Confinement Fusion (ICF) and High Energy Density Physics (HEDP), the ability to image a target with x-rays at an arbitrary time has significantly added to the physics understanding of various experiments. At Sandia's Z accelerator, this so-called backlit imaging technique relies upon the multi-kilojoule, multi-terawatt Z-Beamlet Laser (ZBL) to directly irradiate a manganese (Mn) foil with a ~1-ns duration pulse and create an x-ray flash, which backlights a 6.151-keV curved-Bragg-crystal imaging system.

Laser irradiation of Mn, or any other element, produces a distribution of x-ray energies of course; but the $1s^2$-1s2p triplet transition of He-like manganese generates a narrow 6.151-keV line: Similarly, the singlet transition produces a narrow 6.181-keV emission line, but with higher brightness. There may be plans to operate the system around the 6.181-keV line since both the signal-to-noise and signal-to-background ratios will increase by a 1.5-2x factor. Furthermore, it is believed that an additional 2x image-plane-received backlighter signal can be easily attained by a simple change of the imager setup. (These ideas have been fully communicated to the relevant staff in Center-01600).

Thus far, despite the high-quality images that are routinely obtained, an enhanced 6-keV backlighting flux is still required for every Z experiment using ZBL. The same will be true, even more so, with higher energy imaging where the x-ray source is generated by the Z-Petawatt laser (ZPW). This is because x-rays are generated via a different physics mechanism than the He-α photons of long-pulse ZBL (and the conversion efficiency ε of laser light into x-rays is lower). Specifically, a laser of ZPW's class (eventually multikilojoule, ~1-ps) when focused to a sufficiently high irradiance has an electric field, $\underline{E}$, that is sufficient to accelerate electrons to relativistic speeds. Through the Lorentz force, the electron velocity $\underline{v}$ and charge q interact with the $\underline{B}$ field that is orthogonal to $\underline{E}$ so that the electron is accelerated along the path of the incident laser into the x-ray producing target.

This remarkable mechanism accelerates electrons in the Pointing vector direction to forward-directed relativistic energies. Notably, fairly modest irradiances of the order 1e+18 W/cm^2 (assuming 1 μm laser light) can produce relativistic electron velocities within any material. On the other hand, the forward acceleration of even the lightest ions, a proton say, is not possible due to the 3 decades q/m reduction (where m is the particle mass).

Given that electrons can be easily accelerated to relativistic energies into a simple slab-like target of any material with PW class laser systems, it is important to note that there are several important effects that are relevant to high energy x-ray generation:

[1] The element tin (Sn) for example has a 29.2-keV binding energy for the first of its two 1s electrons. Thus a PW-laser-accelerated electron beam with kinetic energies greater than or equal to 29.2-keV will have a non-zero probability of ionizing the innermost Sn shell via electron impact.

[2] The 1s vacancy can be populated by a 2p electron dropping down into this level; thereby releasing either a 25.2713-keV photon, or releasing energy via a non-radiative process (Auger

transitions) by scattering energy to other electrons within the Sn atom. (Note, a 2s-1s transition is forbidden.)

[3] The electron impact ionization cross section for Sn (and many other elements too), which is normally plotted as barns versus electron kinetic energy, increases logarithmically at relativistic energies.

[4] Laser-accelerated electrons can easily transit and exit a target foil that may be, say, 1 mm thick. However, due to space charge effects, the electrons generally do not escape the charged target, but instead re-circulate or reflux back and forth through the slab. And, providing the kinetic energy is 29.2-keV or more, a finite probability exists for creating one or more K-shell vacancies.

Regarding the last point, it is evident that laser accelerated relativistic electrons may be a useful means of creating a sufficiently-bright x-ray source of ~4-5-ps duration (from a ~1-ps laser pulse duration). Indeed, the so-called Direct-Foil Irradiation (DFI) technique is a standard, albeit inefficient, x-ray generating approach for ICF/HEDP experiments which require both a high x-ray probing energy and a short duration flash.

Generally, the DFI technique has been used to provide an x-ray source for point-projection-imaging; the simplest ICF/HEDP imaging method, and analogous to a dental radiograph.

Long-pulse laser irradiation of a single element foil can also be used to generate x-rays of energies that are > 6-keV; for instance, the singlet and triplet lines of He-like Zn produce near-9-keV radiation but with a lower ε than that of Mn. At some point, it is generally believed that the efficiency of generating Kα radiation at a particular photon energy is better than long-pulse (thermal) production of the singlet and triplet He-like states in the same element.

Moreover, at this cross-over point the short-pulse, non-thermal process has the advantage that the x-ray flash is 3 decades shorter: this has the advantage of essentially eliminating motional blur, which can be problematic for certain ICF/HEDP targets that are moving extremely rapidly.

This document serves as a closeout report for an LDRD project that ran for <2 of the three planned years. (One of the authors, GRB, transferred to Division 05000 during the second year). As a result the SAND report title is a little misleading because the research ended up being purely theoretical and computational in nature.

The work is therefore better described as “High-Efficiency 25-keV Kα Source for Advanced ICF/HEDP X-Ray Imaging: A Theoretical/Computational Physics Study (130805).” In essence, the authors wished to invent a new target concept beyond DFI that would increase ε by >10x. During preparations for the 130805-LDRD application, the first target concept consisted of laser-driven hemispherical „first stage’ that was PW-laser irradiated on the exterior of, say, a C (carbon) foil to produce a focused beam of Target-Normal-Sheath-Accelerated

(TNSA) protons and ions. The beam would then converge onto the x-ray generating target material of interest, Sn, the second stage.

The advantage of, say, a fully-stripped carbon ion over an electron is that the impact ionization cross section is 36x larger at its peak. However for both protons and ions beyond this peak, the cross section rapidly approaches zero instead of logarithmically increasing typical of an electron. In short, because the peak occurs at a high electron kinetic energy and neither ions nor protons reflux, this idea was abandoned.

The particular „Two-Stage' concept instead pursued is described in the next section.

2. TWO-STAGE TARGET SPECIFICS

The short-pulse laser-driven, two-stage Kα target concept that was studied utilized an approximately 30-100 nm "*ultrathin*" (say, carbon) foil, irradiated at 10^{19}-10^{21} W/cm^2 with ultra-high contrast, followed by a μm-to-mm sized converter foil (say, tin). In this scheme, the thin foil is rapidly and fully ionized, laser energy is very efficiently absorbed by the electrons (e) and burns through the foil, and the ions are accelerated in bulk via the relativistic Buneman instability to extremely high energies (>1 GeV, here). [This mechanism, discovered by Los Alamos National Laboratory (LANL) through computational simulations and verified independently by us using different codes and methods, is termed the laser Breakout Afterburner (BOA) effect.]

The resulting high-efficiency ultra-relativistic (γ_e>>1) e cloud, high-efficiency high-energy ions, and remaining laser energy, then impact a tin converter foil and create 25.2713-keV $K\alpha_1$ x-rays. A higher ε is expected largely because of a calculated significant increase in energy efficiency for 25 keV $K\alpha_1$ production from the bulk-heated BOA electrons, which achieve highly-populated ultra-relativistic energy distributions. In this case, the $K\alpha_1$ conversion efficiency shows a broad range of enhancement for electron energies from ~1 to ~200 MeV (γ_e ~3 to ~400), with a peak near 10 MeV (γ_e ~20); such energy levels are not well-populated in conventional DFI schemes involving direct μm-thick-foil laser irradiation. At this time, calculations indicate that the desired >10x ε enhancement over the present ε~10^{-4} of DFI is possible; primarily due to the bulk-heated relativistic electrons.

3. THE BREAK-OUT AFTERBURNER (BOA) EFFECT

The ultrathin foil (carbon) critical to the BOA effect is initially considered to be a fully ionized, stationary C^{6+} plasma with an electron density 660x larger than the critical density to 1 μm light ($\rho_C \sim 2.5$ g cm^{-3}). A PW-class laser is focused onto the front surface of the target. After a brief period of TNSA, wherein ponderomotively-accelerated electrons reflux within a foil to create a virtual cathode on the backside of the target that field ionizes H impurities, and so create a forward-moving energetic proton beam, which propagates normal to the target with a co-moving neutralizing electron cloud, an enhanced TNSA phase occurs during which the laser heats nearly all the target electrons to relativistic energies. Such bulk heating occurs because, when the target is 30-100 nm thin, the laser wavelength is much larger than the target thickness the skin depth is comparable to the target thickness, and both effects cause rapid bulk electron heating to relativistic energies, and increased laser penetration into the thin foil occurs.

Then, the ponderomotive and sheath electric fields (from TNSA charge separation) begin to overlap, the electrons oscillate with the laser and have increased conversion efficiencies into relativistic energies, and the target ions are accelerated in bulk. As the masses of the electrons relativistically increase, the effective critical density (where laser light is reflected due to $\omega_{laser} = \omega_{pe}$) also increases and the solid density target plasma becomes underdense to the laser. When this so-called *relativistic transparency* happens, the laser burns through (or *breaks out* of) the thin foil and the so-called *afterburner stage* continues to heat the electrons, which can contain ~50% of the laser energy and efficiently transfer their energy into directed ion acceleration via the relativistic Buneman (two-stream) instability. Electron energy lost to the ions is rapidly replenished by the continued presence of the laser, hence the overall BOA process efficiency is extraordinarily high. The kinetic modeling of this entire phenomenon was first performed by LANL simulators and demonstrated a large (>10x) theoretical improvement to overall plasma particle energies and efficiencies associated with laser-driven acceleration.

The co-moving high-energy and high-current-density ions (~100 MeV to ~2 GeV) and ultra-relativistic electrons (~1 MeV to ~200 MeV) quasi-neutrally propagate (naturally overcoming space-charge-limited transport) in the same direction as the laser light. Therefore, the demonstration of enhanced ion acceleration from the BOA effect is critical to the goal of impinging a second tin converter foil with ultra-relativistic electrons, in order to take the most advantage of the peak energy efficiency range of Kα production in tin by electron impact (as mentioned in the overview). Kα x-rays are made in the converter foil in the conventional way, via electron refluxing within a μm-sized target, or complete ranging out in a mm-to-cm-sized target, except we expect a substantial improvement to the overall conversion efficiency into 25 keV x-rays because of the sizable relativistic electron component introduced by the BOA mechanism. The heating of bulk electrons deep into the Sn slab material by the ion and proton beams (unlike laser heating, which only heats a small region near the interaction site) is expected to give an additional enhancement of Kα yield proportional to the original laser energy they contain, perhaps an estimated ~20-30%.

To put the context of this work at a higher, general-reader level it is worth noting that successful laser-backlit x-ray imaging requires the optimization of three key items: (1) An exquisitely-sensitive, time-gated image plane detector; (2) A high-collection-efficiency, high-

spatial-resolution imaging optic (unless point-projection imaging is used); And (3), a novel Kα target design with high ε. Items (1) and (2) are already being addressed, but item (3) has not until now been investigated in Center 01600.

4. ELECTRON & PROTON K-SHELL IMPACT IONIZATION CROSS SECTION FOR TIN

It was mentioned earlier that the proton or ion impact K-Shell ionization cross section – for Sn or any other element - had a single peak, the height of which is proportional to the square of the elementary-charge squared. Thus, in Figure 1 below, a fully stripped carbon ion would have a peak cross section value 36x larger than that of the proton shown. The electron on the other hand has a peak occurring at a lower kinetic energy, and after that a logarithmically increasing behavior, a relativistic effect.

When a K-shell vacancy is created, there is a high probability that a $K\alpha_1$ photon (25.2713-keV) will be produced. Such a transition occurs when an L3 electron drops into the K1 shell. The next most likely transition is an L2 electron filling the 1s vacancy. This would result in the emission of a 25.0440-keV photon ($K\alpha_2$), with a probability of 53%, relative to 100% for $K\alpha_1$.

As mentioned earlier, however, there is finite chance that there will be no radiative emission at all – the non-radiative Auger process. For high-Z material though, the probability of this process is quite small. In the case of Sn, the x-ray emission accounts for approximately 90 % of the energy transfer process with the remainder (non-radiative) being 10%. Within the ~90% probability of energy transfer by x-ray emission for Sn, it is important to note that lines other than $K\alpha_1$ and $K\alpha_2$ can be emitted: for example, $K\beta_1$, etc.

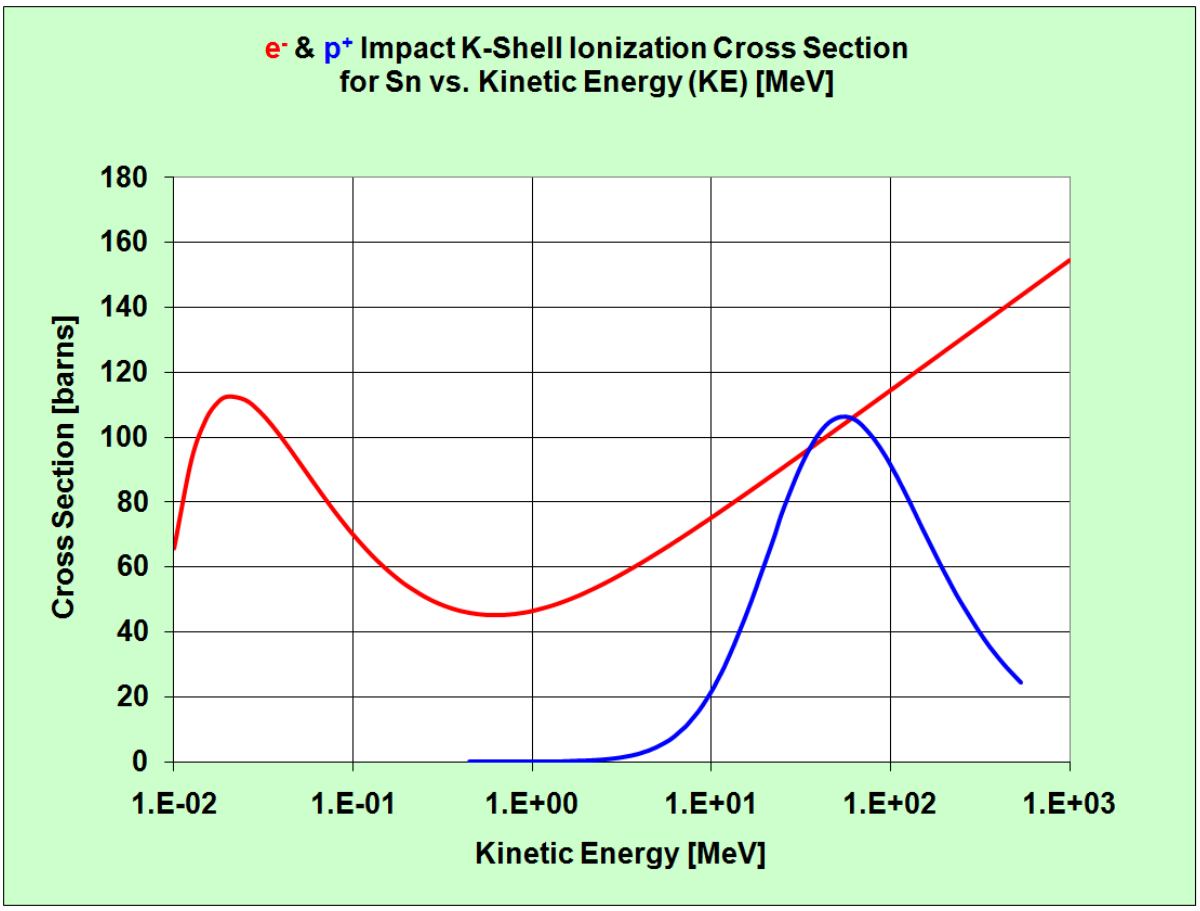

Figure 1. The electron and proton impact K-Shell ionization cross sections [barns] as a function of kinetic energy [MeV] for tin (Sn). In the case of Sn, the first 1s electron to be completely ionized requires 29.200 keV. It is important to notice the logarithmically increasing cross section for the electron impact case, compared to the single peak of a proton. Ion impact has a similar behavior to protons, except the cross section is higher, proportional to the square of the charge state.

5. $K\alpha_1$ PRODUCTION EFFICINECY AS A FUNCTION OF ELECTRON KINETIC ENERGY

As discussed earlier, compared with protons & ions, electrons have the advantage – through the high q/m ratio - that they can re-circulate through a PW-laser-driven target. Indeed, a single 1 GeV electron for example has so much kinetic energy that it can re-circulate generating 1s vacancies many times, until its energy winds down to <29.200-keV.

A critical ε-related question to ask is whether, say, one 1 GeV electron is better than one hundred 10 MeV electrons or one thousand 1 MeV electrons? (In all three examples the total energy is 1 GeV). Figure 2. below answers this important question.

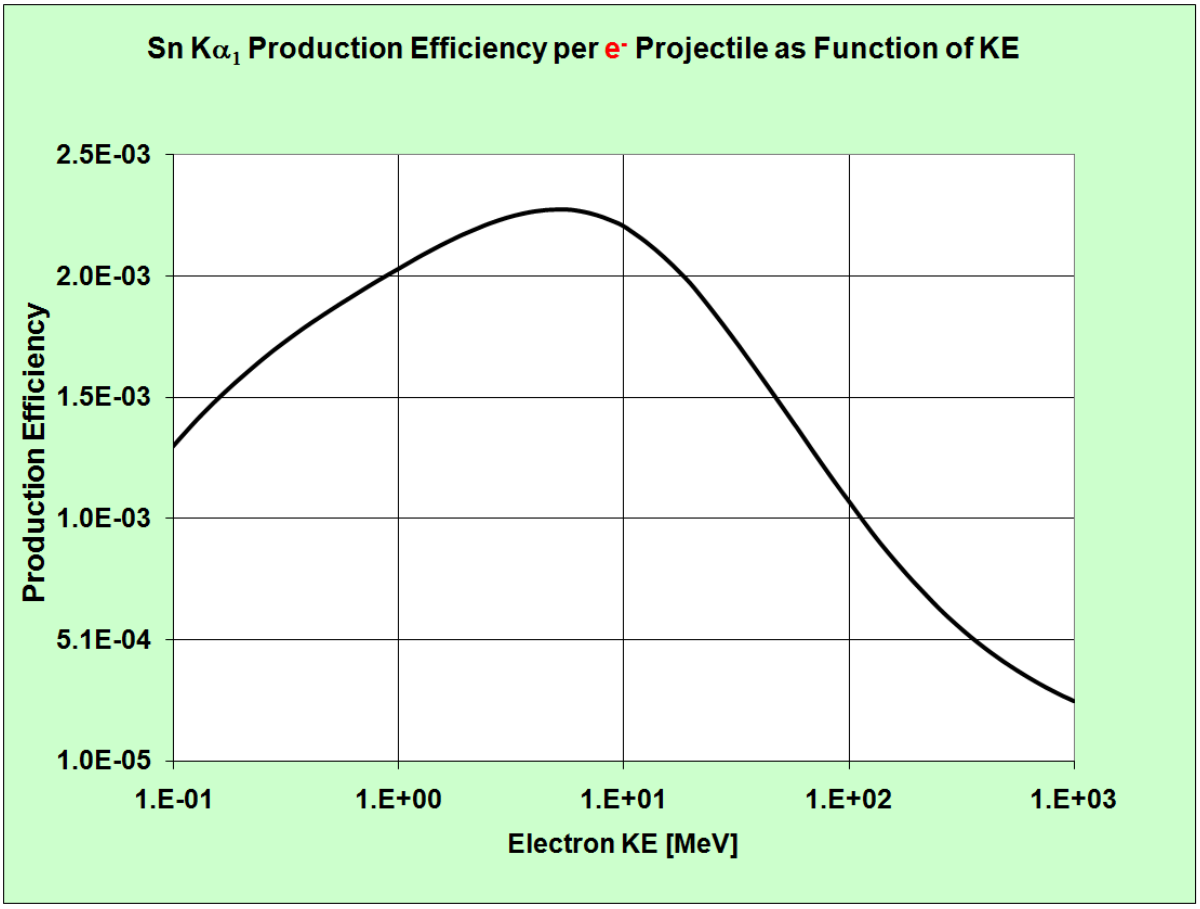

Figure 2. Sn $K\alpha_1$ production efficiency as a function of electron kinetic energy. This calculation takes into account: (a) the energy-dependent cross section (Fig. 1); (b) the energy-dependent stopping power of electrons in Sn; and (c) the probability of 1s vacancy leading to $K\alpha_1$ emission rather than $K\alpha_2$, $K\beta_1$, etc. or non-radiative Auger.

Fig. 2 indicates that given a fixed energy E_0 within which one has a mono-energetic bunch of electrons of, say, 1 GeV, 100 MeV, 10 MeV, or 5 MeV kinetic energies, then the optimum appears to be around 5-10 MeV. To this end, this LDRD project strived to find a novel means of converting PW-laser energy into the maximum number of 5-10 MeV electrons, the "most useful" electron energy, within a Sn target.

Again, two approaches have been studied directly towards this end; (1) optimizing regular DFI, and (2) conceiving an alternative, novel target. The following section describes the theory/computational physics used to predict Sn DFI measurements performed within Center-01600.

6. DIRECT FOIL IRRADIATION SIMULATIONS OF CENTER-01600 TIN X-RAY DATA

First, the LSP Particle-in Cell (PIC) code simulated the Center-01600-performed Sn DFI data with the following conditions: [1] Fully electromagnetic, relativistic, and kinetic; [2] Explicit particles and fields; [3] No implicit or fluid particles, needing an Equation of State; [4] Energy-conserving-push (rather than momentum-conserving-push) algorithm; which is not susceptible to the numerical Debye heating instability; [5] Collision rates included; either Spitzer rates or binary model; [6] Cloud-in-cell interpolation model to reduce particle noise; [7] Double precision operations.

In terms of item [2], three conditions are met: (a) The Courant condition; that is the time step Δt multiplied by the speed of light c must be less that the grid spacing; (b) The plasma angular frequency ω_{pe} multiplied by Δt must satisfy $\omega_{pe}\Delta t<1$; And (c) the electron-cyclotron angular frequency ω_{ce} multiplied by Δt must satisfy $\omega_{ce}\Delta t<1$. These three conditions as well as numerical convergence and statistical convergence of Ka production, were met using a time step of 1e-17 s. A typical simulation duration of 5 ps, therefore, requires 500,000 time steps. A typical 200x200 μm grid had 10,240,000 nodes. Hence, a supercomputer capable of devoting ~1000-2000 processors for a few days to few weeks was required, depending on total particle count.

The laser was directly incident upon a 130 x 130 μm^2 Sn square tilted to 45^o with *p*-polarization, as depicted in Figure 3. (The LSP simulations were limited to 2D Cartesian.) The peak electric field was ~2.08e+08 kV/cm, which corresponds to an irradiance or Poynting vector value of ~5.5e+19 W/cm^2. The laser was modeled as a Gaussian in space and time with 7 μm FWHM and 470 fs FWHM, respectively. The total energy within the 1053 nm wavelength laser pulse was 104 J +/- 10%.

The computational model fixed the Sn ionization distribution to Sn^{+1}; thus the initial electron (n_e) and ion densities (n_i) were $n_e=n_i$~3.66e+22 cm^{-3} for the initial 7.3 g/cm^3 Sn mass density. $K\alpha_1$ and $K\alpha_2$ x-ray powers as a function of time, birth locations, and spectra were passively computed from the electron distributions (density and kinetic energy as a function of space) in conjunction with the Sandia-developed/compiled ITS tables for electron impact cross sections.

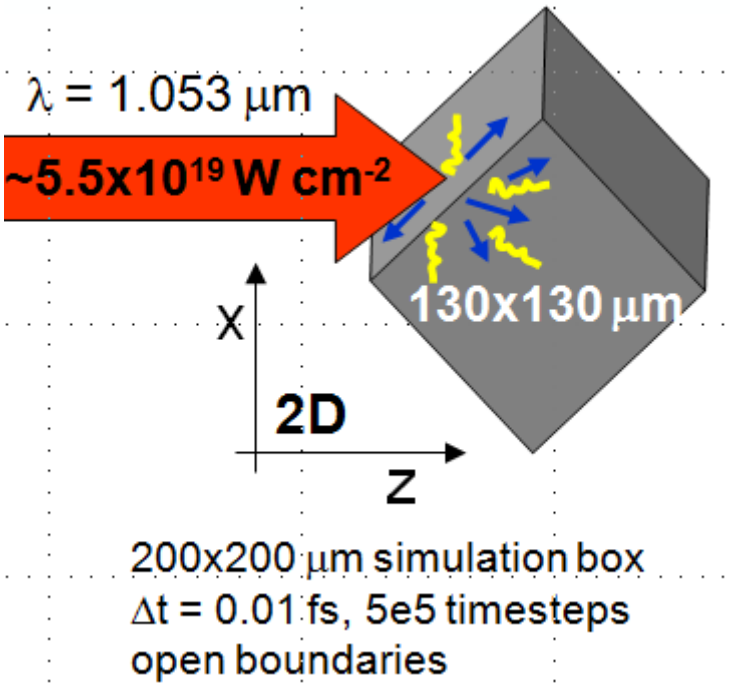

Figure 3. Part of the setup for the computational model used to study Center-01600 DFI x-ray DFI data.

Figure 4 shows the electric field (left) and electron temperature (right) at t=1000 fs, for the target depicted in Fig. 3. The electric field scale ranges from 4e+03 to 4e+08 kV/cm, and the electron temperature covers 0.001-400 keV. The $K\alpha_1$ and $K\alpha_2$ x-ray powers integrated over 4 ps are within the error bars of the measured x-ray yield for this particular 104-J laser shot. The simulated ε is ε~1.00e-04, where the measured ε is 0.5-2e-04.

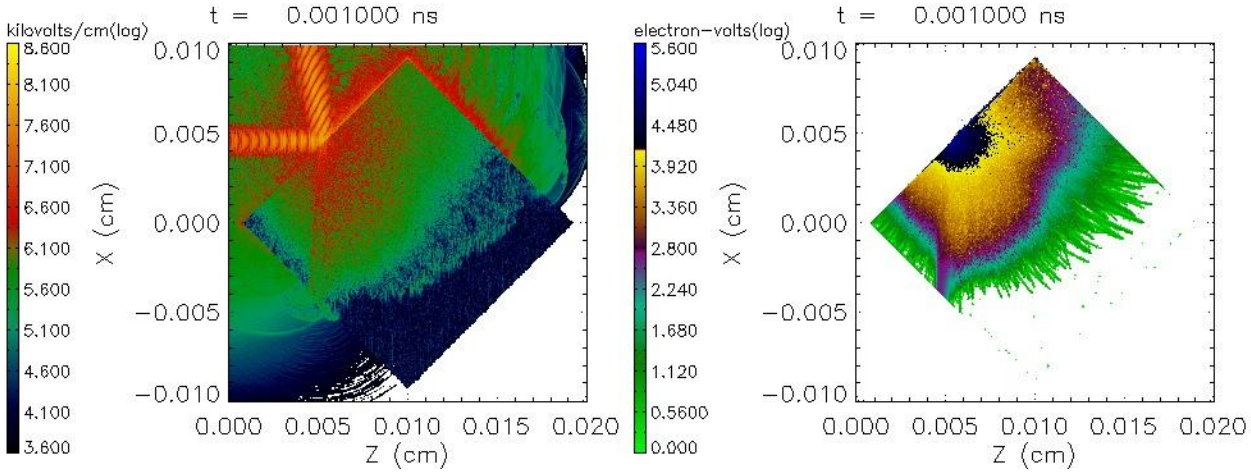

Figure 4. The electric field (left) and electron temperature (right) at t=1000 fs for the Sn target depicted in Fig. 3.

Figure 5 below shows the predicted and measured ε values for three data sets as a function of irradiance (Wcm^{-2}).

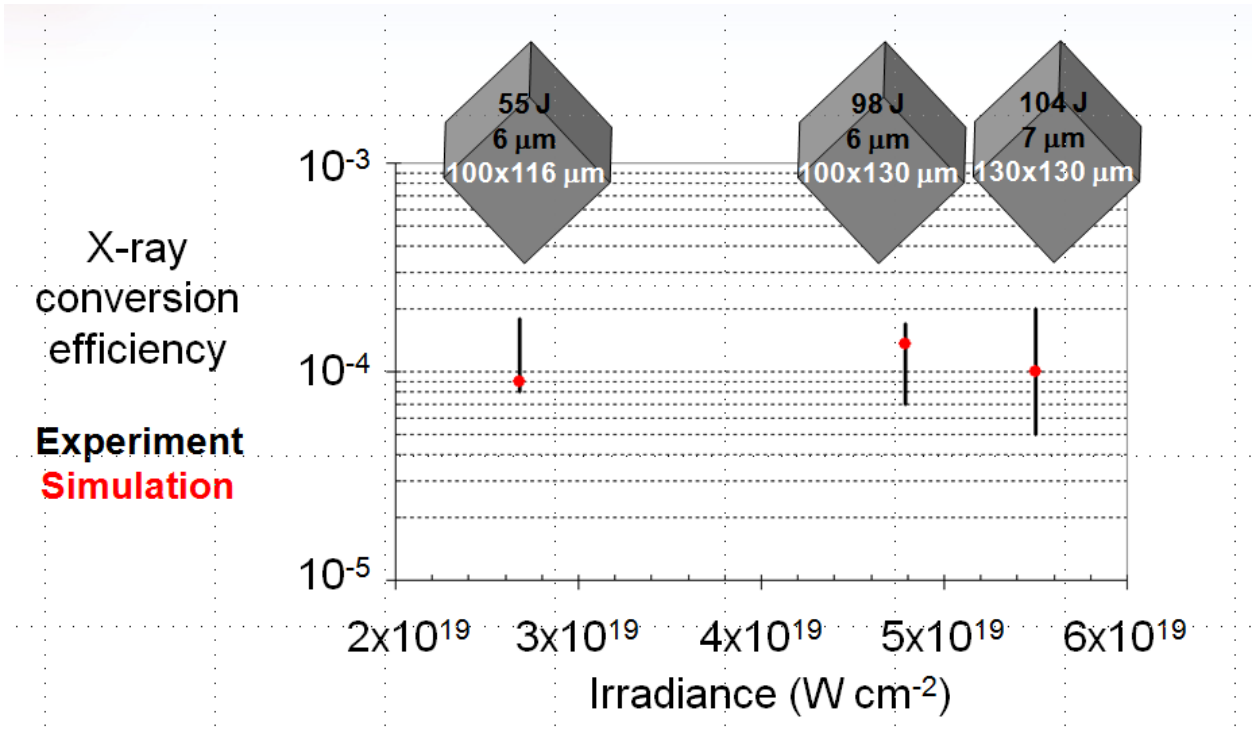

Figure 5. Two additional data points (55 and 98 J) that also indicate simulated ε within measurement error bars.

The level to which LSP PIC simulations were able to reproduce the measured ε values gave confidence in the computational predictive capability, and therefore allowed one to proceed towards studying/conceiving methods with the goal of a >10x ε enhancement.

7. THE TWO-STAGE CONCEPT

The Two-Stage concept is illustrated in Figure 6 below, but with the addition of an extra couple of secondary Sn stages. Fig. 6 is self-explanatory through the detailed annotations, and those comments will not be repeated here.

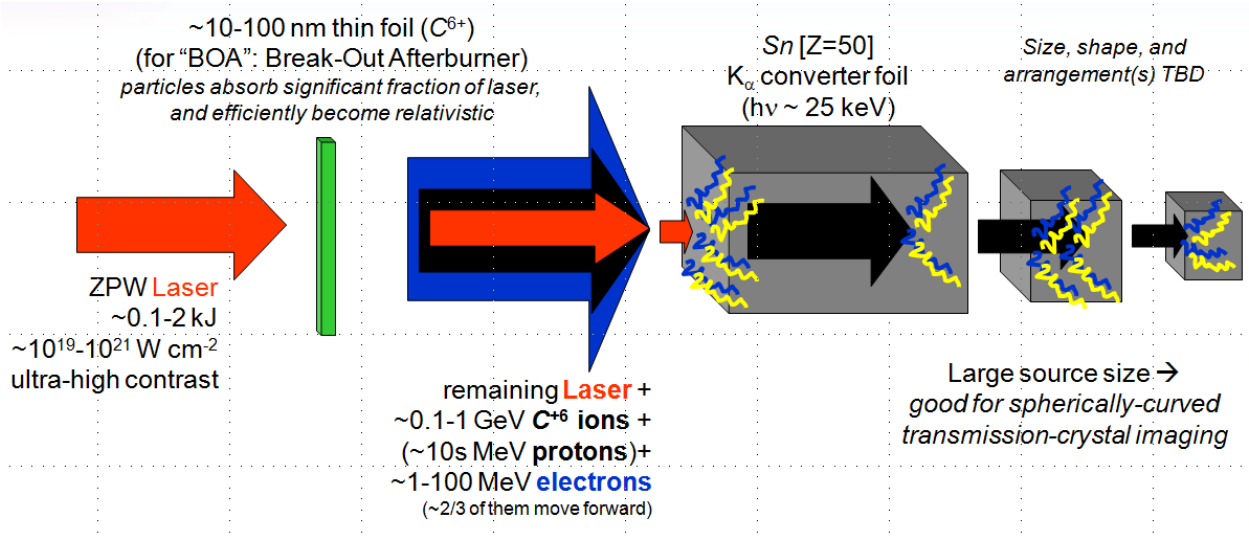

Figure 6. Illustrative cartoon of the two-stage concept using a BOA-produced "superbeam" (electrons+ions+laser) to significantly increase the efficiency of a fixed amount of laser energy into Kα x-rays.

Note the high 1e+21 W/cm^2 irradiance level that may be required to initiate the BOA effect. Also note that double plasma mirrors will likely be needed in order to achieve the necessary ultrahigh contrast. The goal is to convert as much laser energy as possible into fully-ionized carbon ions and electrons, with the highest possible fraction of beam energy in the forward direction. The electron beam can create $K\alpha_1$ directly but the C^{+6} beam does this too by heating electrons deep inside the S target.

Figure 7 illustrates the details used in a BOA simulation where a 2600 J laser is contained within a 300 fs FWHM (Gaussian) pulsewidth. Also, the laser is assumed to have no significant prepulse (other than the Gaussian rise of the main pulse) – which can otherwise adversely affect the BOA initiation – and the focal spot is 8 μm FWHM (Gaussian). Again, the simulation is 2D Cartesian.

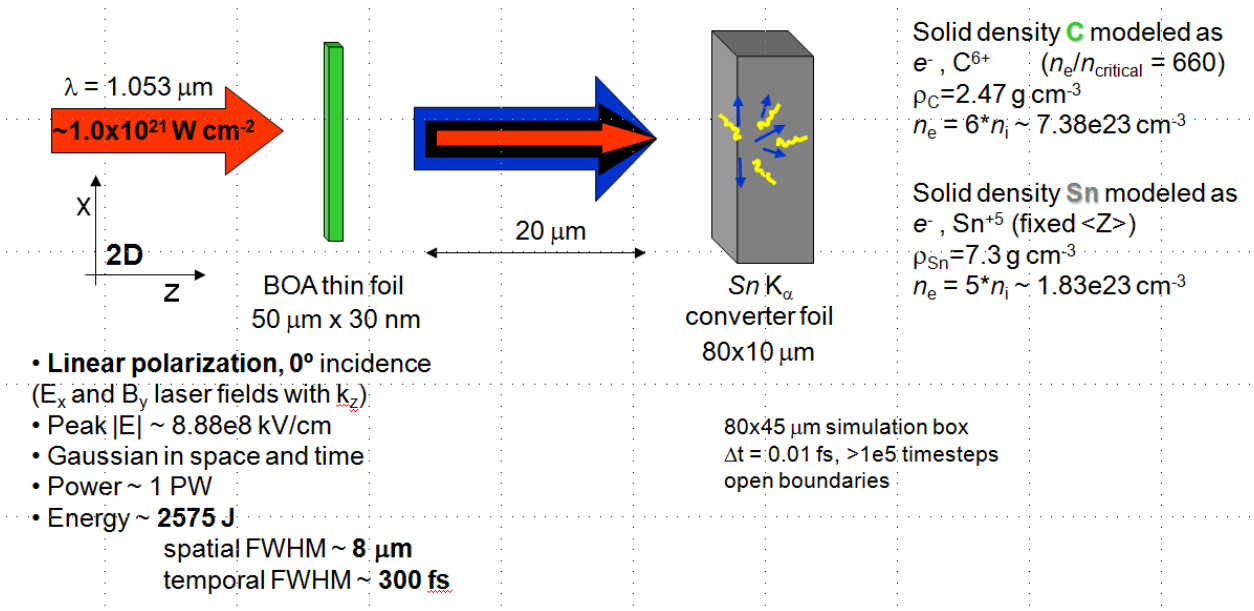

Figure 7. Simulation setup specifics of a Two-Stage target.

In this instance the Sn is fixed to the Sn^{+5} ionization state. The carbon BOA foil, 20 μm ahead of the Sn Kα target, is assumed to be fully ionized at t=0 leading to the 660x overdense case (annotated in the figure). The following figures, Figure 8(a) etc., contains time snapshots of five quantities throughout the Δx=80 μm, Δz=45 μm space: (1, top left) Electric field; (2, top middle) BOA foil electron density [1/cc] normalized to the Sn solid density; (3, top right) BOA foil fully-ionized carbon density [1/cc] normalized to the Sn solid density; (4, bottom left) BOA foil electron temperature; (5, bottom right) Tin foil electron temperature. Since temperatures in these simulations are actually ill-defined, the plotted "temperatures" are actually kT = 2/3 E_{ave}, where E_{ave} is the average electron energy within each cell.

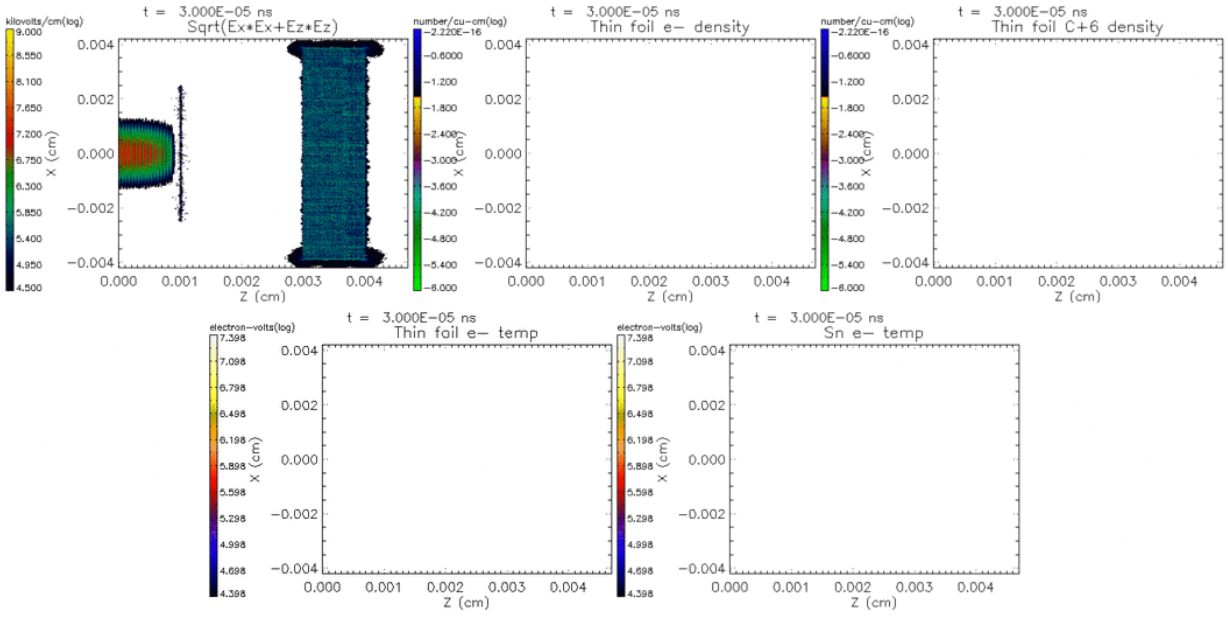

Figure 8(a). At t=30 fs the laser is about to strike the fully-ionized carbon BOA foil.

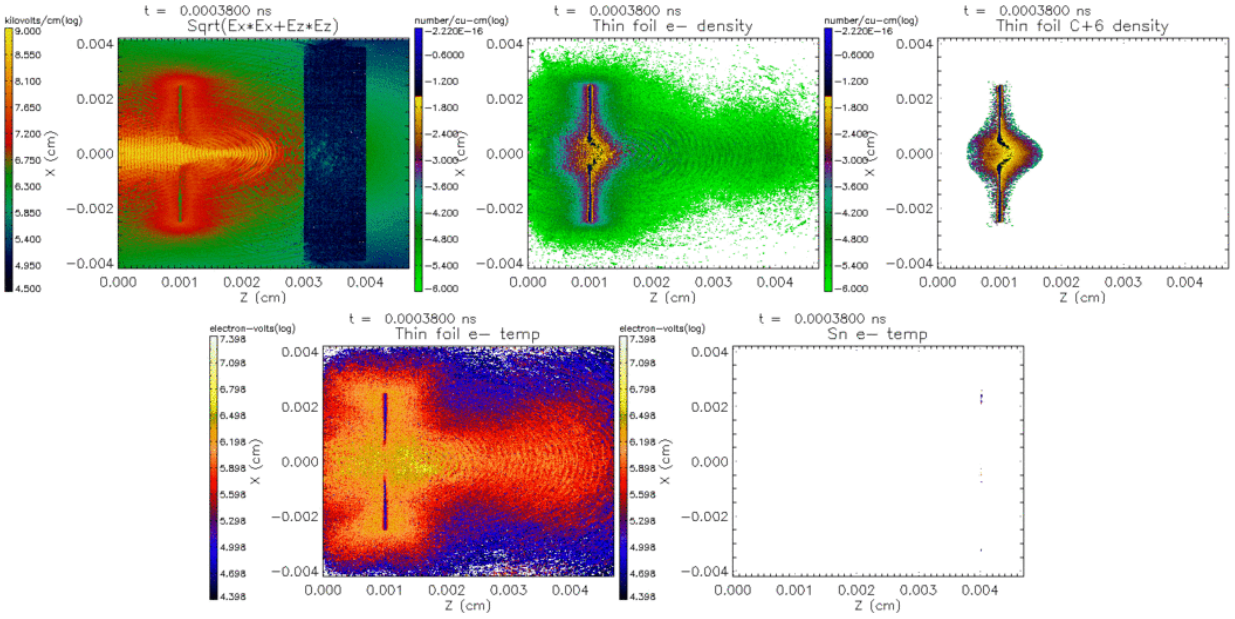

Figure 8(b). At t=380 fs the laser field is a little more than midway between the BOA foil and the Sn target. Notably the electron density has not necessarily dropped by a 660x factor, but rather the electrons have increased their mass relativistically to the extent that the plasma frequency has decreased in proportion to $\gamma^{-1/2}$.

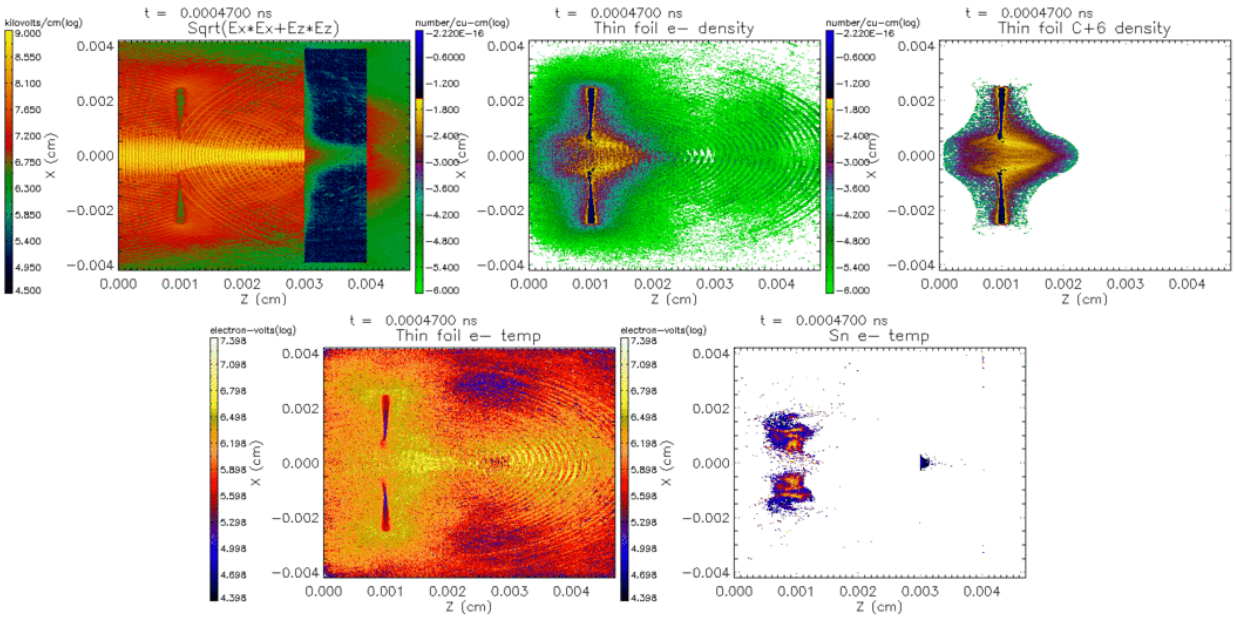

Figure 8(c). At t=470 fs an apparently coherent electron beam has reached and then passed through the 10-μm-thick Sn target. The carbon ion beam is now established but, being slower moving, it is mid way between the BOA foil and Sn target. Sn electrons are beginning to heat up, likely due to direct laser irradiation.

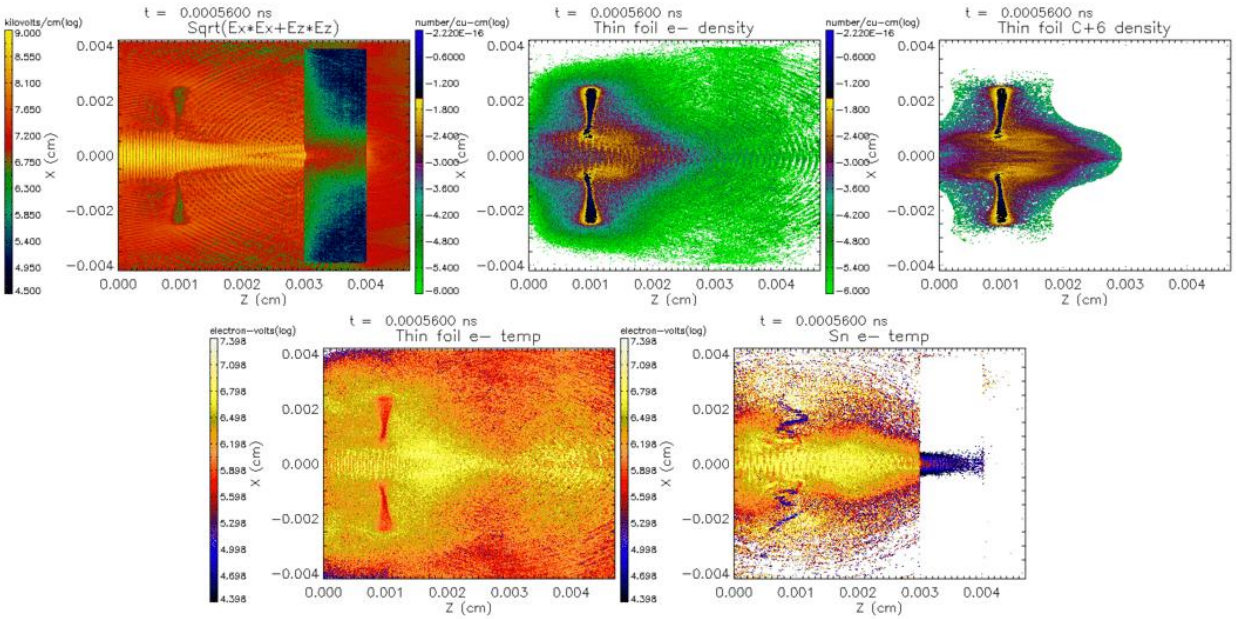

Figure 8(d). At 560 fs Sn electrons within the Sn slab have heated to approximately 100 keV, and the temperature profile almost extends through the 10 μm target thickness (z-axis). The profile is tightly centered about the origin of the x-axis, because the heating is mostly due to the self-focused laser field.

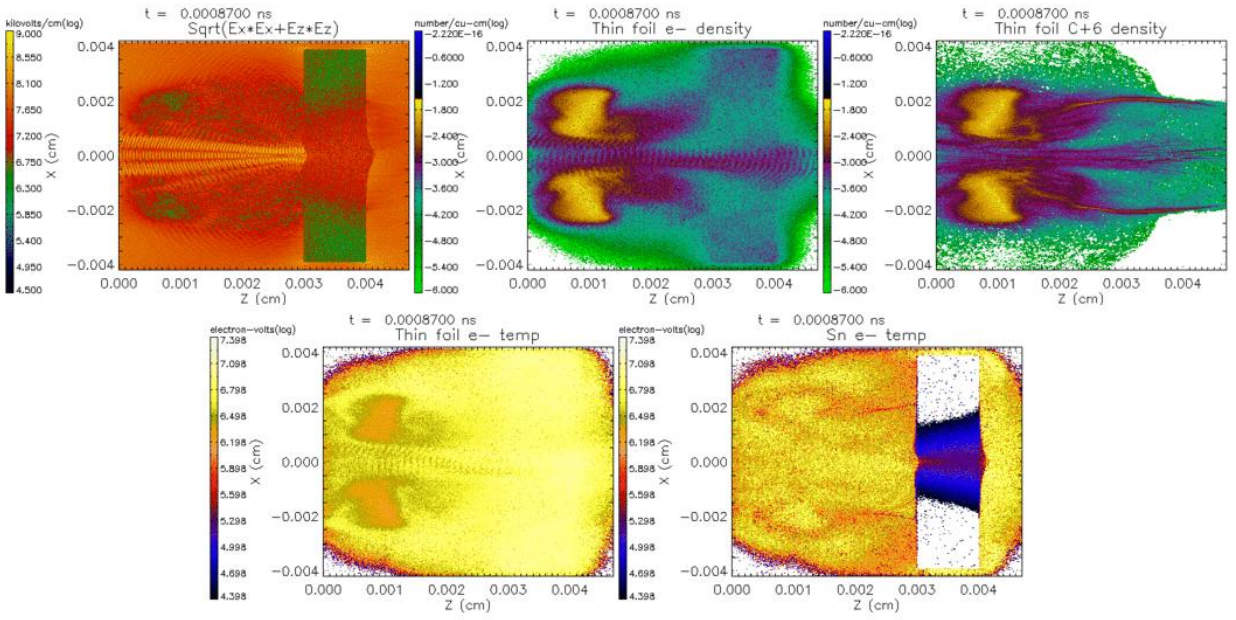

Figure 8(e). At 870 fs the ion beam has reached the Sn slab and passed through it. The beam has high density at z>45 μm, implying no refluxing. The BOA and Sn electrons on the other hand are recirculating. The BOA electrons within the Sn may have reached their peak "temperature" at this point, 13-25 MeV; which is above the 5-10 MeV *kinetic energy* corresponding to peak efficiency. Note 1: one cannot use $E_{ave,e}=(3/2)K_BT_e$ is this case because the normal Maxwell-Boltzmann distribution is relativistically skewed. Note 2: for comparison, the lower-irradiance, lower-laser-energy DFI case in Fig. 4 reaches a peak <0.4 MeV electron temperature.

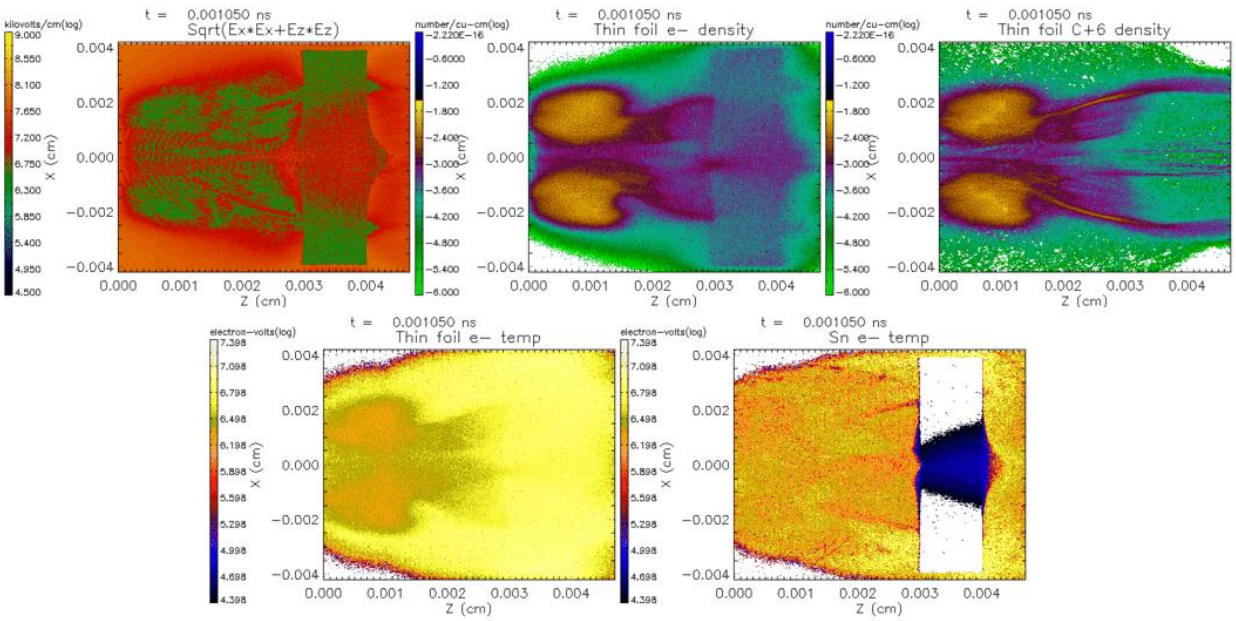

Figure 8(f). At 1050 fs the ion beam has widened in the x-direction but it is possibly losing energy. Bulk tin electrons are beginning to cool, as are the BOA-originating electrons. For the latter, a uniform temperature of 6-13 MeV appears to exist throughout the Sn volume. It may be the general case that recirculating BOA electrons within Sn are creating more x-rays than recirculating Sn-electrons.

This initial, non-optimized Two-Stage simulation demonstrates beam transport, refluxing of both BOA- and Sn-electrons, and an approximately uniform BOA electron temperature within the Sn volume corresponding to kinetic energies close to the optimum, Fig.2.

8. BOA FOIL INTEGRITY IN PRESENCE OF PREPULSE

As noted earlier, BOA simulations assume that the laser field reaches a 1e+21 W/cm^2 irradiance essentially instantaneously (within a few hundred fs). Therefore, the 30 nm carbon foil does not expand significantly towards the underdense limit. In the realm of laser physics/engineering, such a pulse is impossible, but it is feasible to limit effects originating from spontaneous amplified emission, and so on, with new technological breakthroughs.

Assuming the 1e+21 W/cm^2 irradiance main pulse, it is interesting to study the effect of constant (in time) 1e+09, 1e+10, 1e+11, and 1e+12 W/cm^2 irradiance prepulses upon the BOA foil integrity. First, the lowest prepulse irradiance, 1e+09, corresponds to a 4 kbar pressure as prescribed by a well-known empirical formula from the field of ICF. The same formula yields a 400 kbar pressure for the 1e+12 case.

The irradiance-dependent pressure can be substituted into the standard ideal-gas sound speed expression and, using the 30 nm thickness divided by this quantity, a *hydrodynamic expansion* time-scale „t_{hydro}' can be obtained. For example, in the 1e+09 case the 4 kbar shock crosses the 30 nm thickness in t_{hydro}~55.2 ps: whereas the 400 kbar shock from the 1e+12 prepulse crosses in t_{hydro}~5.52 ps.

In Figure 9(a) below, the left plot shows the BOA foil mass density (2.255 g/cc initially) as a function of z at t=0. The right plot will show the normalized overdense thickness as a function of time for the 1e+09, 1e+10, 1e+11 and 1e+12 W/cm^2 irradiance cases.

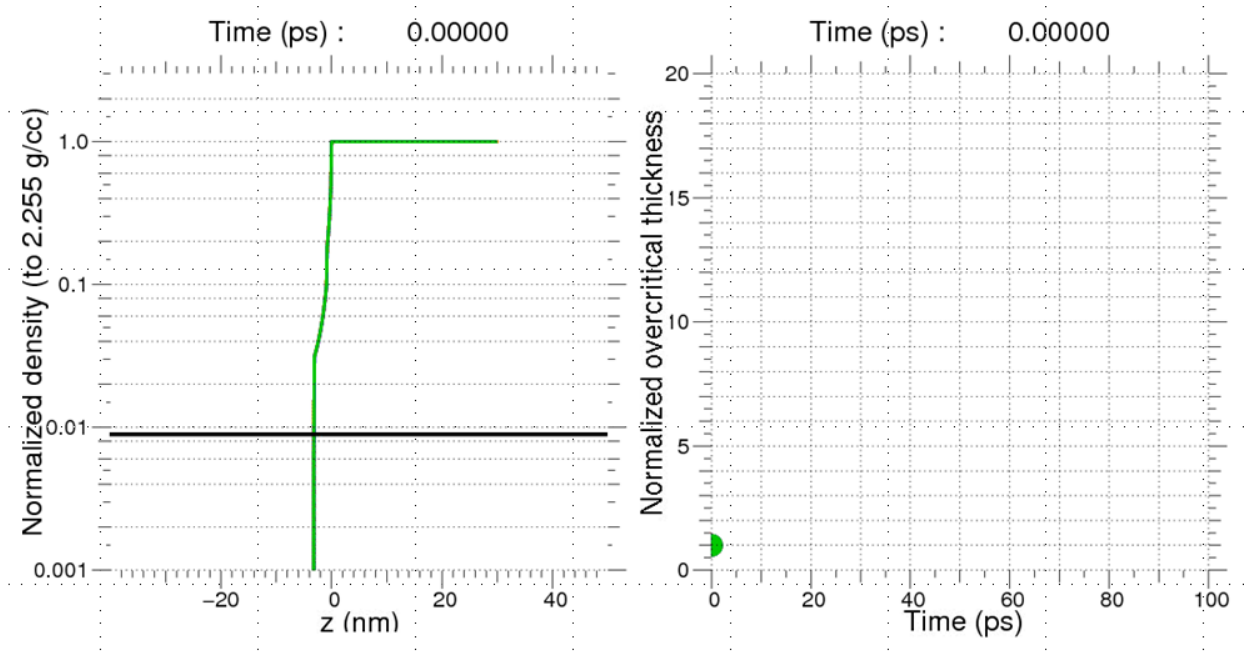

Figure 9(a). At t=0 ps there is of course no expansion.

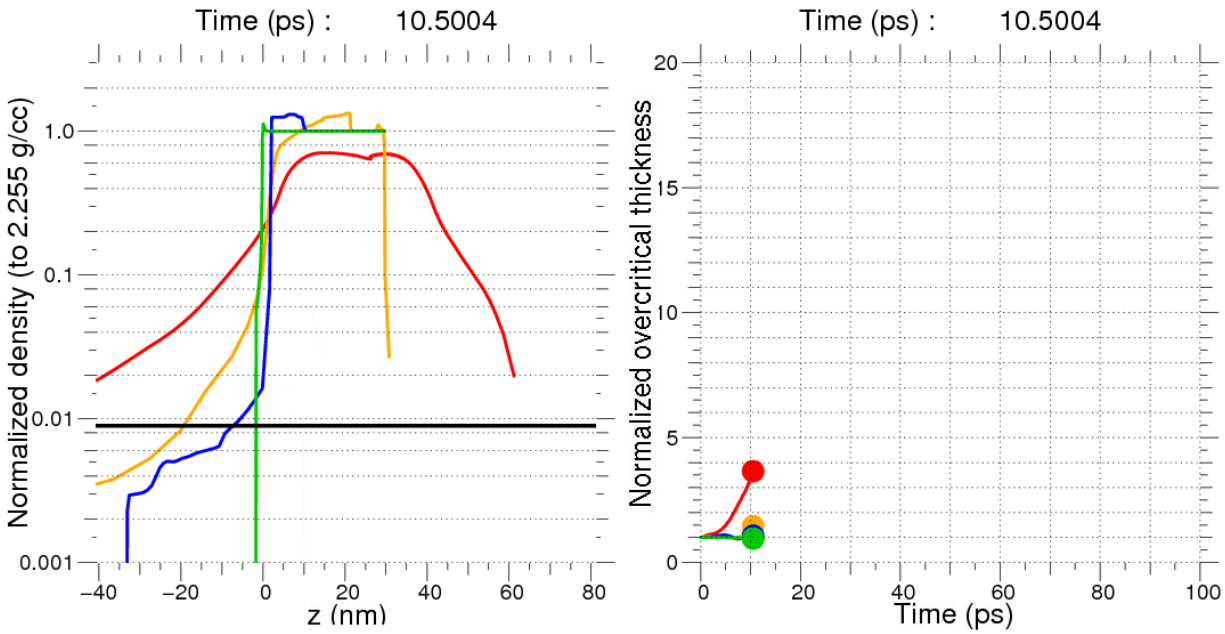

Figure 9(b). At t=10.5 ps only the highest irradiance prepulse, 1e+12, has increased in its normalized overdense thickness (right panel); by a factor of ~3.75x in fact. It is not yet known whether a 3.75x30=112.5 nm thick, 2.255/3.75 g/cc density foil will initiate the BOA mechanism.

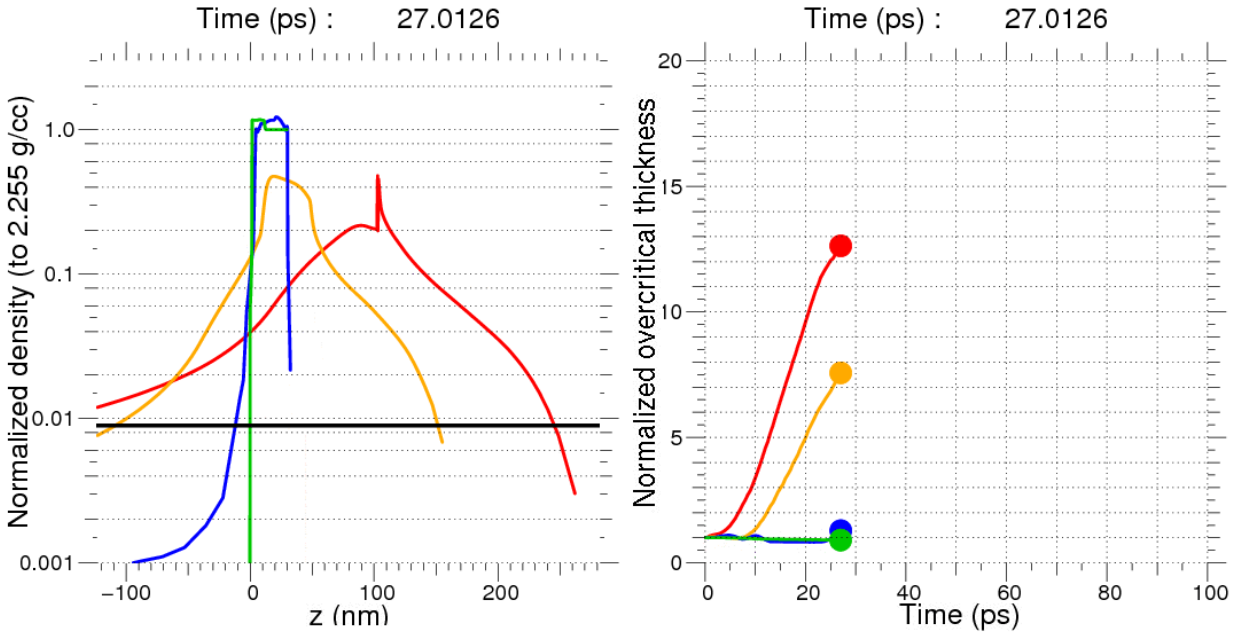

Figure 9(c). At t=27 ps both the 1e+12 and 1e+11 prepulses have led to 13x and 7.5x normalized overdense thicknesses. The other two lower irradiances however, 1e+09 and 1e+10, have yet to expand significantly.

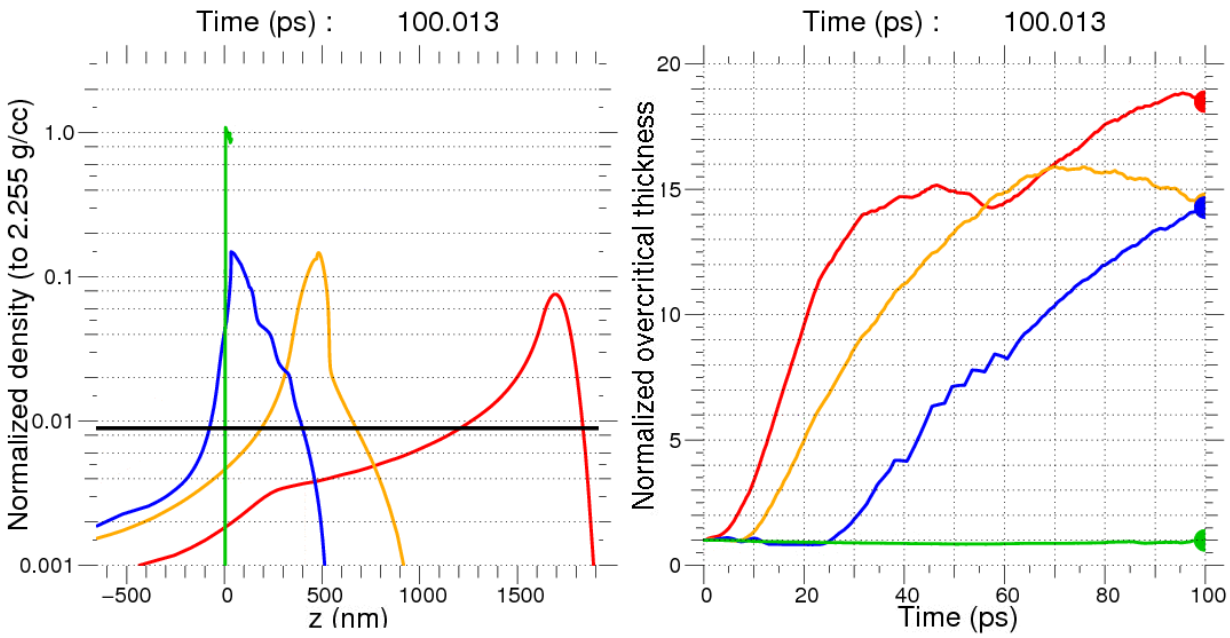

Figure 9(d). At t=100 ps only the 1e+09 irradiance case has not expanded significantly, because the specified intensity lacks the energy necessary to melt the thin foil (according to the QEOS model used for the carbon).

Figures 9(a) – 9(d) give an excellent indication of the time that the normalized overdense thickness remains near unity (30 nm) for a variety of irradiances. It is however unclear at this writing precisely what level of foil perturbation BOA initiation can tolerate. Although it is likely that double plasma mirrors will be necessary.

9. CONCLUSIONS

A state-of-the-art predictive/computational capability has been established allowing $K\alpha_1$ & K α_1 x-ray production to be modeled for a target of any material irradiated by a Petawatt short-pulse laser. The capability is continuingly being advanced, but at present the tool has closely predicted the measured x-ray yields from simple Sn targets irradiated by the so-called 100TW system within Center-01600. This device will eventually become the „Z-PetaWatt' laser, ZPW. (Ongoing numeric advances include investigating the effect of a preplasma created by the finite prepulse of a PW-class laser.)

The computational tool's success gives one confidence that more complicated, novel target concepts can be numerically investigated with accuracy; in particular, the Two-Stage BOA idea. The BOA-produced beams from the „first stage' are used to effectively heat a larger source(s) second stage. (Sn has been the main interest so far). Notably, the Los Alamos National Laboratory (LANL) published BOA simulations were reproduced during the early course of this work. Moreover, the preplasma level as a function of prepulse can now be predicted; however, incorporation of a particular preplasma into a BOA simulation has not yet been performed.

Although the goal of this prematurely-ended LDRD (Guy R. Bennett's decision to transfer to a different Division part way during the 2nd year of this 3-year project) was to increase ε, it is noted that two other fundamental requirements are required for the very highest quality ICF/HEDP-relevant x-ray imaging:

[1] An exquisitely sensitive Multiframe Ultrafast Digital X-ray Camera (MUDXC).

[2] A high-collection-efficiency, high-spatial-resolution 25-keV x-ray imager.

Please see appendix II which discusses item [2] in some detail. In terms of item [1], if a MUDXC device is realized, the effective 1 ns gate time (affecting „motional blur' if any) between frames will fortunately limited by the 1-10 ps timescale of the $K\alpha$ emission time.

Should the Two-Stage concept be successful for, say, Sn-$K\alpha_1$ (25.2713 keV, and success is defined as a >10x ε enhancement), the technique should also work for higher atomic number (Z) elements, too: Except, it is believed that the electron impact K-shell ionization cross section σ for such elements decreases. The overall outcome would likely be a ε lower than that of Sn (Z=50), despite the fact that the non-radiative Auger 'loss' would be close to zero. For elements $Z<50$ it is believed that σ rapidly increases. This could dramatically increase ε for x-ray energies around 6 keV, a photon energy that is routinely used on many Z accelerator experiments. This would require the use of a low-Z element, with the drawback that the non-radiative Auger loss is high. At this writing it is therefore unclear if a low-Z Two-Stage target would *win* over long-laser-pulse, thermally generated 6.151-keV radiation from Mn. If the low-Z Two-Stage technique does indeed win, then it would be recommended that consideration be given towards converting the long-pulse Z-Beamlet Laser (ZBL) into a ZPW device: With the option of reverting to long-pulse mode, if desired. The Two-Stage, non-thermally-produced 6-15 keV (elements Co through Zr) x-rays would – unlike ZBL – create blur-free images.

APPENDIX A:

PREDICTIVE CAPABILITY FOR Z-PETAWATT-DRIVEN HIGH-ENERGY K-ALPHA X-RAY YIELDS USED TO IMAGE HEDP EXPERIMENTS ON THE Z MACHINE

Predictive capability for Z-Petawatt-driven high-energy K_α x-ray yields used to image HEDP experiments on the Z Machine

A. B. Sefkow, G. R. Bennett, M. Geissel, M. Schollmeier
Sandia National Laboratories
Albuquerque, NM 87185, USA

On behalf of the
Z experiment, theory and design, and laser teams

Z100 Meeting
August 25th, 2010

Sandia is a multiprogram laboratory operated by Sandia Corporation, a Lockheed Martin Company, for the United States Department of Energy's National Nuclear Security Administration under contract DE-AC04-94AL85000.

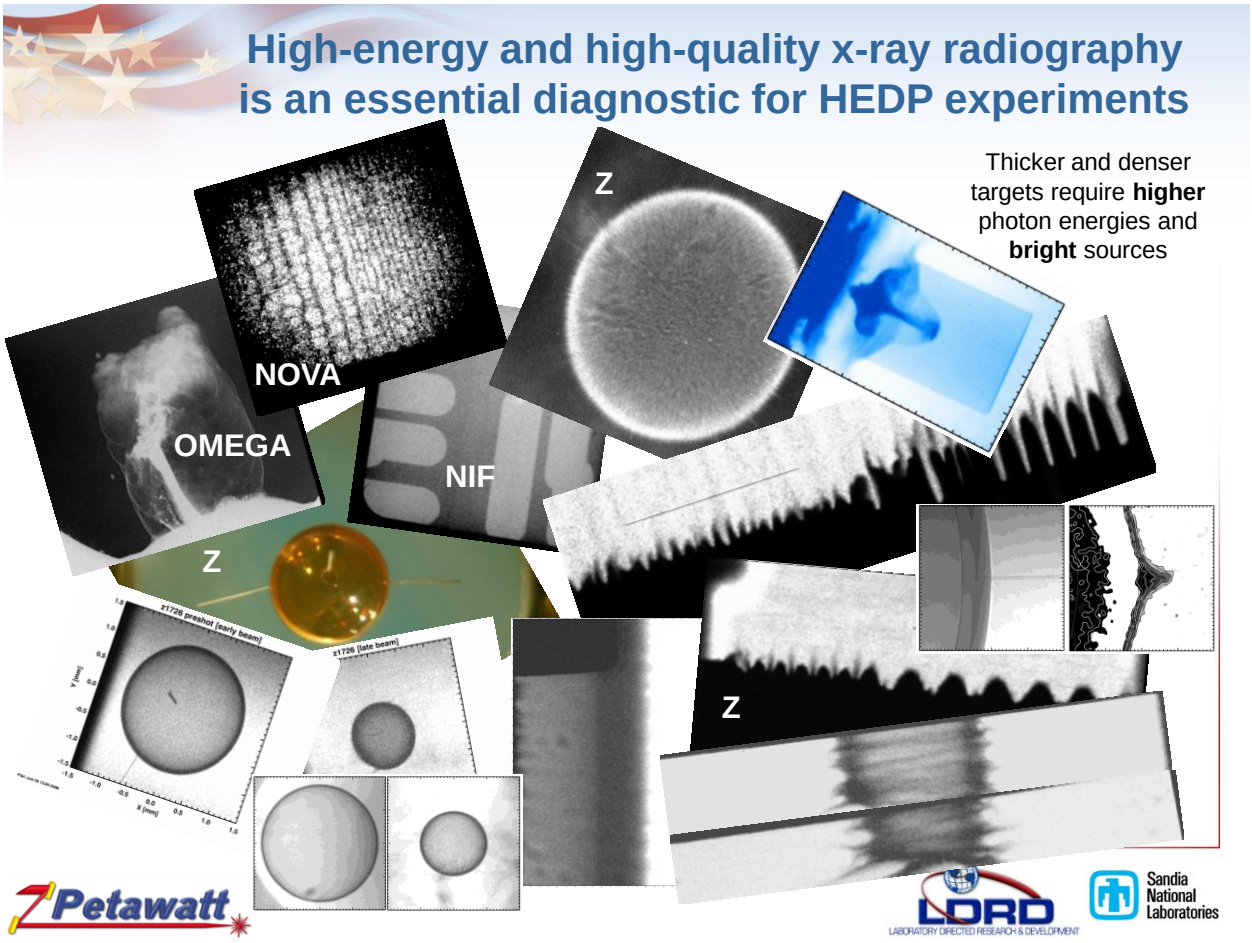
High-energy and high-quality x-ray radiography is an essential diagnostic for HEDP experiments
Thicker and denser targets require **higher** photon energies and **bright** sources
NOVA
OMEGA
NIF
Z
Z
Z
Petawatt
LDRD
LABORATORY DIRECTED RESEARCH & DEVELOPMENT
Sandia National Laboratories

Laser-driven K_α x-ray production using thin foils can produce ~10-80 keV x-ray sources

High intensity lasers
produce
hot electrons in targets
which generate
K_α x-ray emission

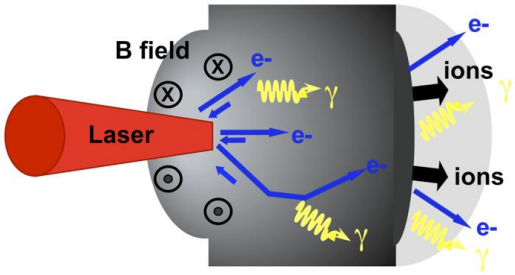

Choice of material Z determines K_α x-ray energy

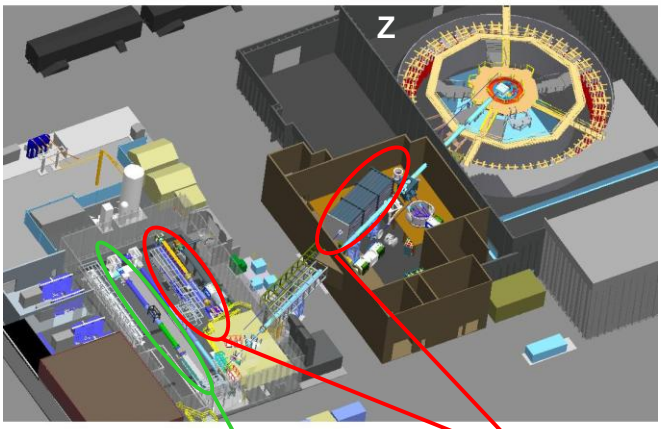

Z Beamlet
long pulse (~ 4-6 kJ)
~ few ns

Z Petawatt
short pulse (≤ 2 kJ)
~0.5-10 ps

~**1 ps** short pulse laser gives **~4-5 ps K_α x-ray pulse**
→ **little-to-no motion blur**
100 km/s (ICF target) only moves 0.5 μm in 5 ps

Z Petawatt

LDRD Laboratory Directed Research & Development

Sandia National Laboratories

First, we seek to develop a predictive capability for measured K_α yields from traditional thin foils

~100s x 100s x 10s μm

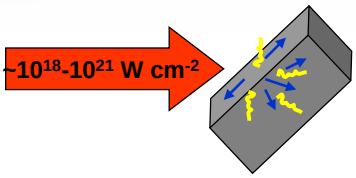

Small source size → *good for point-projection imaging*

Typical efficiencies for high-energy K_α production are **~1e-4 or less** (relatively low)

H. S. Park, et. al., Phys. Plasmas 15, 072705 (2008).

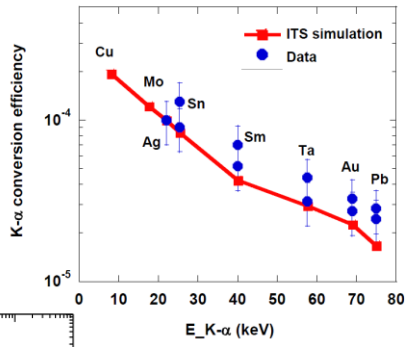

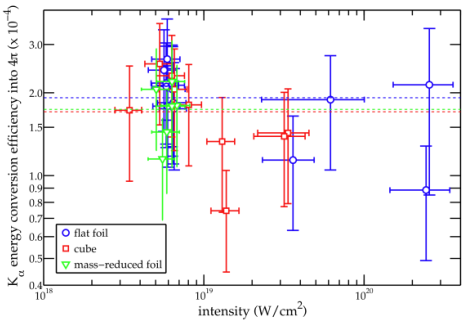

M. Schollmeier, et.al., in preparation (2010).
Sn (Z=50) targets, hν ~ 25 keV

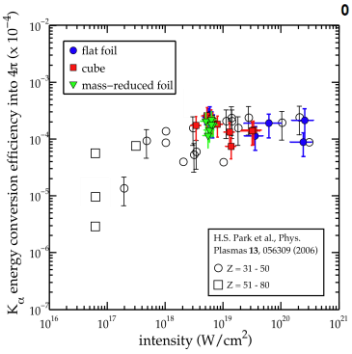

H. S. Park, et. al., Phys. Plasmas 13, 056309 (2006).

If successful, then try to engineer novel target (and imaging) concepts to increase efficiency

Petawatt

LDRD LABORATORY DIRECTED RESEARCH & DEVELOPMENT

Sandia National Laboratories

25 keV (*Sn* K_α) source characterization

100-200 TW target area (PW in-progress)

Laser parameters:

- E = 60-160 J (eventually ≤ 2 kJ), t_{pulse} ~ 0.5 – 50 ps
- focal spot: 6.5 µm FWHM (~35-50% energy)

***Sn* targets:**

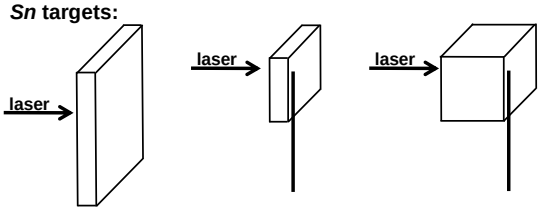

mm-size **"flat foils"** 20 µm or 100 µm thick

20 µm x (150 µm)^2 **"mass-reduced foils"**

"cubes" with 100 µm sides

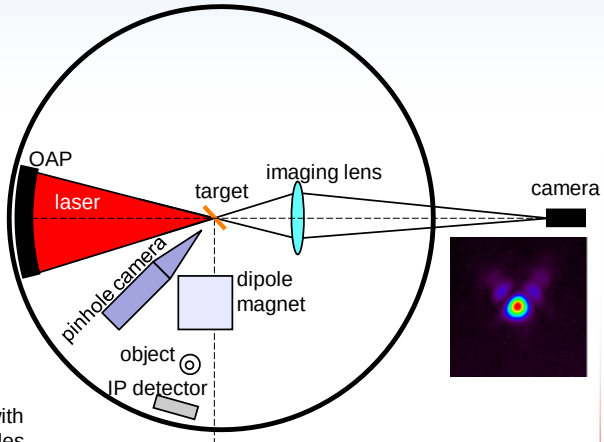

100 TW target chamber (top view)

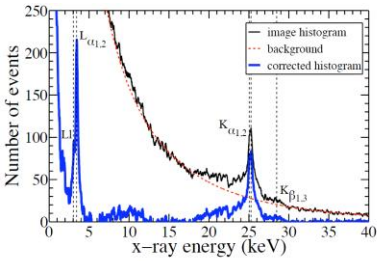

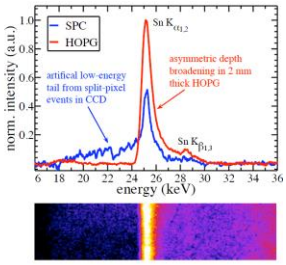

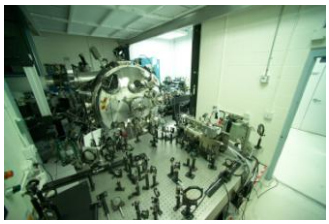

SPC = single photon counter
HOPG = highly oriented pyrolitic graphite spectrometer

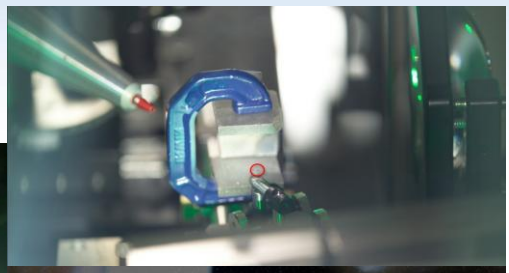

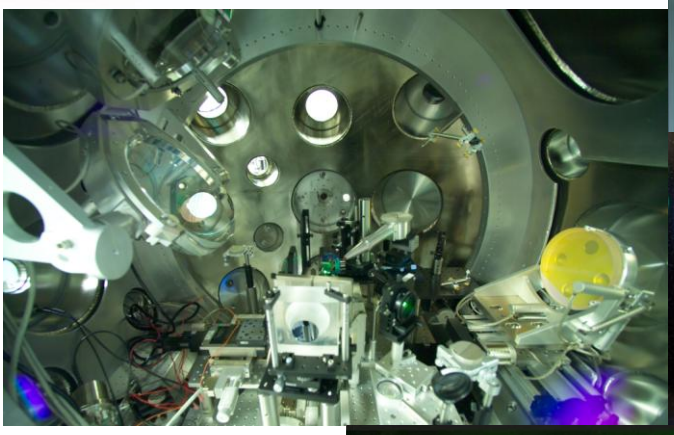

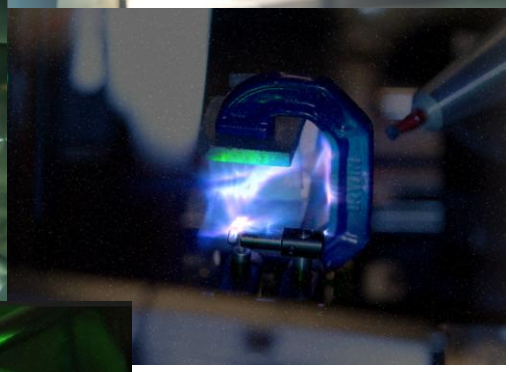

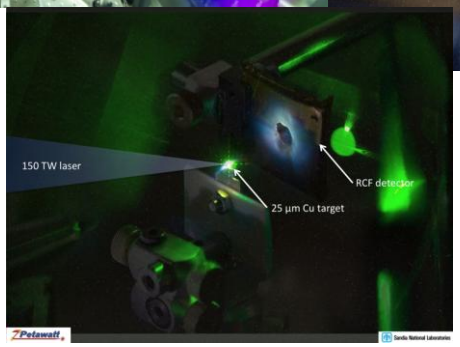
150 TW laser
RCF detector
25 µm Cu target

25 keV (*Sn* K_α) radiograph of test objects

Spatial characterization

'cube' target

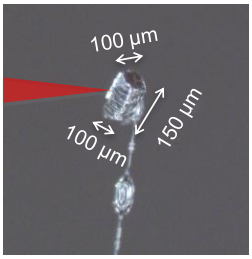

pinhole image with 'cube' target

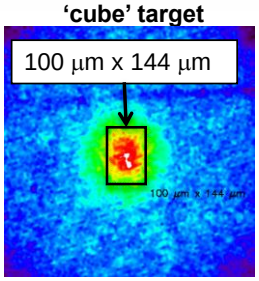

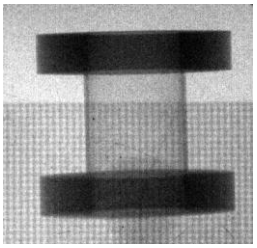

radiograph

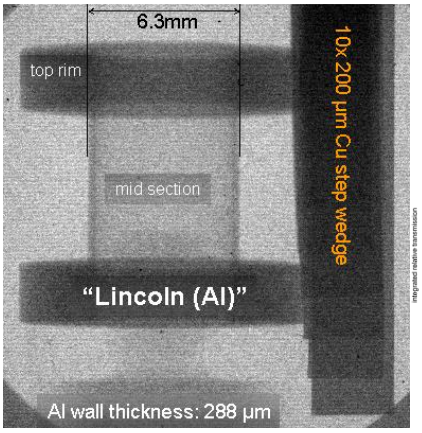

Nested aluminum cylinders

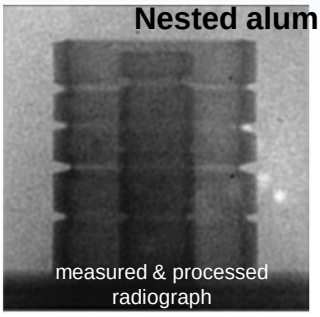

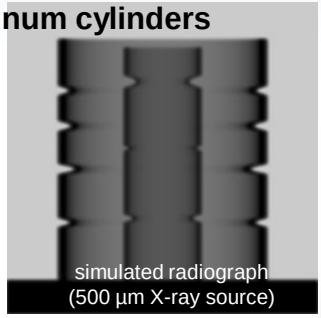

- *Laser : ~100 J, ~7 ps, ~10 μm FWHM*
- *Liner thicknesses: 890 μm (outer), 560 μm (inner)*

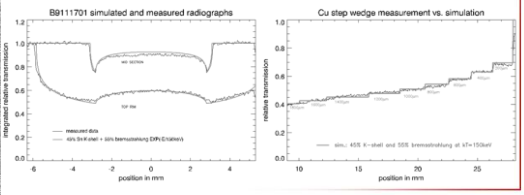

Petawatt

LDRD LABORATORY DIRECTED RESEARCH & DEVELOPMENT

Sandia National Laboratories

A single photon counter is used to determine the laser-to-K_α conversion efficiency

- absolutely calibrated for detection efficiency ε
  Fe^{55} (5.9 keV) and *Cd*^{109} (22 keV), will add *Sn*^{113} and *Sb*^{125}
- 4π conversion efficiency into $K_{\alpha 1}$+$K_{\alpha 2}$: η ~ 0.8-2.5 x 10^{-4}
- flat foils perform best
- mass-reduced targets: slightly smaller efficiency, but higher spatial resolution

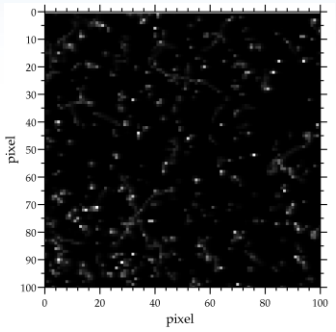

$$E_{\text{x-ray}} = \frac{N_{CCD} \times 25\,\text{keV}}{\varepsilon \times \Omega \times T} \qquad \eta = \frac{E_{\text{x-ray}}}{E_{\text{laser}}}$$

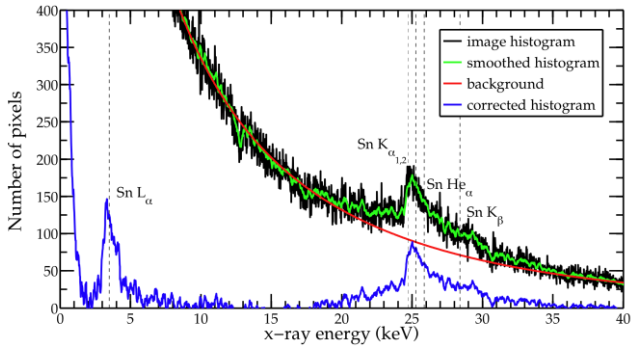

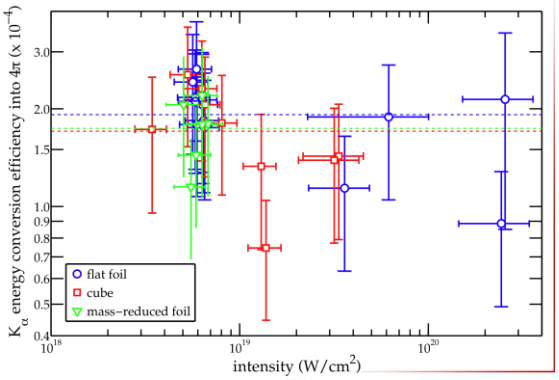

Experimental error bars are presently ~40-100%

Description of simulation used to predict experimental K_α yields measured by ZPW

- **Linear p-polarization, 45°** incidence (E_x and B_y laser fields with k_z)
- Peak |E| ~ 2.04e8 kV/cm
- Gaussian in space and time
- Energy ~ **104 J** and 50% energy within
  spatial FWHM ~ **7 μm**
  temporal FWHM ~ **470 fs**

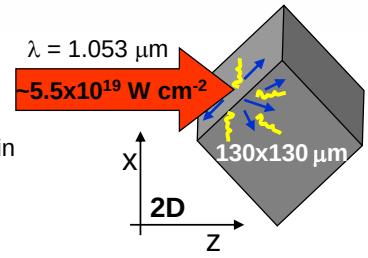

200x200 μm simulation box
Δt = 0.01 fs, 5e5 timesteps
open boundaries

Solid density Sn modeled as
e^- , Sn^{+1} (fixed <Z>)
ρ_{Sn}=7.3 g cm^{-3}
$n_e = n_i$ ~ 3.66e22 cm^{-3}

There are no free parameters in this simulation:

No ad-hoc injection of e^- beam. Actual laser parameters injected as fields, including some pre-pulse. The code has an opinion on laser absorption, e^- distribution, etc.

LSP code (Particle-In-Cell "PIC") treatment:

- fully electromagnetic, relativistic, and kinetic
- explicit particles and fields ($\omega_{pe}\Delta t < 1$, $\omega_{ce}\Delta t < 1$, $c\Delta t < \Delta z$)
- no implicit or fluid particles (needing an EOS)
- energy conserving push (not susceptible to λ_{De} instability)
- collisions included (Spitzer rates or binary model)
- cloud-in-cell interpolation model (reduces particle noise)
- double precision

K_α x-ray powers(t) , birth locations, and spectra are passively computed from e^- distributions and ITS electron impact σ_{ioniz} data (cold σs)

(… presently thinking about improvements, e.g. tracking multiple charge states, in-line atomic kinetics sub-routine, photon transport, etc. …)

Petawatt

LDRD LABORATORY DIRECTED RESEARCH & DEVELOPMENT

Sandia National Laboratories

Results of simulation to predict K_α yields measured by ZPW

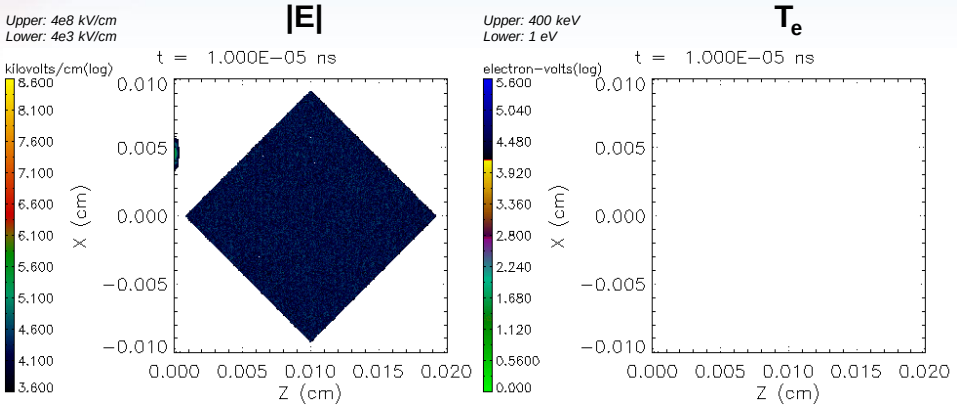

Log

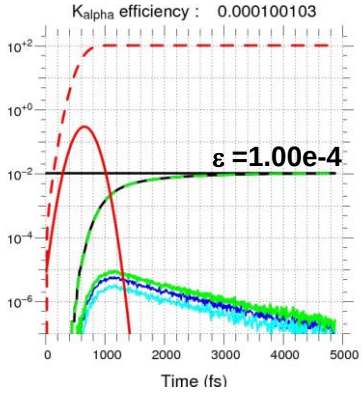

Linear (same plot)

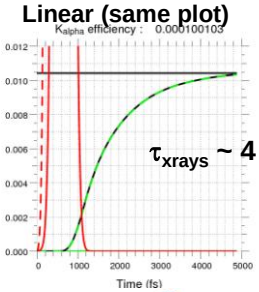

τ_{xrays} ~ 4 ps

Laser
$K_{\alpha 1}$
$K_{\alpha 2}$
$K_{\alpha(1+2)}$

Power (J fs^{-1})
Energy (J)

Petawatt

LDRD
LABORATORY DIRECTED RESEARCH & DEVELOPMENT

Sandia National Laboratories

Predictive capability for Z-Petawatt-driven K_α x-ray yields has been established

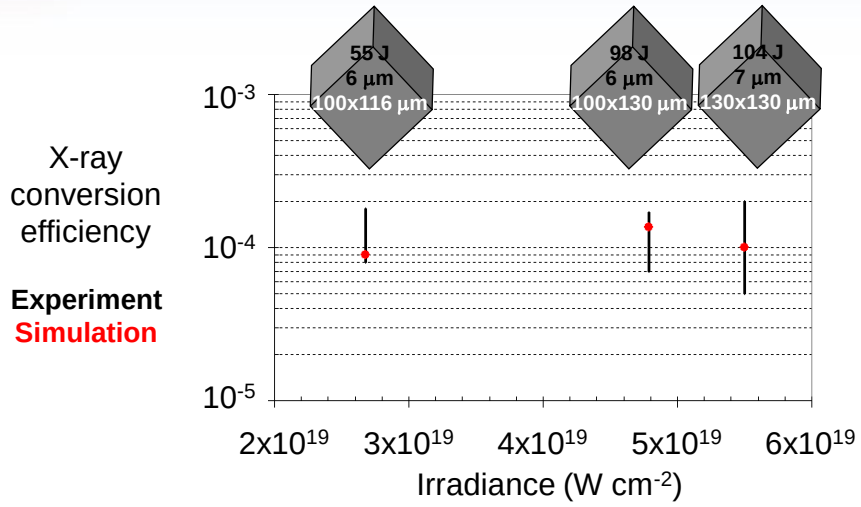

Having established a predictive capability for laser-driven K_α yield,

we now study novel target and imaging concepts aimed at *dramatically increasing* the production and collection efficiency in order to **enhance the quality** of our HEDP experiments on Z.

In ICF/HEDP x-ray imaging, "one can never have enough backlighter photons"

In the continuous quest to improve spatial resolution, it should be realized that the optical system must be fully illuminated (the brightest possible laser-produced x-ray source) and that the detector should be exquisitely sensitive

To this end, we envision three key components for advancing ps-scale, blur-free x-ray imaging for ICF/HEDP:

(1) **A novel K_α target concept with the highest possible conversion efficiency ε**
A target+imaging solution to achieve a factor of ≥10 improvement in ε might involve:
- a *large source size* (not limited to point-projection and small sources with low-ε)
- *shielding* of unwanted radiation from Z and ZPW between object and image planes

(2) **An optic with the highest possible collection efficiency**: we are developing a prototype 25 keV x-ray imager based on a spherically-curved, very-thin *Ge* (111) Bragg crystal in *transmission* mode.

The *transmission* approach, if it works, has 3 main advantages over 25-keV imaging in *reflection* mode:
[a] Almost 200x less monochromatic than equivalent device in *reflection* mode: better capture of a wide, ionization-broadened $K_{\alpha 1}$ line
[b] Very high spatial resolution (in principle): if the optic is sufficiently illuminated
[c] Works at 22-28 keV by slight Bragg angle change, w/o changing the crystal

(3) **A detector with highest sensitivity, dynamic range, and 1 ns gate times:**
Sandia is developing a solid state Multiframe Ultrafast Digital X-Ray Camera (MUDXC) based on CMOS7 microelectronics and *Si* pin diodes [G. R. Bennett et al, Rev. Sci. Instrum. **77,** 10E322 (2006).]

Full details of an alternate, ultrahigh spatial resolution 13-keV x-ray microscope have been published [G. R. Bennett et. al., Applied Optics, **40,** 25, 4570 (2001) & G. R. Bennett et. al., Applied Optics, **40,** 25, 4588 (2001).]

Petawatt

LDRD LABORATORY DIRECTED RESEARCH & DEVELOPMENT

Sandia National Laboratories

The ideal upper bound on K_α production efficiency per particle can be estimated

Given the stopping power, and e^- impact K_α ionization cross section (w/ relativistic enhancement), the *maximum* production efficiency can be estimated:

Stopping power

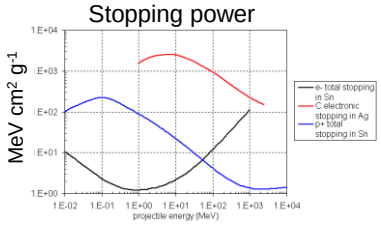

Range in *Sn* (μm)

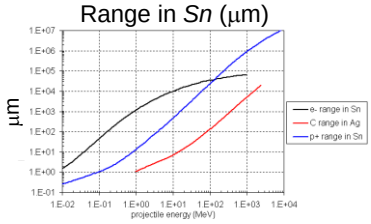

K_α^{mfp} (μm) ~ $(n_{Sn}*\sigma_{K\alpha}[E])^{-1}$

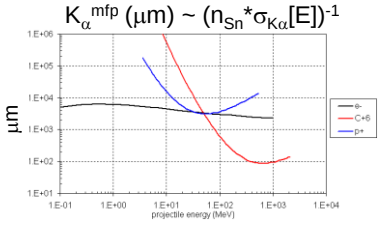

Range(E)/ K_α^{mfp}(E)

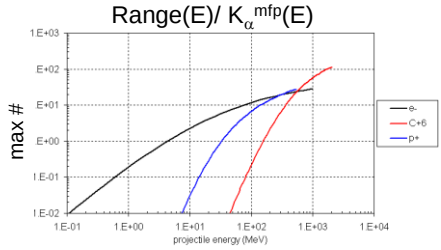

The max # of K_αs generated per particle, assuming no hydro expansion, no re-absorption, no other realistic effects, *and* complete ranging out

(requires refluxing for e^- or long target for ions)

{Range(E)/ K_α^{mfp}(E)} * {(0.025 MeV)/(projectile energy)}

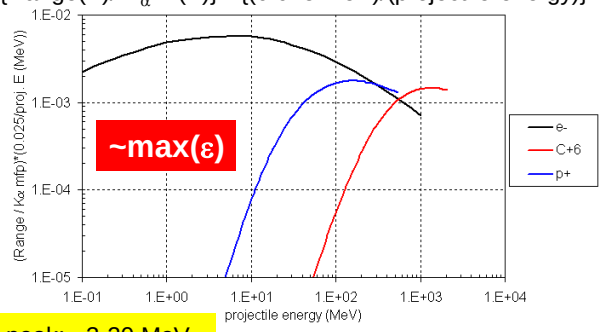

The broad e^- peak: ~3-20 MeV in a single particle sense
(Note: 10 MeV e^- → γ_e ~ 20)

Petawatt

LDRD LABORATORY DIRECTED RESEARCH & DEVELOPMENT

Sandia National Laboratories

The literature suggests an optimum T_e^{hot} exists for K_α production efficiency

Consider a simplistic toy problem (without laser):
Initialize *Sn* slab with one T_e and count K_α photons

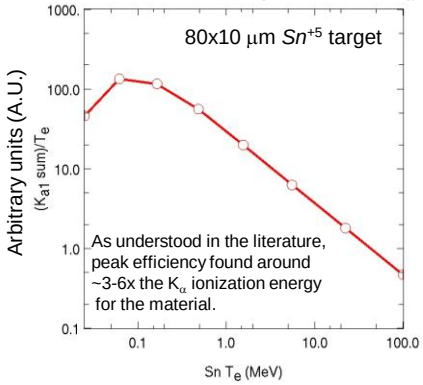

Given a target material and laser energy, K_α emission maximized for one foil volume and one hot T_e. [Salzmann, et. al., Phys. Rev. E **65**, 036402 (2002).]

"TOO HOT" : Too much energy lost to bulk particles and motion. Increasing cold *T* shifts and broadens K_α features, and energy-integrated emission rate can decrease.

"TOO COLD" : Not enough hot e^- to ionize K shell.

"JUST RIGHT" : Balances effects of actual two-temp EEDF.

One would prefer to increase efficiency into *just* the effective hot electron K_α producers

The "BOA" mechanism efficiently generates mostly relativistic e^-s, unlike regular TNSA or K_α generation in MRTs or FFs:

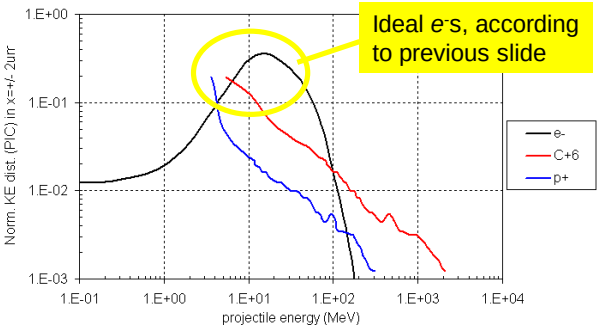

Two paths to seek increased efficiency (not mutually exclusive): (1) multiple small targets optimally heated by one laser pulse, and/or (2) generation of "better" two-temperature EEDF within target

Petawatt

LDRD LABORATORY DIRECTED RESEARCH & DEVELOPMENT

Sandia National Laboratories

Two-stage concept using "BOA" beams may couple more energy into hot electrons for larger K_α yield

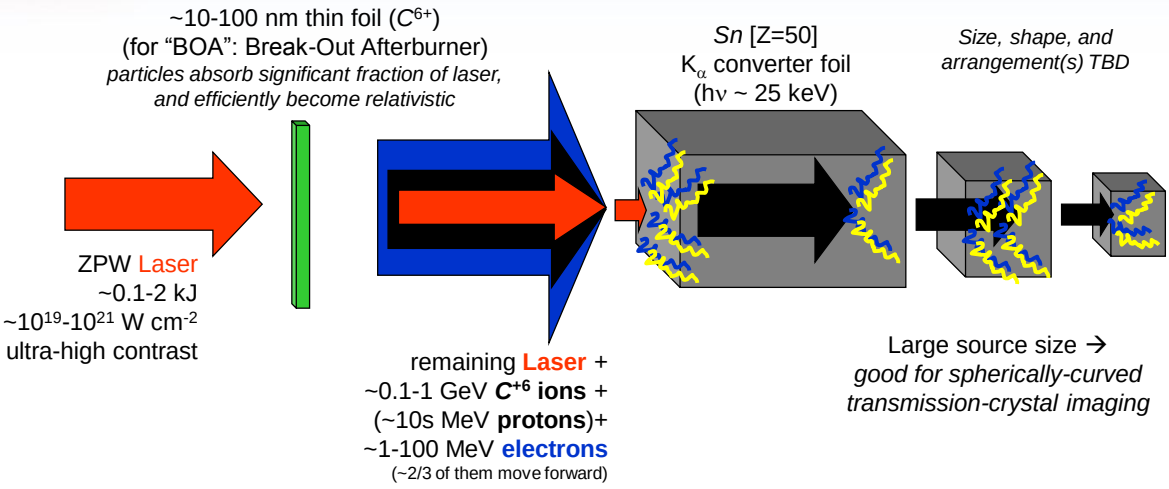

1) **Ion beam** energy deposition heats **electrons** in **target** deeper than **laser**
2) Creates two-temperature **electron** distribution in **target** (traps relativistic e^- **cloud**)
3) Imaging concept based on spherically-curved Bragg transmission crystals may provide good spatial resolution even with large source lengths (100 μm to ~few mm)

(but ~10s um lateral dimension for high transmission)

We seek to exploit all three as favorable properties for enhancing K_α yield by heating as much material as possible to ideal T_e

Petawatt

LDRD LABORATORY DIRECTED RESEARCH & DEVELOPMENT

Sandia National Laboratories

Description of simulation used to study novel target concepts for increasing K_α yields

First, we reproduced original LANL 2D VPIC results on BOA:
L. Yin, et al., Laser Part. Beams **24,** 291 (2006).
(Also, recall Tuesday evening Plenary talk by L. Yin [LANL])

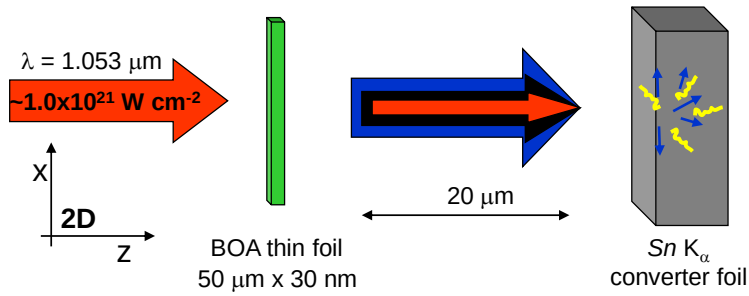

BOA thin foil
50 μm x 30 nm

Sn K_α converter foil
80x10 μm

Solid density **C** modeled as
e^- , C^{6+} ($n_e/n_{critical}$ = 660)
ρ_C=2.47 g cm^{-3}
$n_e = 6*n_i$ ~ 7.38e23 cm^{-3}

Solid density **Sn** modeled as
e^- , Sn^{+5} (fixed <Z>)
ρ_{Sn}=7.3 g cm^{-3}
$n_e = 5*n_i$ ~ 1.83e23 cm^{-3}

- **Linear s-polarization, 0º** incidence (E_x and B_y laser fields with k_z)
- Peak |E| ~ 8.88e8 kV/cm
- Gaussian in space and time
- Power ~ 1 PW
- Energy ~ **2575 J**
  spatial FWHM ~ **8 μm**
  temporal FWHM ~ **300 fs**

80x45 μm simulation box
Δt = 0.01 fs, >1e5 timesteps
open boundaries

Initial work is promising for the two stage concept to improve K_α yield and overall efficiency

This initial (suboptimal) simulation of novel PW-driven target concept demonstrates (1) beam transport, (2) refluxing of ultrarelativistic BOA electrons, and (3) significant K_α yield

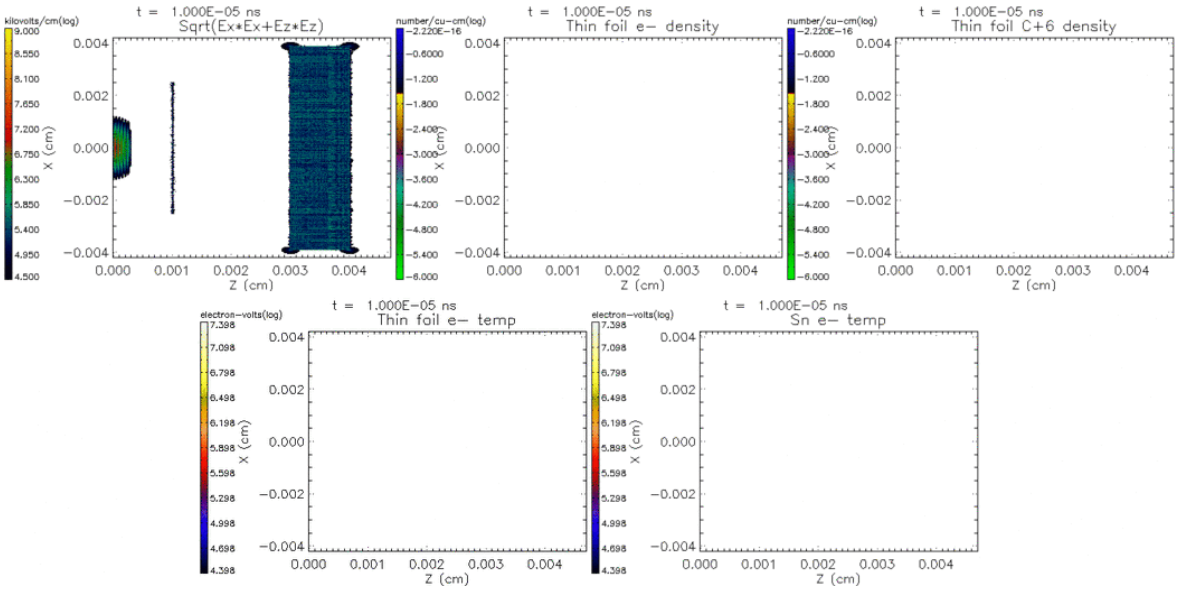

All plots on $\log_{10}$ scale,
density plots normalized to respective Sn species,
and temp. plot range: [25 keV, 25 MeV]

Thin nanometer-scale targets have been acquired and characterized for initial experiments

Acquired large-area ultrathin carbon films of 8, 17, & 38 nm
+/- 30% thinness, assuming 2.255 g/cc

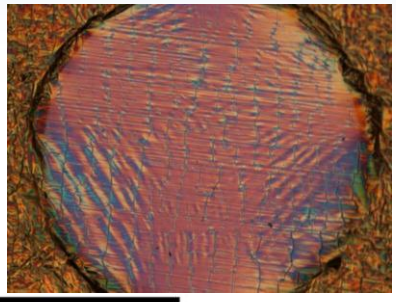

Diffraction-limited focus of ZPW (~10 μm) contains ~300-700 nm ripples.

Looking into small-area, free-standing ultrathin diamond targets

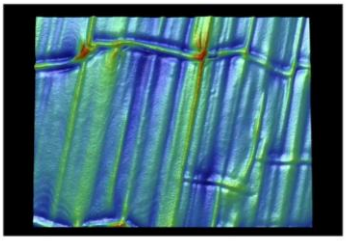

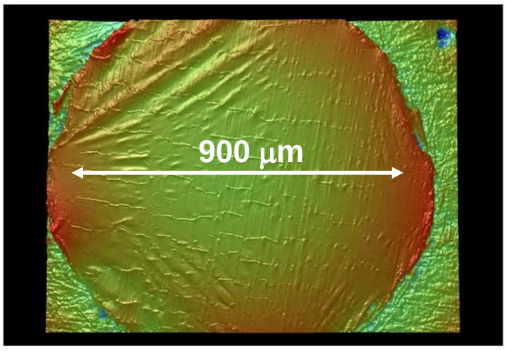

Analytic estimates and hydro sims (discussed next) indicate prepulse < ~10^9 W cm^{-2} for ~t > -100 ps
(or a 30 nm *C* target would prematurely melt and expand)

→ **plasma mirrors required … *in development***
→ **hydro sims capable of evaluating measured prepulse(t)**

Petawatt

LDRD LABORATORY DIRECTED RESEARCH & DEVELOPMENT

Sandia National Laboratories

How good does the prepulse contrast have to be so the ultra-thin nm foils survive until the main pulse?

Old contrast measurement:
Is such a pre-pulse good enough to maintain
Δz ~ 30 nm target integrity? (for 10^0 ~ 10^{21} W cm^{-2})

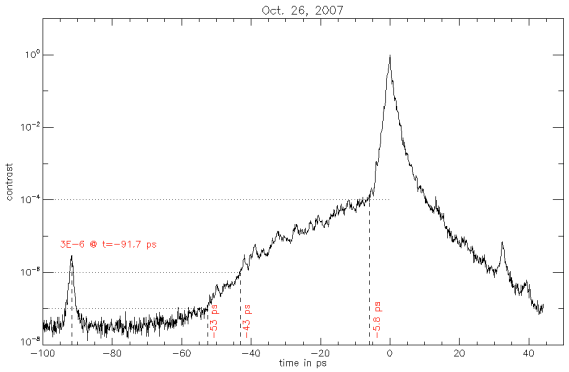

P_{laser}[Mbar] ~ 40 (I_{laser} [1e15 Wcm^{-2}]/ λ_{laser} [μm])$^{2/3}$
(Eqn 5.6 in Lindl's ICF book, direct-drive approx.)

C_s [nm/ps] ~ 10*Sqrt(γ P_{laser}[Mbar]/ρ [g cm^{-3}])

t_{hydro} [ps] ~ Δz [nm]/ C_s

For Δz = 30 nm and ρ ~ 2.255 g cm^{-3},

I_{laser} = 1e12 W cm^{-2} gives t_{hydro} ~ 5.52 ps
I_{laser} = 1e11 W cm^{-2} gives t_{hydro} ~ 11.9 ps
I_{laser} = 1e10 W cm^{-2} gives t_{hydro} ~ 25.3 ps
I_{laser} = 1e9 W cm^{-2} gives t_{hydro} ~ 55.2 ps

(P_{laser} range from 400 to 4 kbar)

Plasma mirrors are essential for BOA experiments involving ultra-thin nm foils

I_{laser} = **C***1e21 W cm^{-2}, where **C** = 1e-9, 1e-10, 1e-11, 1e-12
(I_{laser} [W cm^{-2}] = 1e12, 1e11, 1e10, 1e9)

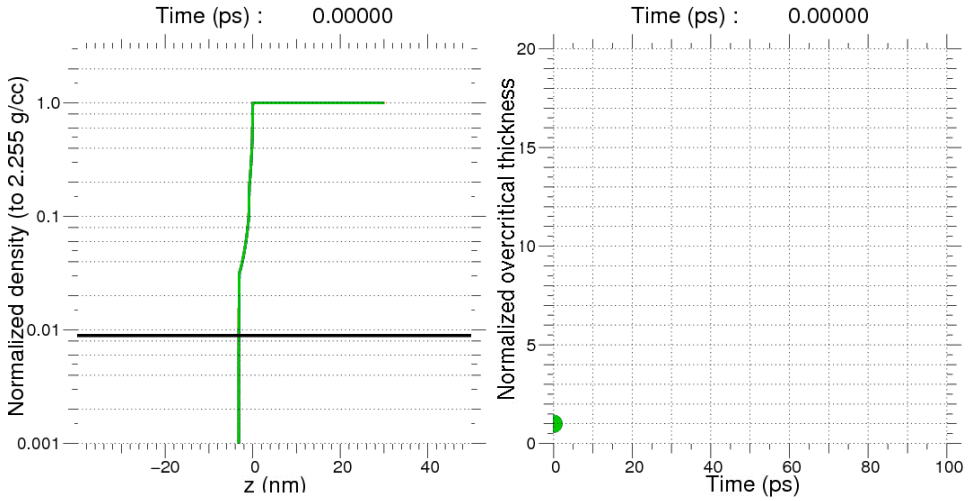

t_{hydro} ~ 5.52 ps
t_{hydro} ~ 11.9 ps
t_{hydro} ~ 25.3 ps
t_{hydro} ~ 55.2 ps

This capability has been established in order to simulate arbitrary laser intensity profiles, so future measurements of laser contrast can provide feedback to simulations

Petawatt

LDRD LABORATORY DIRECTED RESEARCH & DEVELOPMENT

Sandia National Laboratories

HYDRA is also used to evaluate the dynamics of the prepulse-generated pre-plasma

1D HYDRA: *Evolution of preplasma creation and hydro under influence of prepulse*
10 nm contaminant layer on ~25 um slab of Cu

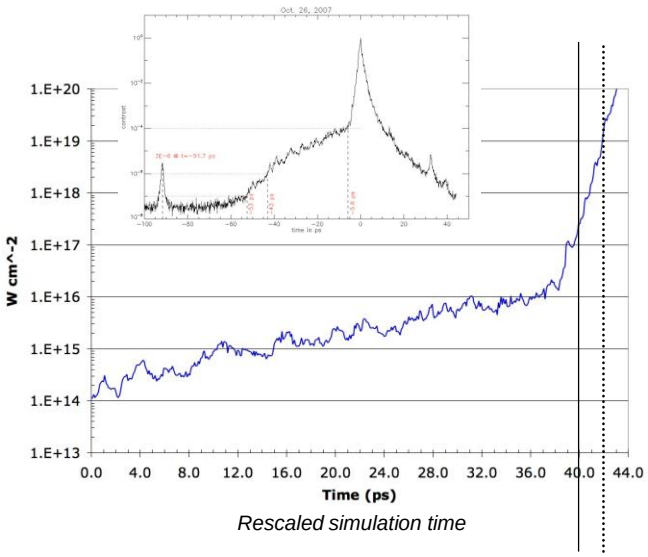

Rescaled simulation time

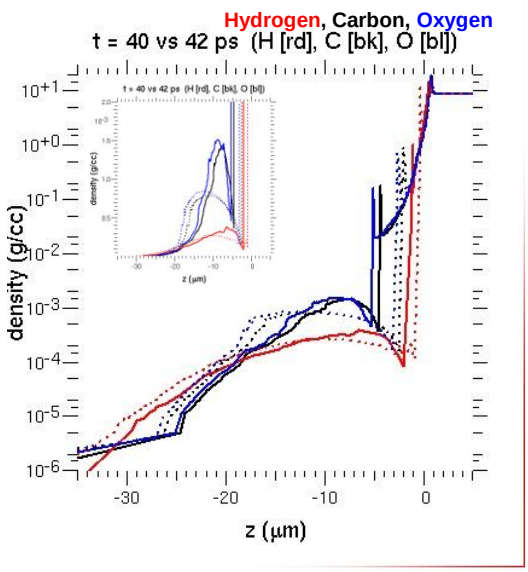

The Z-Backlighter Facility laser group (Org. 1672) has more target ideas that can also be simulated

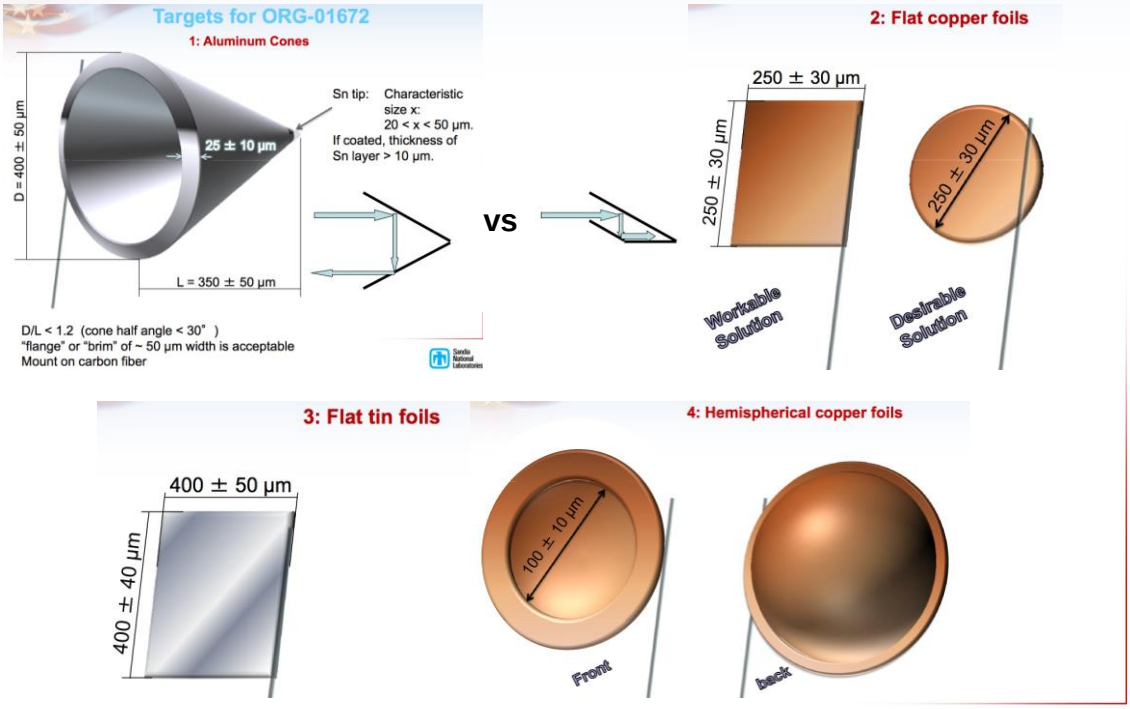

Petawatt

LDRD LABORATORY DIRECTED RESEARCH & DEVELOPMENT

Sandia National Laboratories

Simple, ideal simulations of injected e^- beams predict the estimated efficiency enhancement is real

Sn [Z=50]
K_α converter foil
($h\nu$ ~ 25 keV)

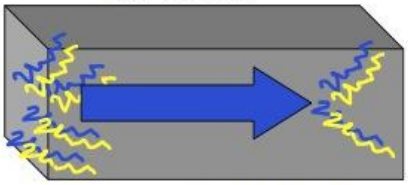

Range in *Sn* (μm)

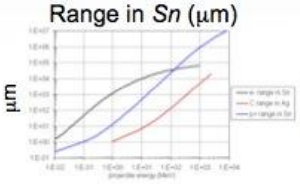

Range(E)/ K_α^{mfp}(E)

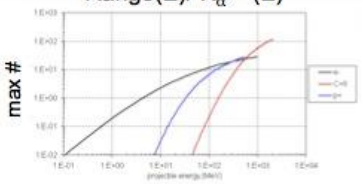

10 MeV e^- range: 10 mm. Since v_e~c, Δt_{xrays} ~ 33.33 ps
e^- beam slows to 1 MeV by 9th mm (90%)
also 90% of K_α contribution (range/mfp) from 10 to 1 MeV

Monoenergetic electron beam injection:
constant 10 MeV ($\gamma\beta$~20.55) for Δt = 1 ps is 1 kJ
for P = (100 MA)(10 MeV) =1 PW, n_{hot}/n_{cold} ~ 5e-3
(assumed from ~2 kJ, ~2 PW **Laser** striking BOA foil)
(neglects heating from leftover laser and ~6 MeV-2 GeV C^{+6} **ions** and ~3-300 MeV **protons**)

K_α x-ray power increases ~t until ~1 ps, then stays constant for t > 1 ps.

Total K_α x-ray energy increases ~t^2 until ~1 ps, then increases ~t for t > 1 ps.

Efficiency ε enhancement (*relative to typical 0.5-1.0e-4*):
ε reaches 1.0e-4 by t ~ 1.6 ps (~0.5 mm) (ε up ~1-2x)
ε reaches 6.8e-4 by t ~ 6.7 ps (~2.0 mm) (ε up ~7-14x)
ε reaches 3.4e-3 by t ~ 33 ps (~10 mm) (ε up ~34-68x)

Δt_{xrays} ~ 33 ps allows a 100 km/s ICF target to move 3.3 μm (typical resolution ~15 μm)

To-do list:
#1: Need to include **p^+ and C^{+6} beam** depositions
(heating of **electrons** in target deeper than **laser**)
#2: Need to include heating near surface from leftover **laser** energy
#3: Need to *design and evaluate* integrated two-stage target concepts

Z Petawatt

LDRD LABORATORY DIRECTED RESEARCH & DEVELOPMENT

Sandia National Laboratories

Summary

Predictive capability has been established for ZPW-driven K_α production in *Sn* targets, providing confidence in our ability to predict x-ray yields in other novel target arrangements
- Studies ongoing, investigating role of preplasma, model improvements in development

Novel target idea relies on "BOA"-produced beams to effectively heat larger source(s)
- Reproduced underlying BOA physics originally published in 2D by LANL
- Numerical and analytical estimates: plasma mirrors essential (development underway)

Experimental and numerical investigation of high-ε targets and imaging are promising and ongoing
- If successful, the idea is applicable to blur-free imaging of user-chosen K_α energies

(Not discussed) Experimental prototype investigations ongoing of novel x-ray imager and MUDXC

LANL and others are interested in collaborations (BOA in thin foils, K_α production and measurement, simulations, etc.)

Novel high-efficiency targets, a high-collection imager, and a multiframe ultrafast digital x-ray camera may offer the most advanced high-energy x-ray radiography to Z

Quality improvements in high-energy (~10-80 keV) x-ray imaging, whether from traditional or novel sources, **are directly beneficial to HEDP platforms such as Z and NIF.**

Petawatt

LDRD LABORATORY DIRECTED RESEARCH & DEVELOPMENT

Sandia National Laboratories

APPENDIX B:

NOVEL(?) HIGH-COLLECTION-EFFICIENCY HIGH-SPATIAL-RESOLUTION 25.2713-KEV X-RAY IMAGER CONCEPT

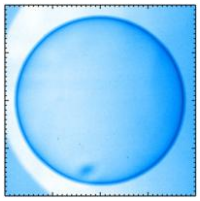

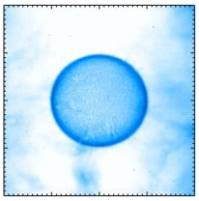

Successful ICF/HEDP x-ray imaging requires four key components

[1] The highest possible conversion efficiency of laser light into the x-ray energy of interest. Hence the Bennett/Sefkow LDRD

[2] An optic with the highest possible collection efficiency. Predicted high spatial resolution is useless unless the system S/N is very high

[3] An exquisitely sensitive time-gated image-plane detector; with high dynamic range

[4] Full use of state-of-the-art image processing for, say, pattern recognition of features expected in MRT growth of a Z100 target. Work with Division 5000 and, say, Goddard Space Flight Center

Note; in the ICF/HEDP field there are never, never enough backlighter photons

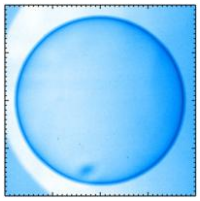

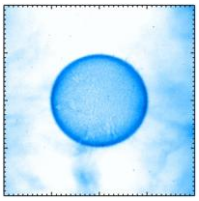

Towards ZPW-driven 25-keV x-ray imaging on Z

2-Frame, 6.151-keV ZBL-driven x-ray imaging is well-established on Z

01672 is investigating a variety of methods to improve the S/N, S/B, etc. for this important diagnostic

We are also investigating both [1] a point-projection imaging, and [2] an object-plane-to-image-plane solution for ZPW-driven 25-keV x-radiography on Z

This presentation pertains to [2]

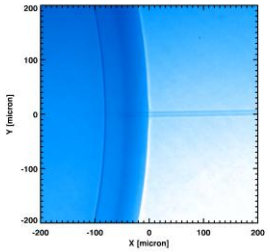

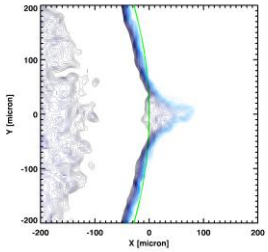

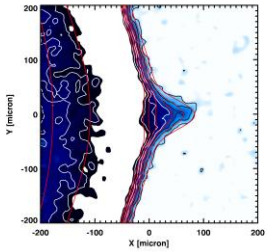

Above example data published in **PRL** (G. R. Bennett, M. C. Herrmann *et al)*

25-keV x-ray imager

We have developed a prototype 25-keV x-ray imager that uses a curved Bragg crystal, Si(111), in transmission rather than reflection

The *transmission* approach, if it works, has 3 main advantages over 25-keV imaging in *reflection* mode:

[1] Device is 287x less monochromatic than 6.151-keV system, allowing for much better capture of a wide, ionization-broadened $K_{\alpha 1}$ line

[2] Neglecting fabrication errors, crystal rocking curve, etc.; excellent spatial resolution

[3] Our 25-keV prototype can also work at 22- to 28-keV; without the need to change the crystal. This is quite unlike the *reflection* mode

Compared to 25-keV point-projection imaging, the imager should yield a significantly higher rejection of Z- and ZPW-generated Bremsstrahlung and other unwanted x-rays

Simple schematic extracted from Zemax

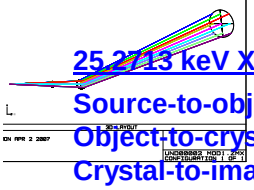

25.2713 keV X-RAY MICROSCOPE SCHEMATIC

Source-to-object: 223.591 mm
Object-to-crystal: 150.000 mm
Crystal-to-image: 749.463 mm
Bragg angle: 4.48707078°

100-micron Si(111) Bragg crystal curved over a transmissive support substrate

4.996x image plane showing nine chief rays of nine object points

200-μm-diam, 25.2713-keV source

10.24 x 10.24 mm^2 object field

Operation at 22.16292-keV would only require a Bragg angle change to 5.1179683°

Bragg diffraction: a quick review

X-rays irradiating an atom move electrons, which re-radiate em radiation with the same wavelength: Rayleigh Scattering (elastic scattering)

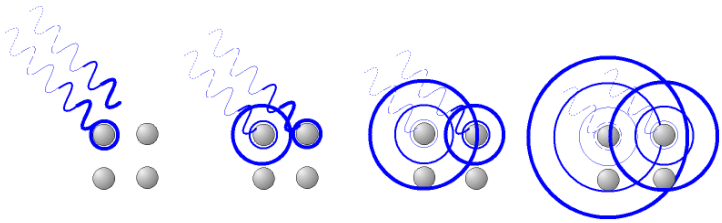

Constructive interference occurs when the Bragg law is satisfied….

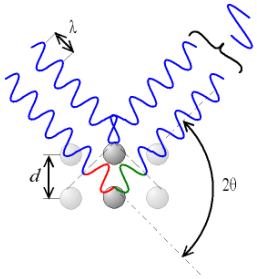

$n\lambda = 2d\sin\theta_B$

where *d* is the spacing between the planes of the atomic lattice

Bragg diffraction: a quick review

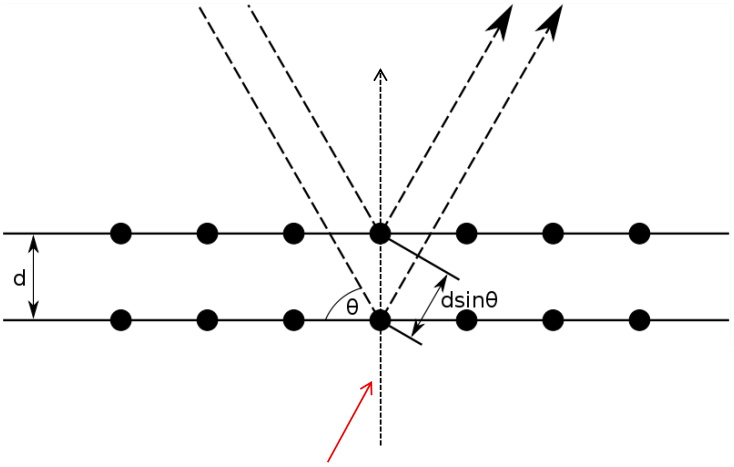

Note; if the crystal is rotated about this axis, Bragg diffraction will still occur

A special case of Bragg diffraction, namely *Laue diffraction in reflection*

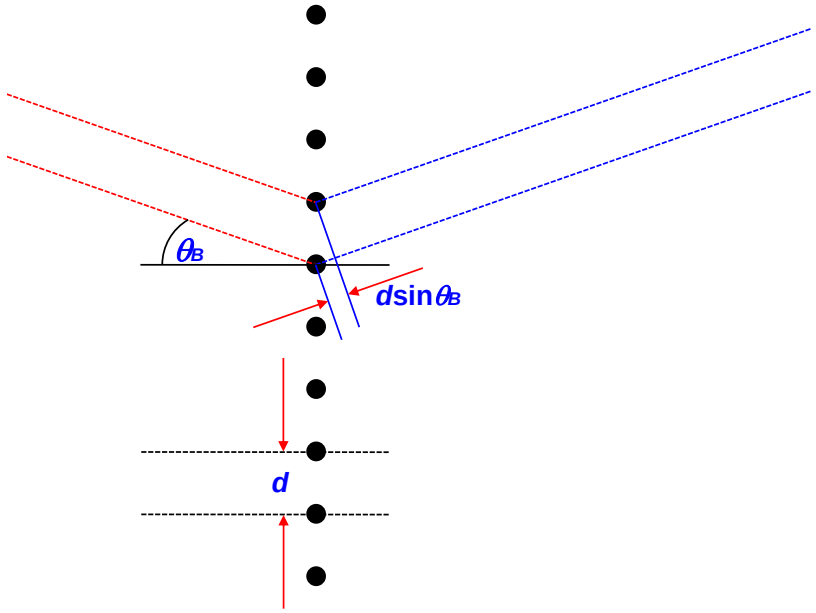

Bragg diffraction: a quick review

A special case of Bragg diffraction, namely *Laue diffraction in reflection*

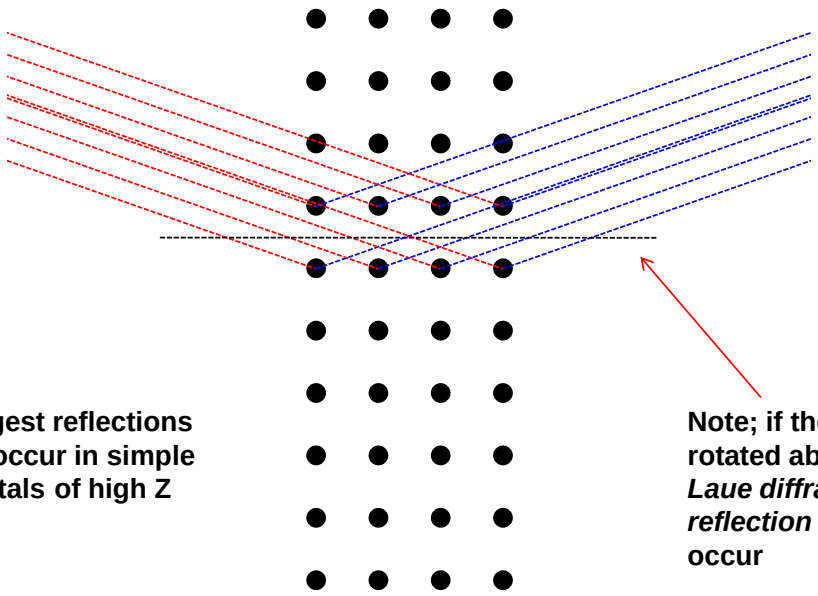

The strongest reflections generally occur in simple cubic crystals of high Z and (111)

Note; if the crystal is rotated about this axis, *Laue diffraction in reflection* will still occur

6.151-keV imaging (*reflection*): A reminder

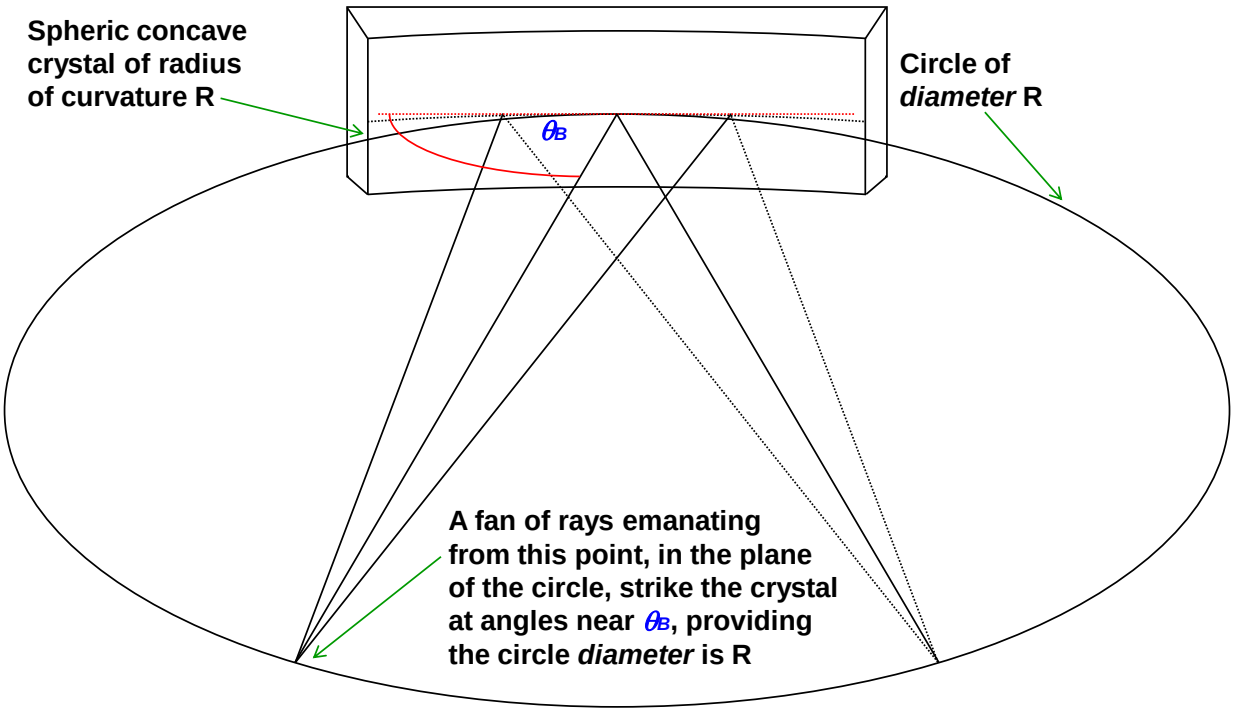

6.151-keV imaging (*reflection*): A reminder

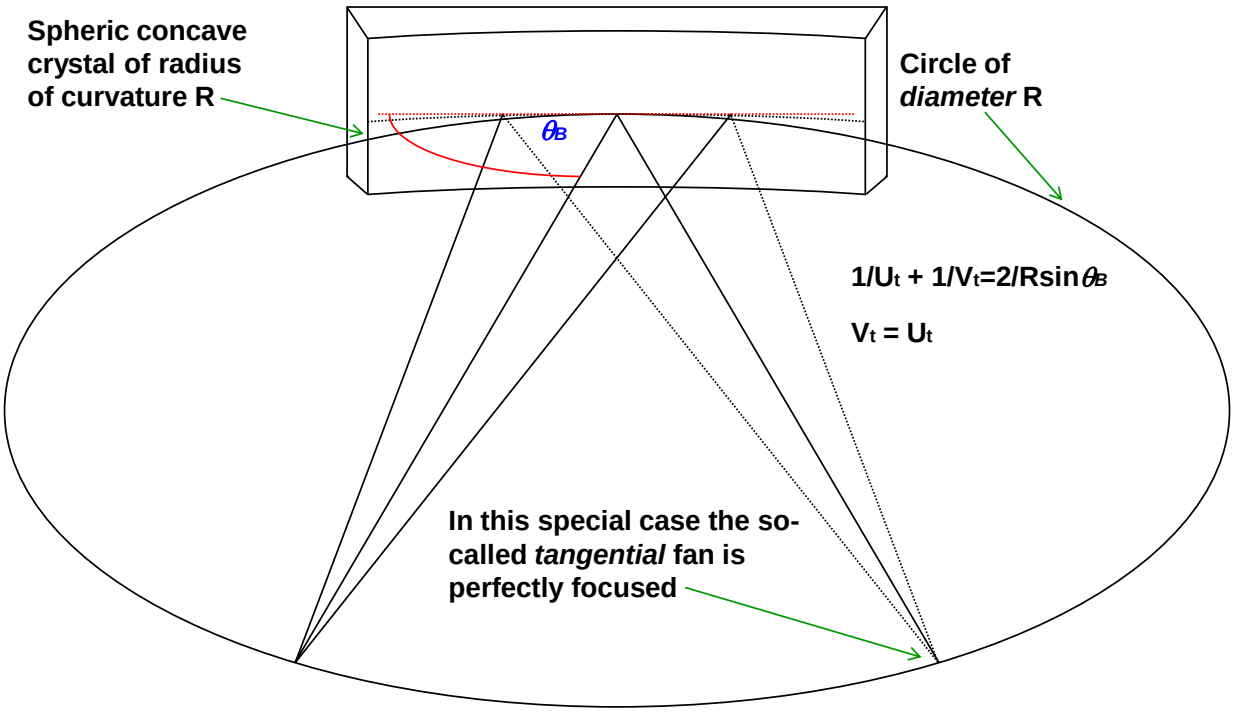

6.151-keV imaging (*reflection*): A reminder

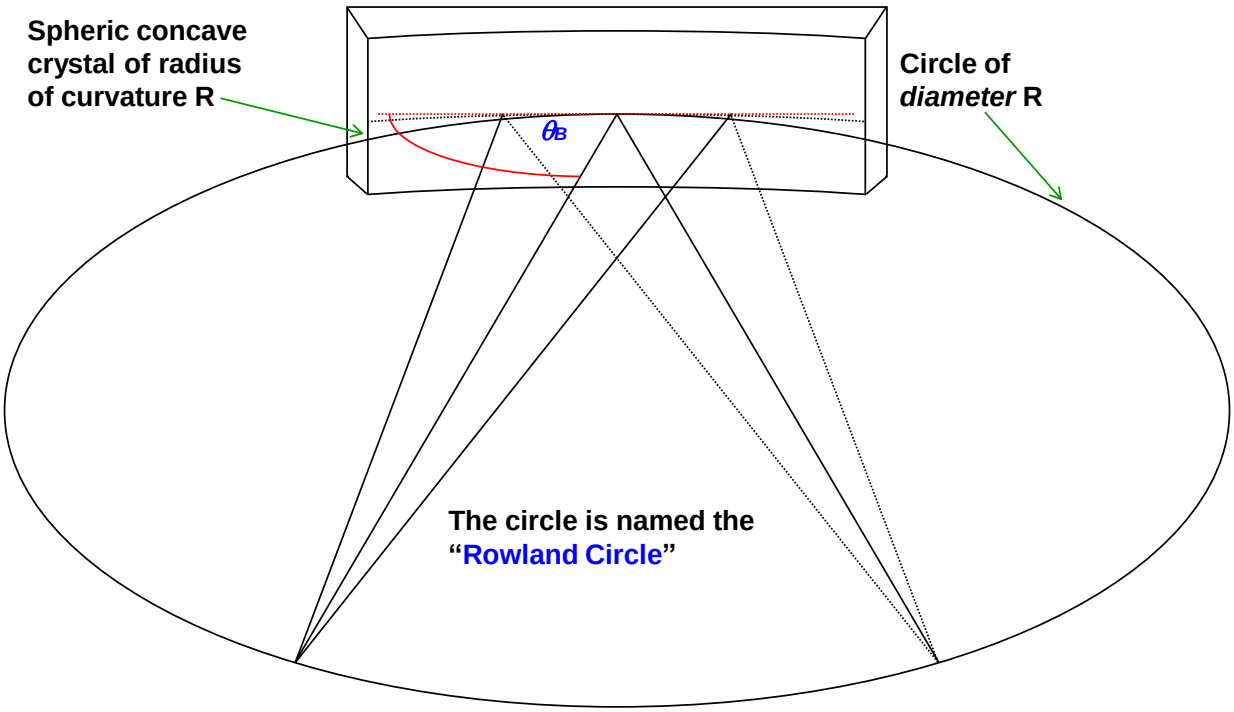

6.151-keV imaging (*reflection*): A reminder

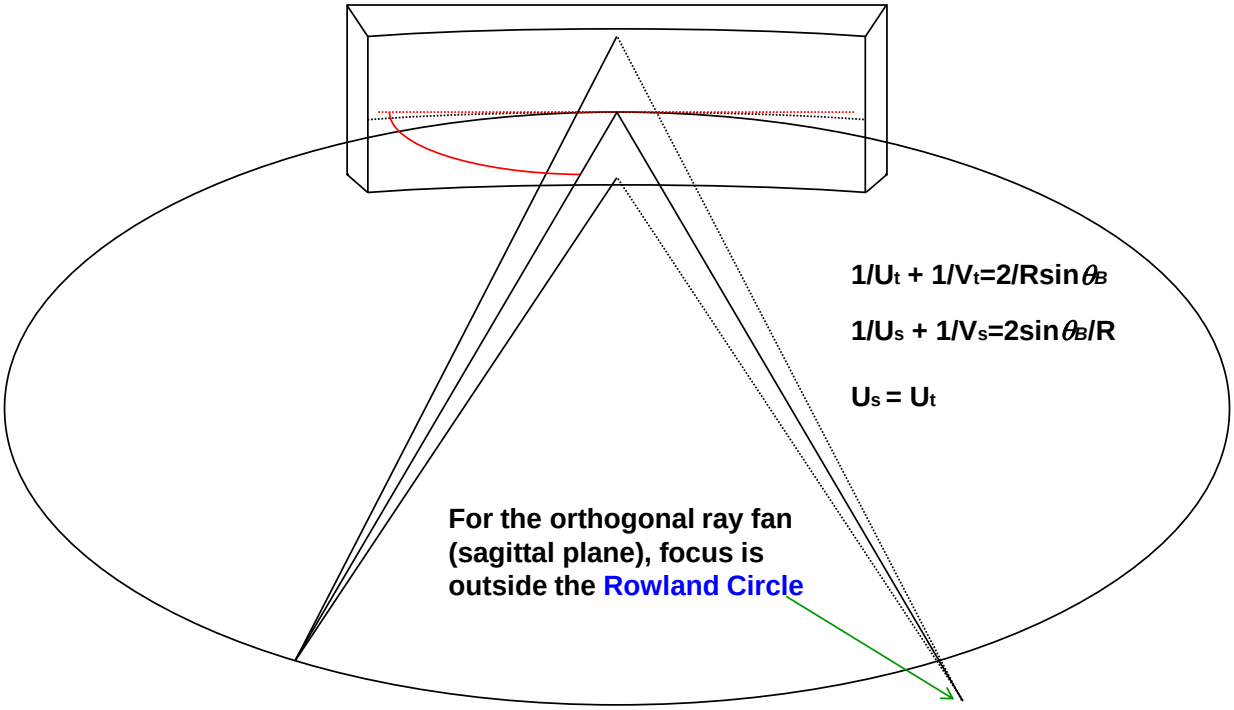

6.151-keV imaging (*reflection*): A reminder

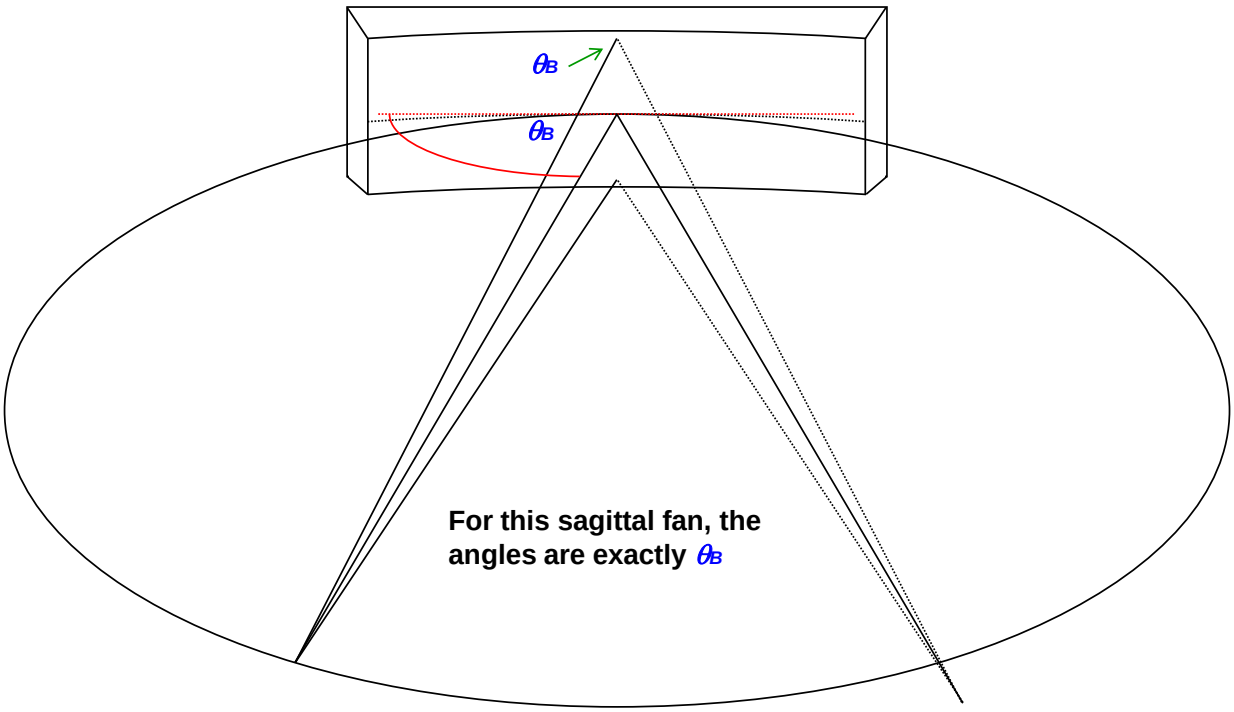

6.151-keV imaging (*reflection*): A reminder

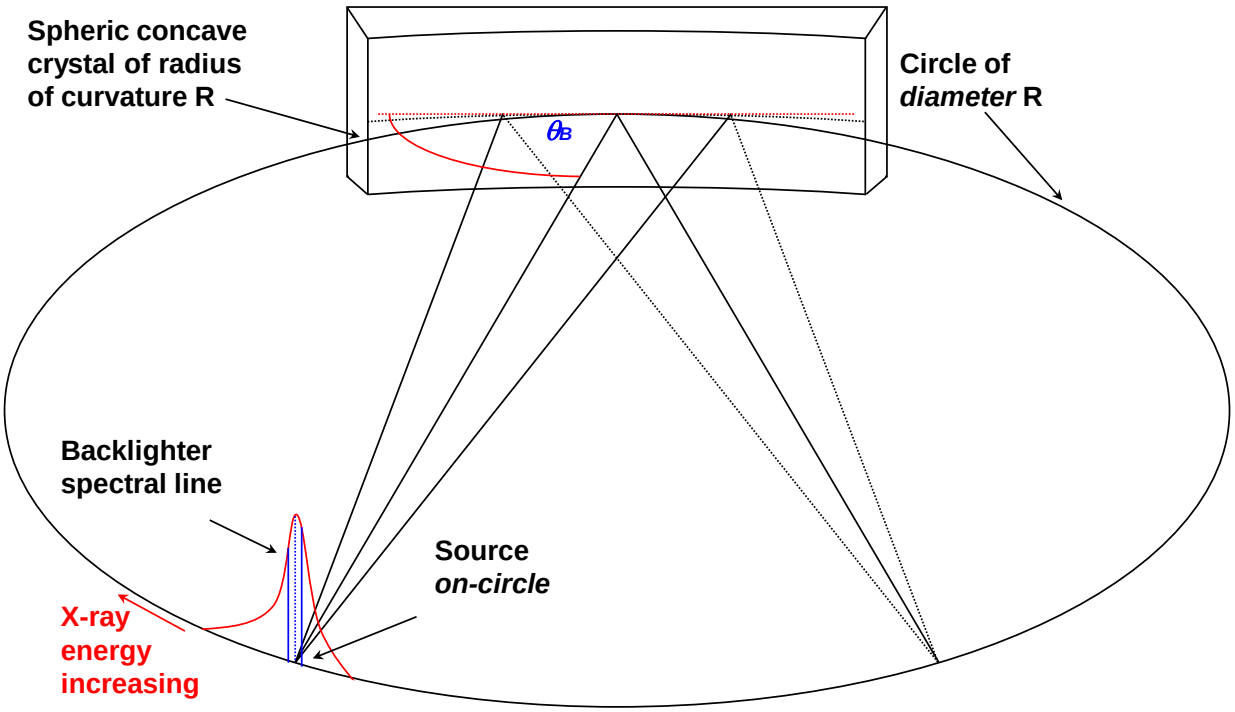

6.151-keV imaging (*reflection*): A reminder

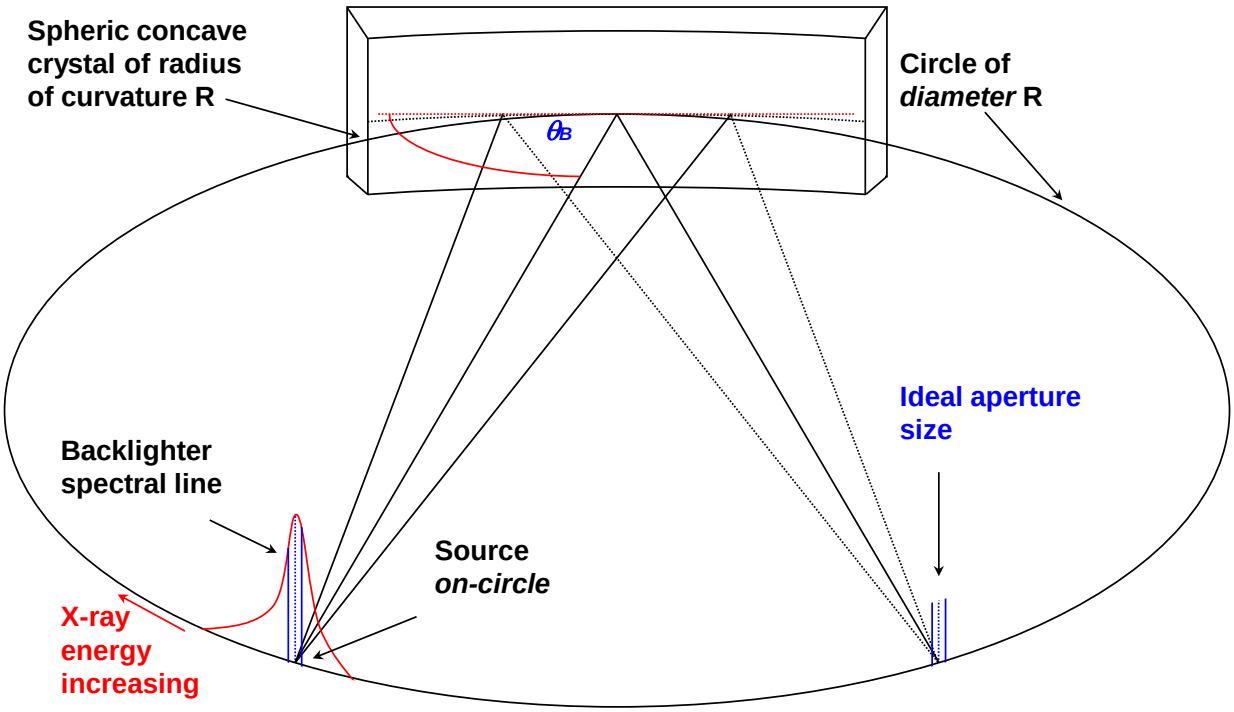

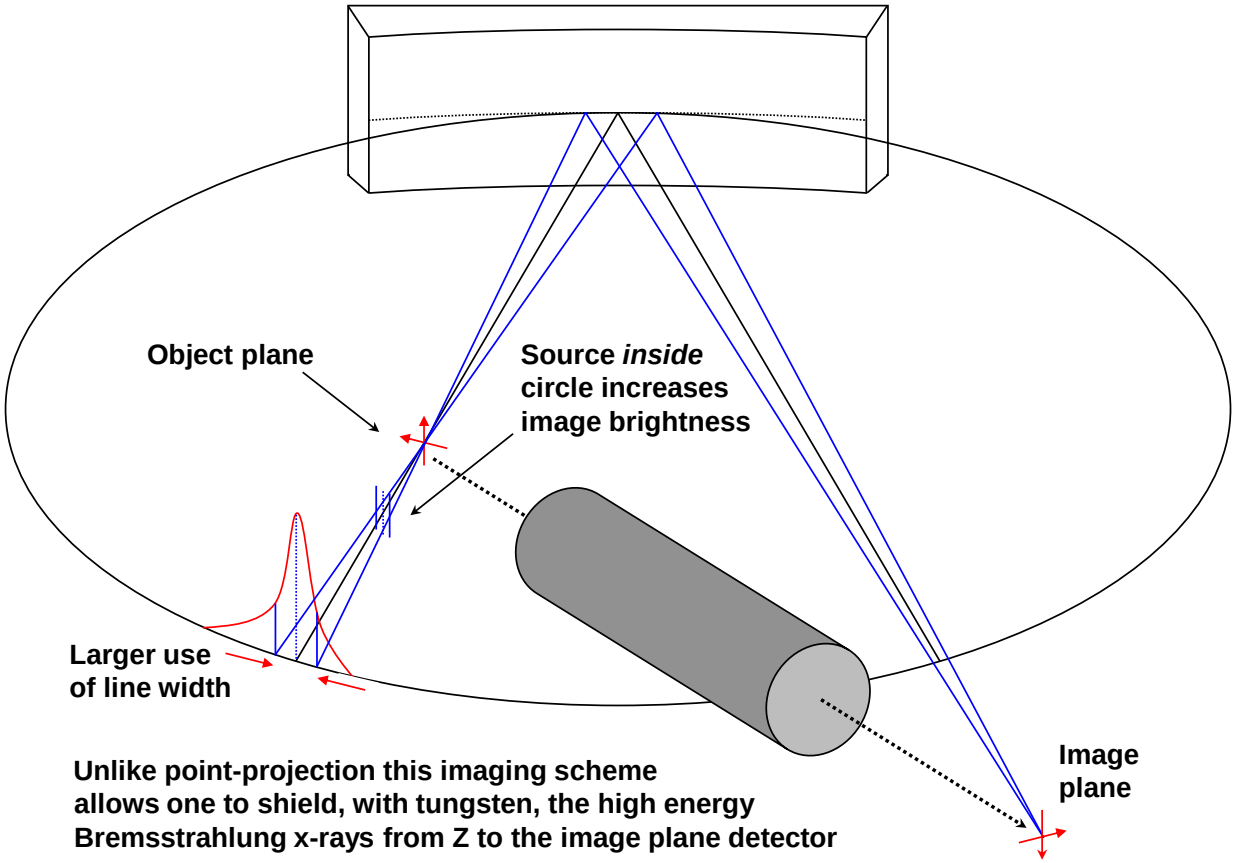

Unlike point-projection this imaging scheme allows one to shield, with tungsten, the high energy Bremsstrahlung x-rays from Z to the image plane detector

Source inside circle increases brightness but narrow FOV obtained, as evident here.

May have solution to overcome this limitation

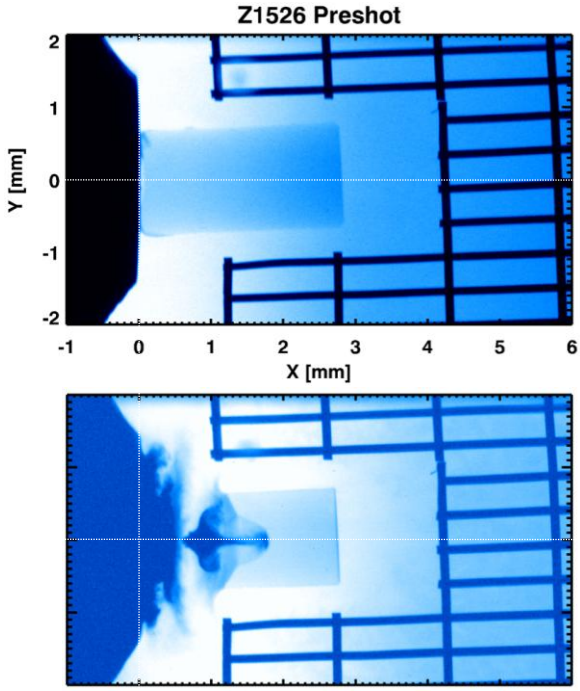

Z1526 pre-shot and down-line images overlaid

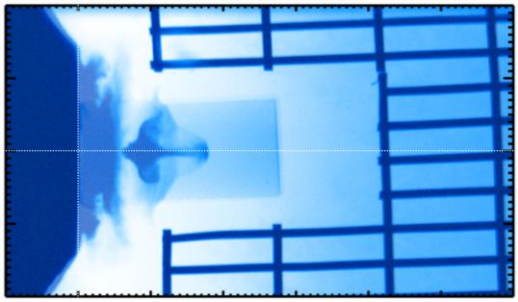

25-keV imaging in reflection is difficult

Given the Bragg condition, $n\lambda=2d\sin\theta_B$, and the desire to image at energies >>6.151-keV in reflection mode and at a small off-axis angle (low astigmatism), there are 3 options:

[1] Keep n=1 but search for a crystal 2d spacing <<2 Angstrom. No such crystal!

[2] Use n>>1 and retain a favorably large θ_B. Poor reflectivity!

[3] Retain n=1 but reduce θ_B. This requires a toroidally-curved optic to correct the now severe astigmatism. The resulting image unfortunately reveals a strongly field-dependent magnification

Possible 22.16292-keV toroidally-curved-crystal imaging system backlit by ZPW-generated 50-μm x-ray source

---

To the same spatial scale, object and image plane of a 4-mm x 4-mm grid. Note the strong field-dependent magnification

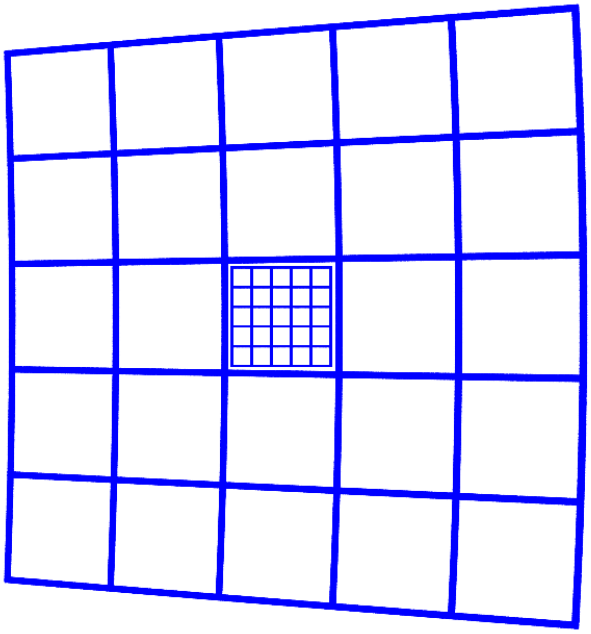

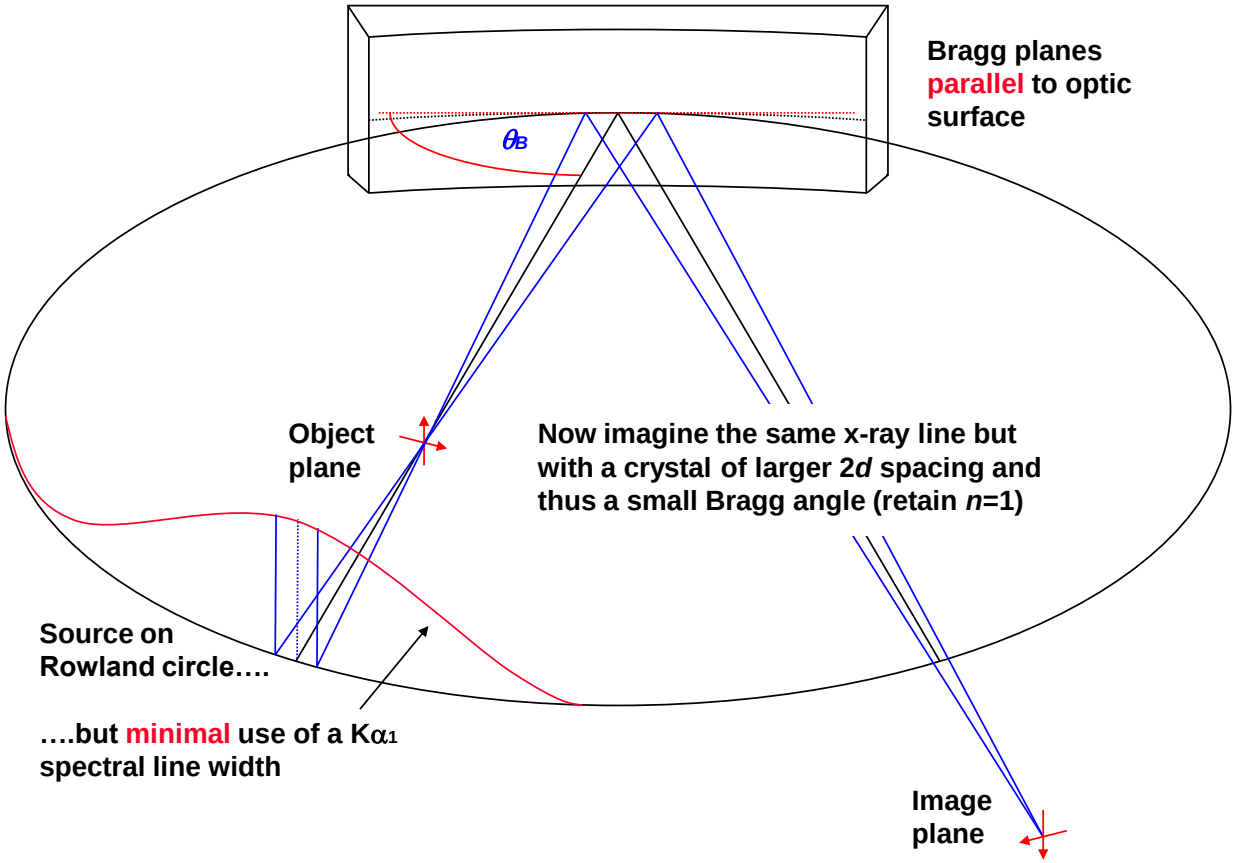
Bragg planes
parallel to optic
surface
θ_B
Object
plane
Now imagine the same x-ray line but
with a crystal of larger 2*d* spacing and
thus a small Bragg angle (retain *n*=1)
Source on
Rowland circle….
….but minimal use of a Kα1
spectral line width
Image
plane

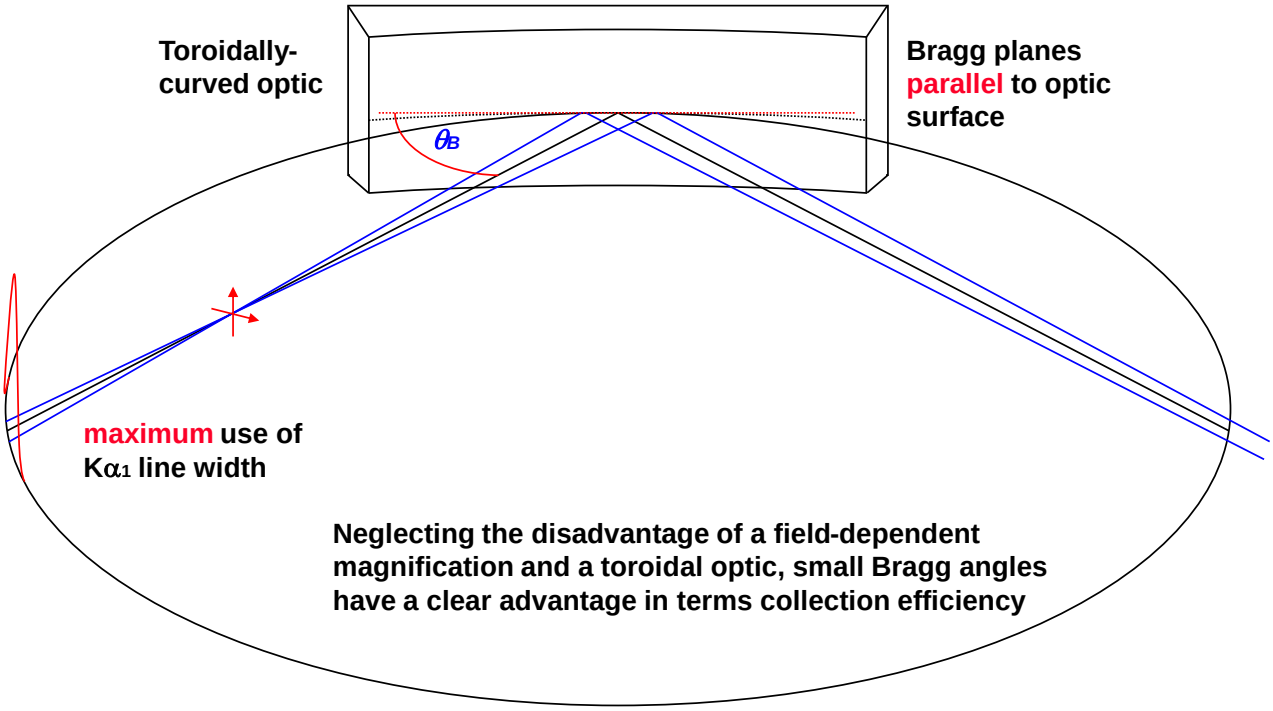

Neglecting the disadvantage of a field-dependent magnification and a toroidal optic, small Bragg angles have a clear advantage in terms collection efficiency

Is there some configuration where a small Bragg angle, for *line compression*, can be utilized near on-axis? Yes!

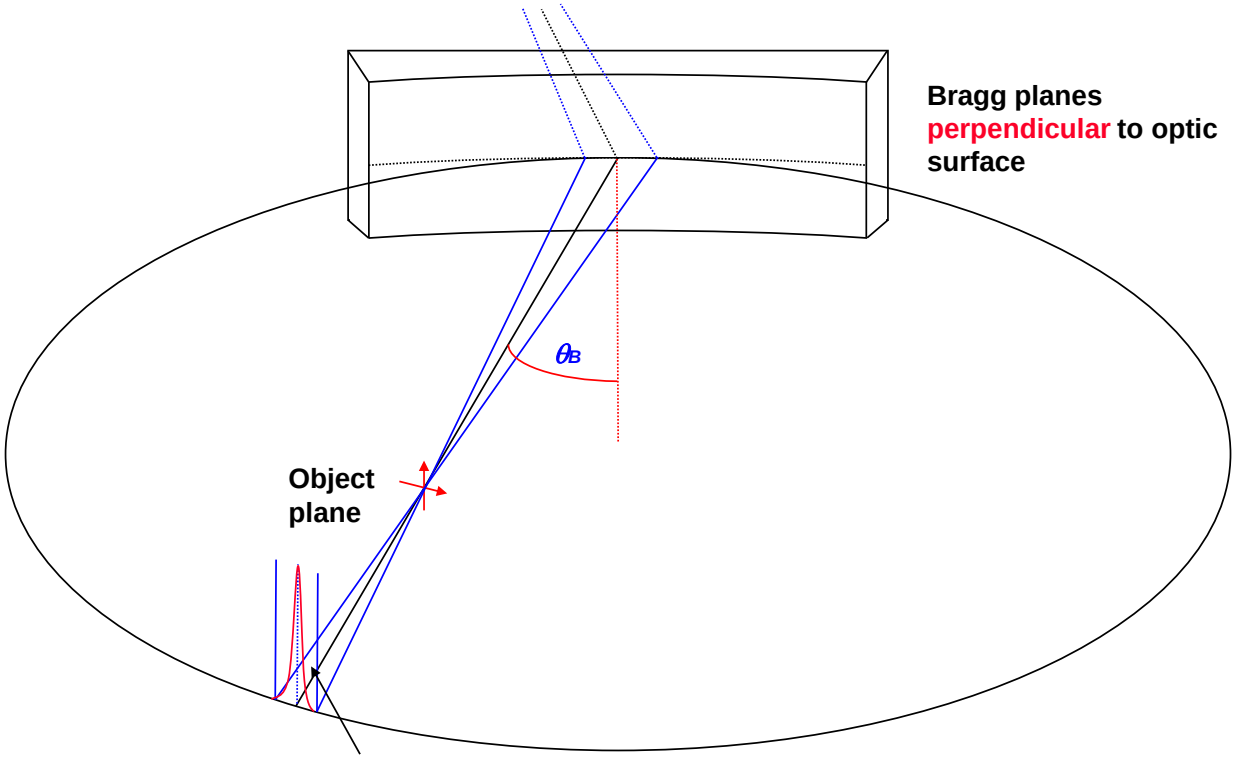

Maximum use of 25.2713 keV spectral line width at n=1

Our prototype 25-keV imager uses *Laue diffraction in reflection*, and thus *line compression*, over a spherical concave surface to (theoretically) achieve high quality imaging

For a spherical concave mirror of radius R with a point source placed at R/2, a collimated beam is formed

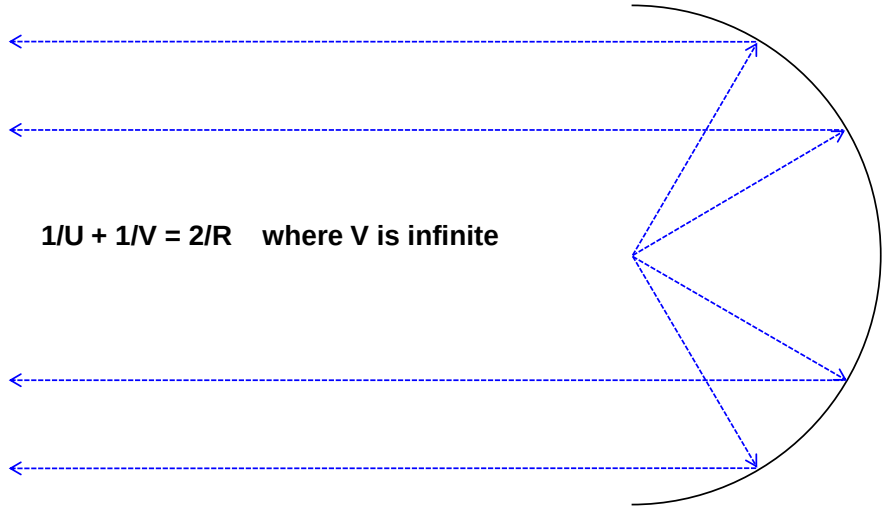

If the point source is placed at a distance <R/2, a virtual image is formed behind the mirror; V<0

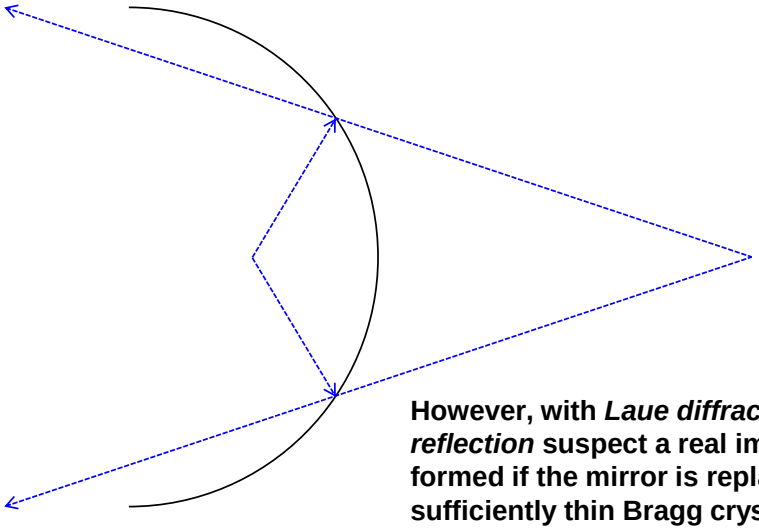

However, with *Laue diffraction in reflection* suspect a real image can be formed if the mirror is replaced by a sufficiently thin Bragg crystal

If the point source is placed at a distance <R/2, a virtual image is formed behind the mirror; V<0

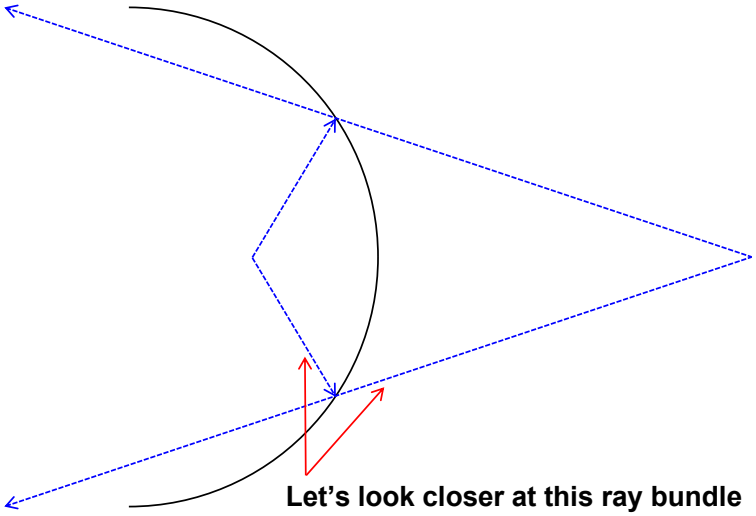

Let's look closer at this ray bundle

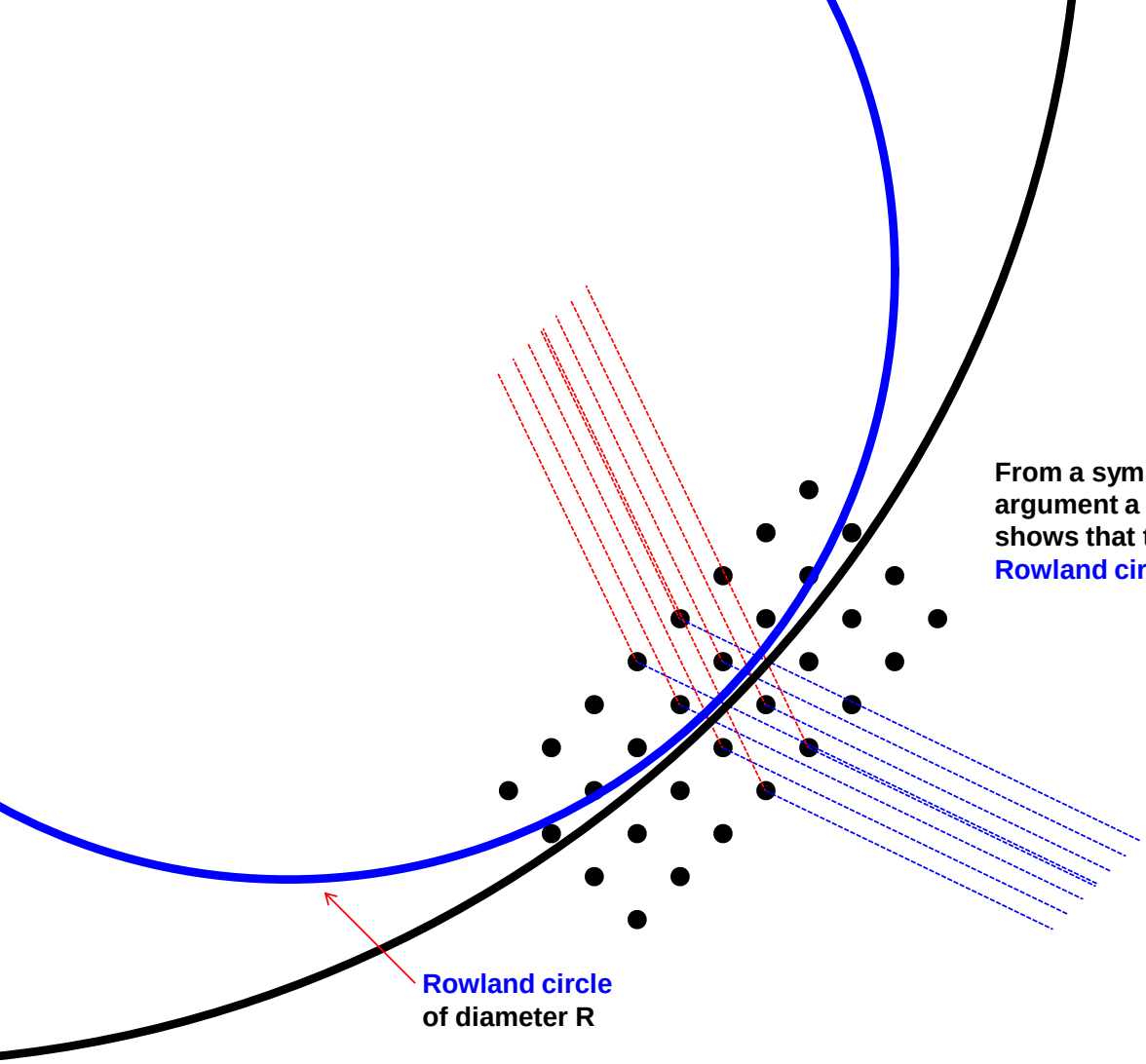
From a symmetry argument a little thought shows that there is still a Rowland circle, as shown
Rowland circle of diameter R

The basic optical principle

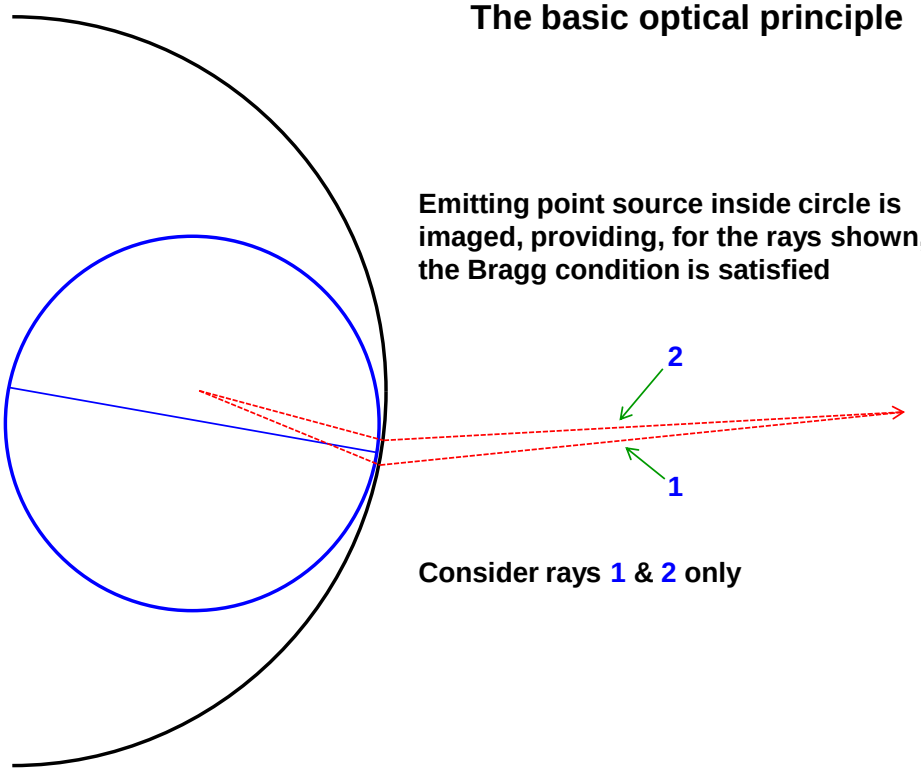

Emitting point source inside circle is imaged, providing, for the rays shown, the Bragg condition is satisfied

Consider rays 1 & 2 only

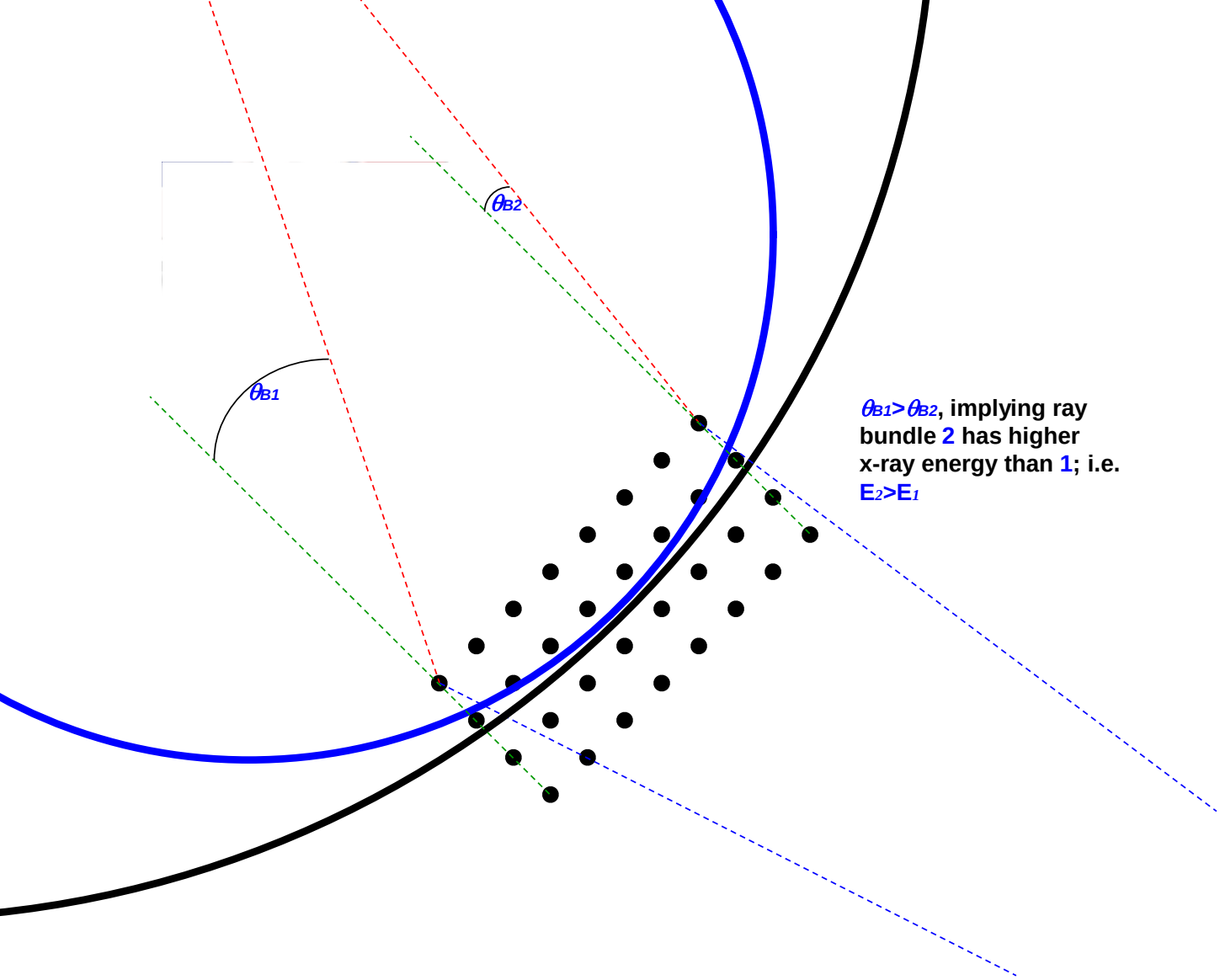

$\theta_{B1}>\theta_{B2}$, implying ray bundle 2 has higher x-ray energy than 1; i.e. $E_2>E_1$

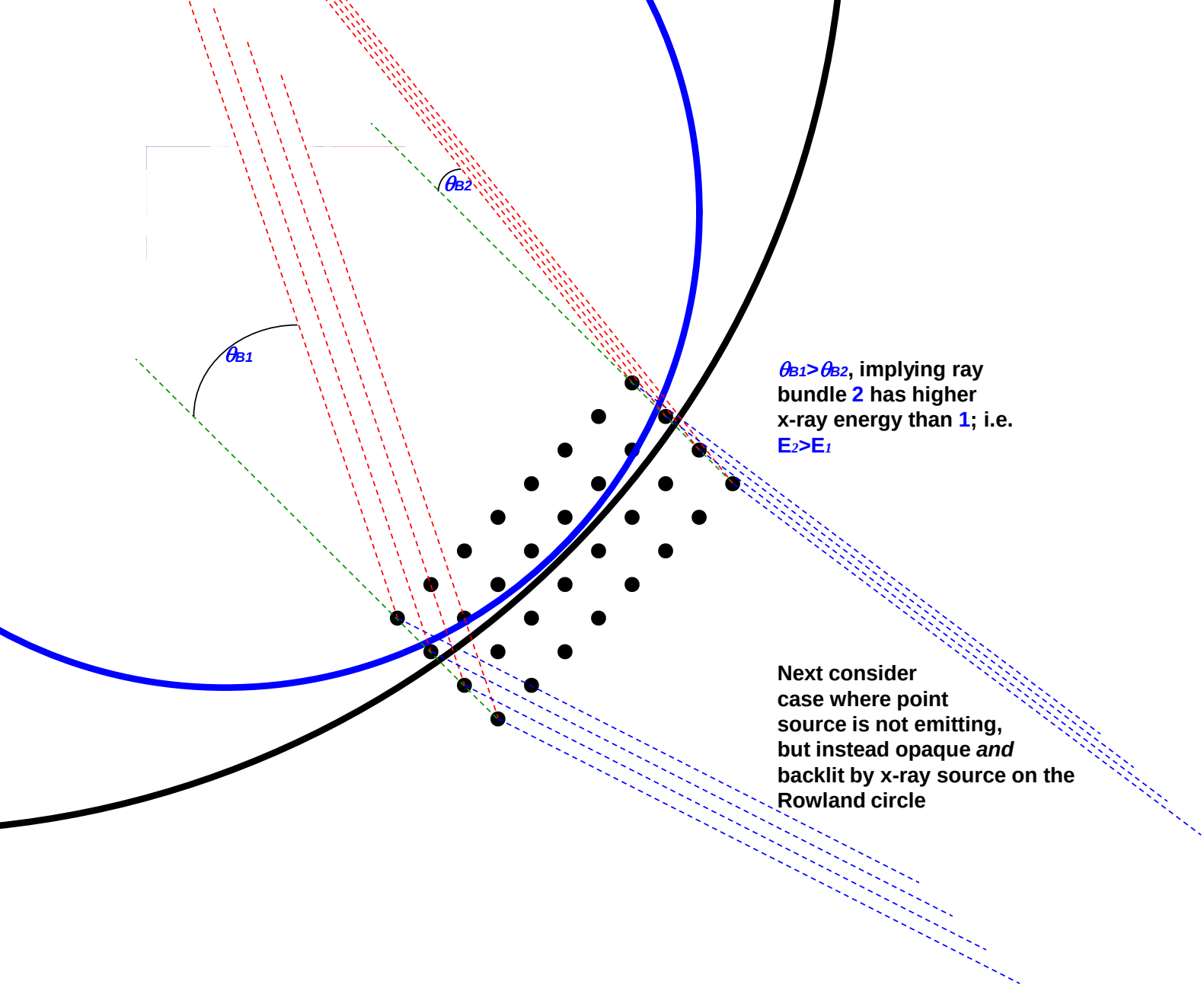

$\theta_{B1}>\theta_{B2}$, implying ray bundle 2 has higher x-ray energy than 1; i.e. $E_2>E_1$

Next consider case where point source is not emitting, but instead opaque *and* backlit by x-ray source on the Rowland circle

The basic optical principle

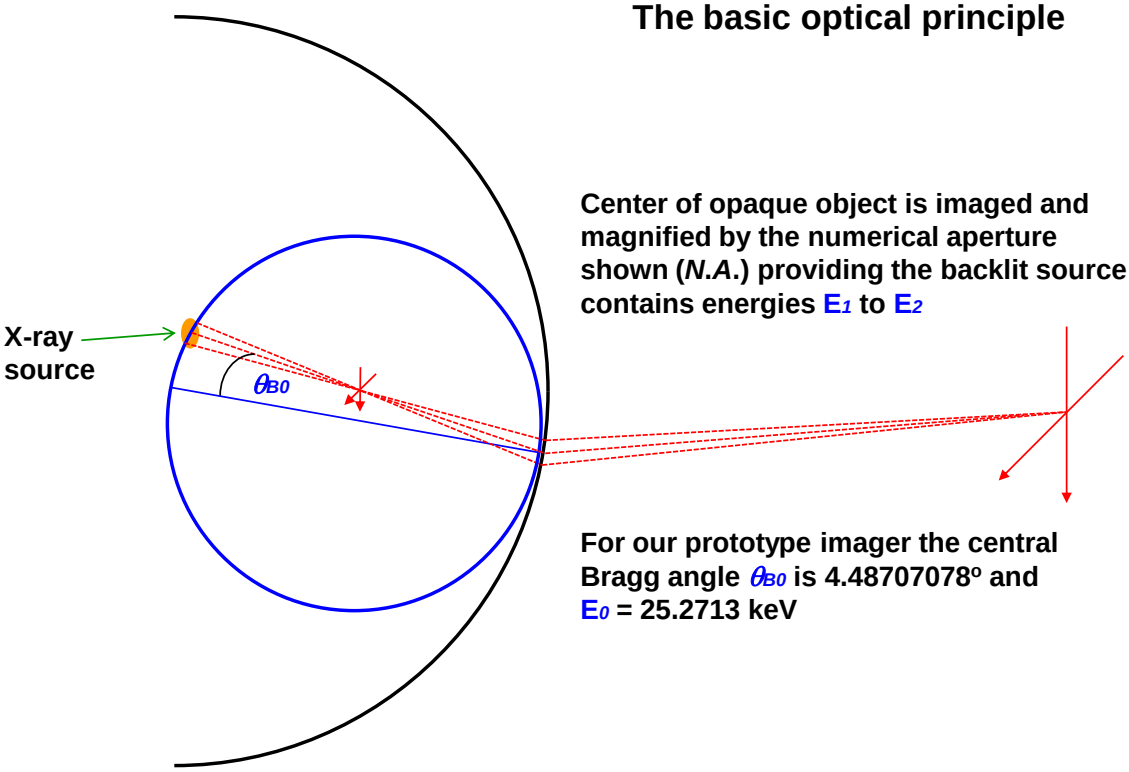

Center of opaque object is imaged and magnified by the numerical aperture shown (*N.A.*) providing the backlit source contains energies E_1 to E_2

For our prototype imager the central Bragg angle θ_{B0} is 4.48707078° and E_0 = 25.2713 keV

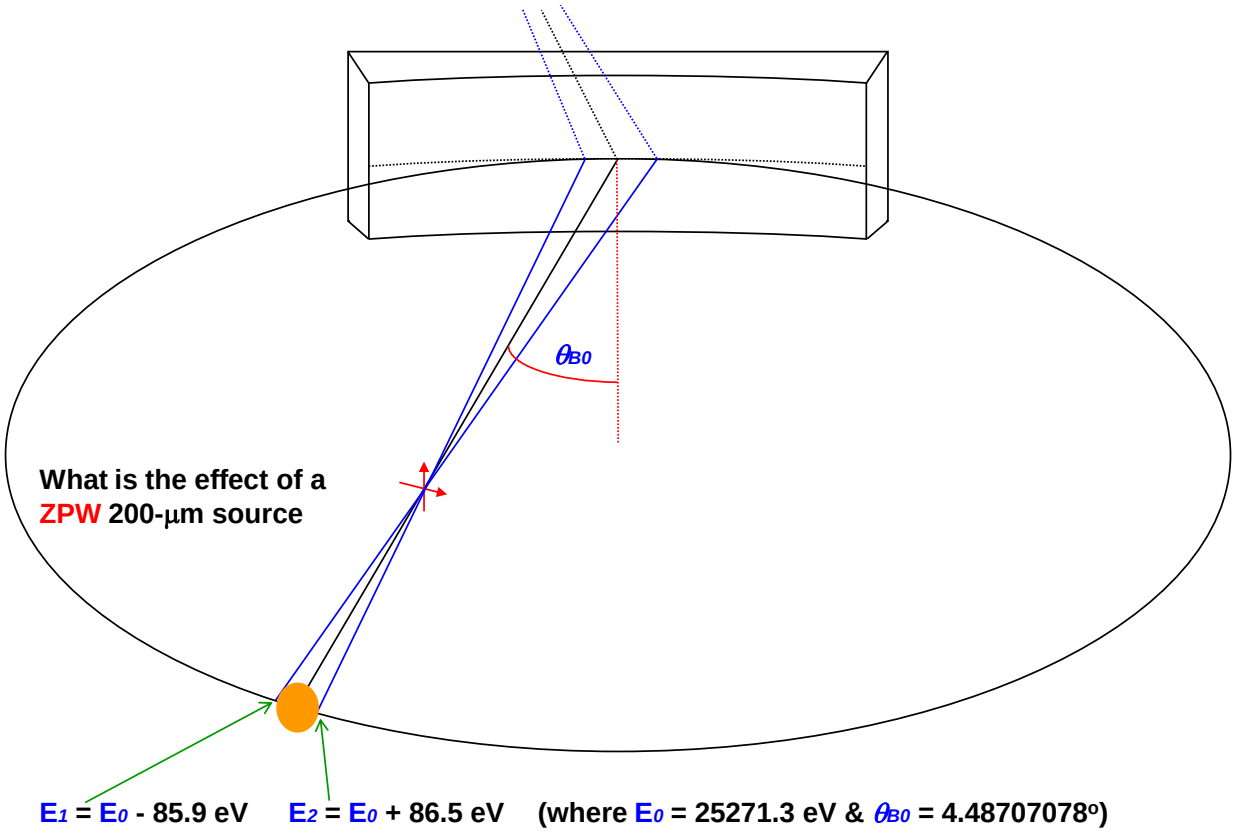
θ_{B0}
What is the effect of a
ZPW 200-μm source
$E_1 = E_0 - 85.9$ eV
$E_2 = E_0 + 86.5$ eV
(where $E_0 = 25271.3$ eV & $\theta_{B0} = 4.48707078^o$)

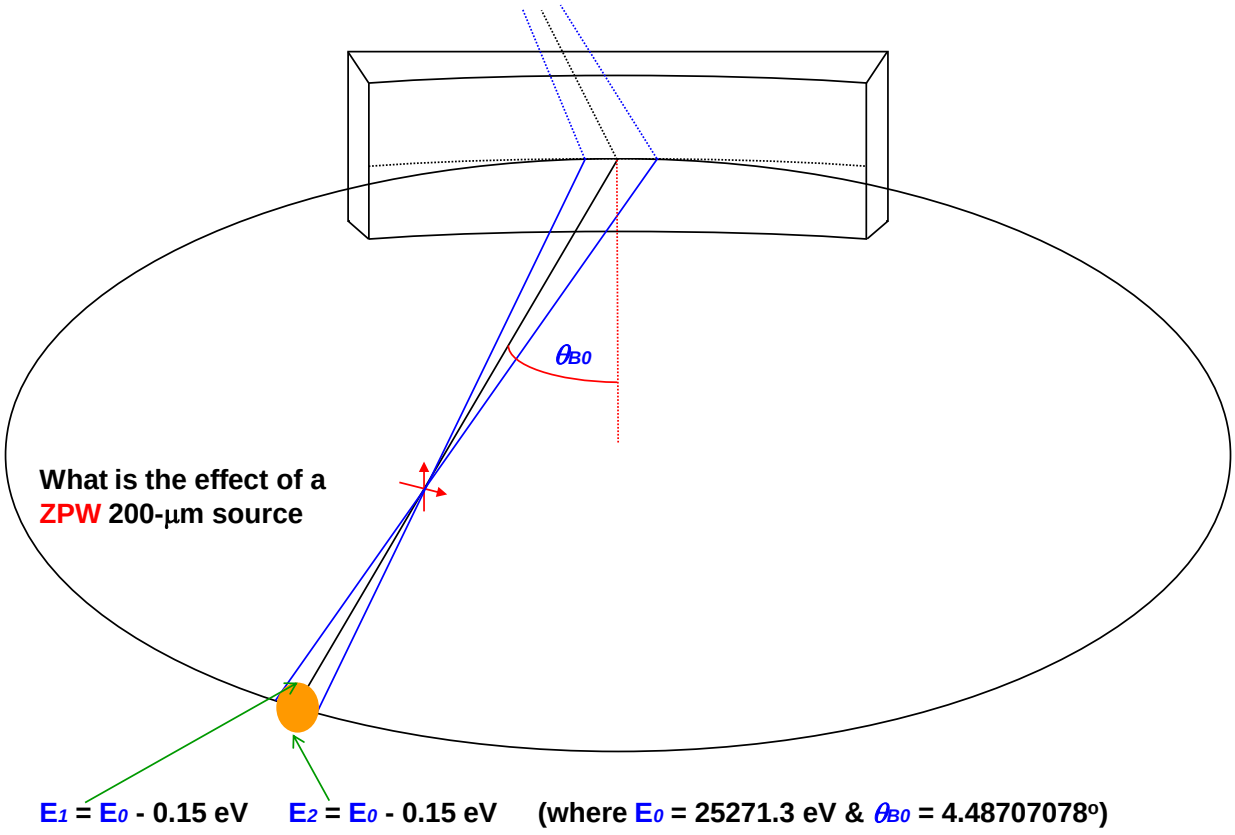
θ_{B0}
What is the effect of a
ZPW 200-μm source
$E_1 = E_0 - 0.15$ eV
$E_2 = E_0 - 0.15$ eV
(where $E_0 = 25271.3$ eV & $\theta_{B0} = 4.48707078^o$)

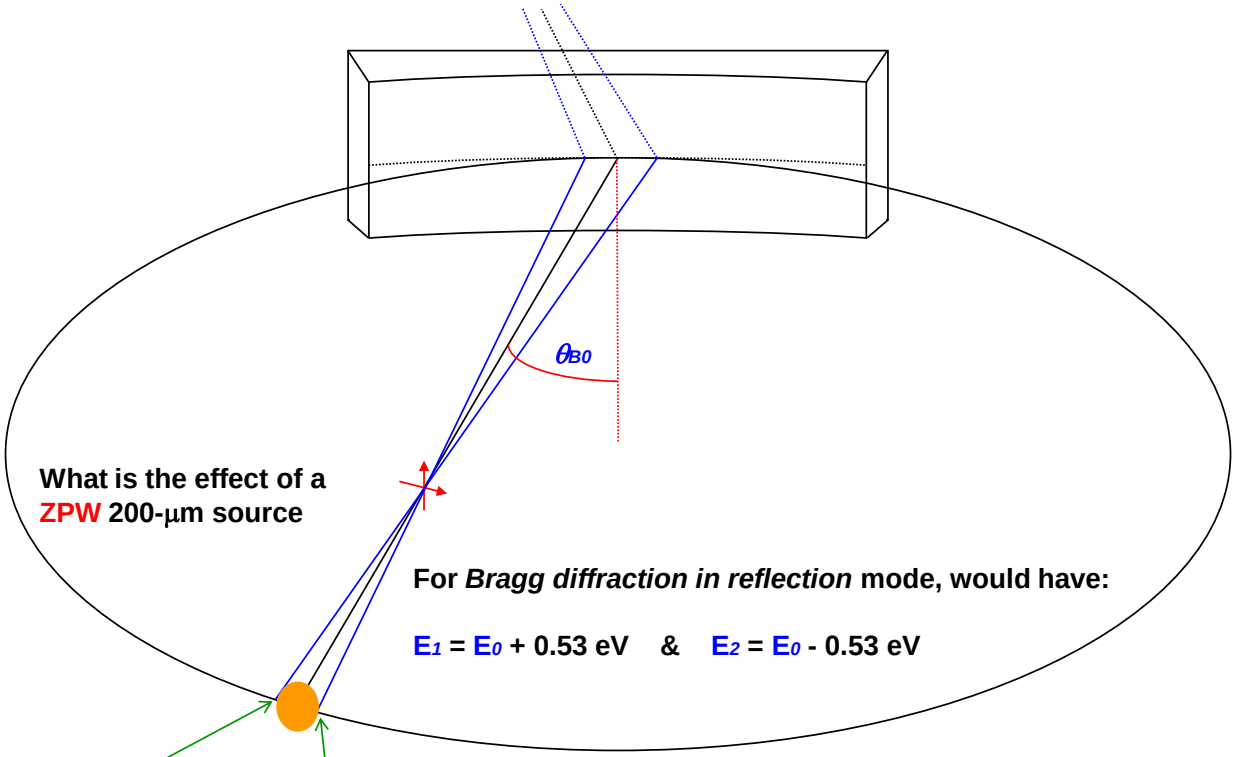
θ_{B0}
What is the effect of a
ZPW 200-μm source
For *Bragg diffraction in reflection* mode, would have:
$E_1 = E_0 + 0.53$ eV & $E_2 = E_0 - 0.53$ eV
$E_1 = E_0 - 85.9$ eV
$E_2 = E_0 + 86.5$ eV
(where $E_0 = 25271.3$ eV & $\theta_{B0} = 4.48707078^o$)

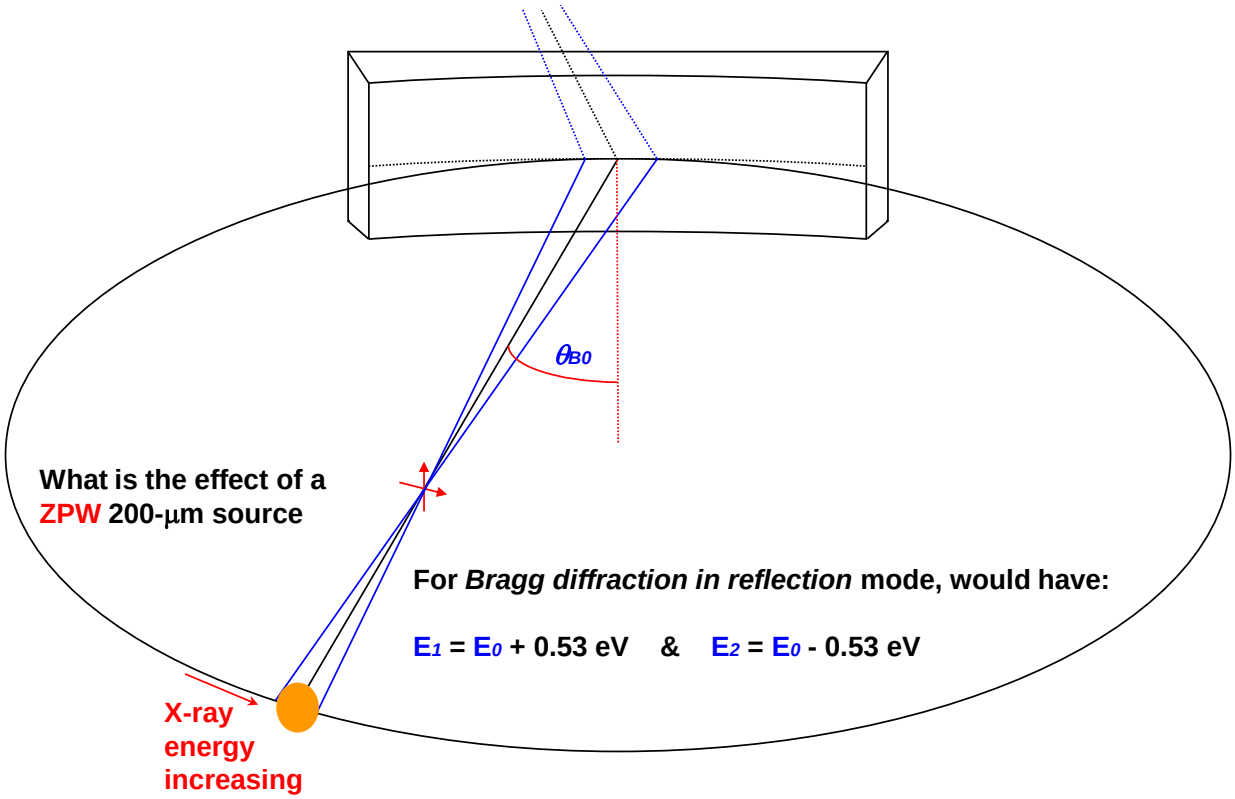
θ_{B0}
What is the effect of a
ZPW 200-μm source
For *Bragg diffraction in reflection* mode, would have:
$E_1 = E_0 + 0.53$ eV & $E_2 = E_0 - 0.53$ eV
X-ray
energy
increasing

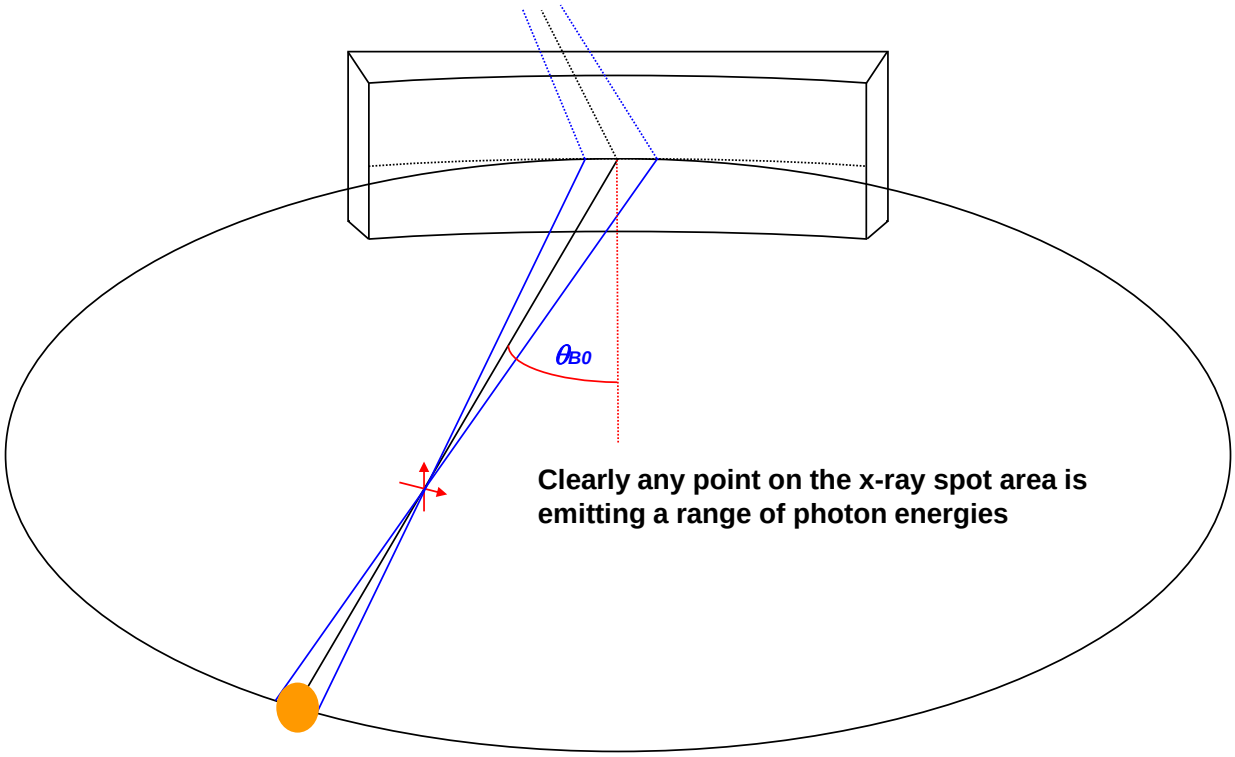
θ_{B0}
Clearly any point on the x-ray spot area is emitting a range of photon energies

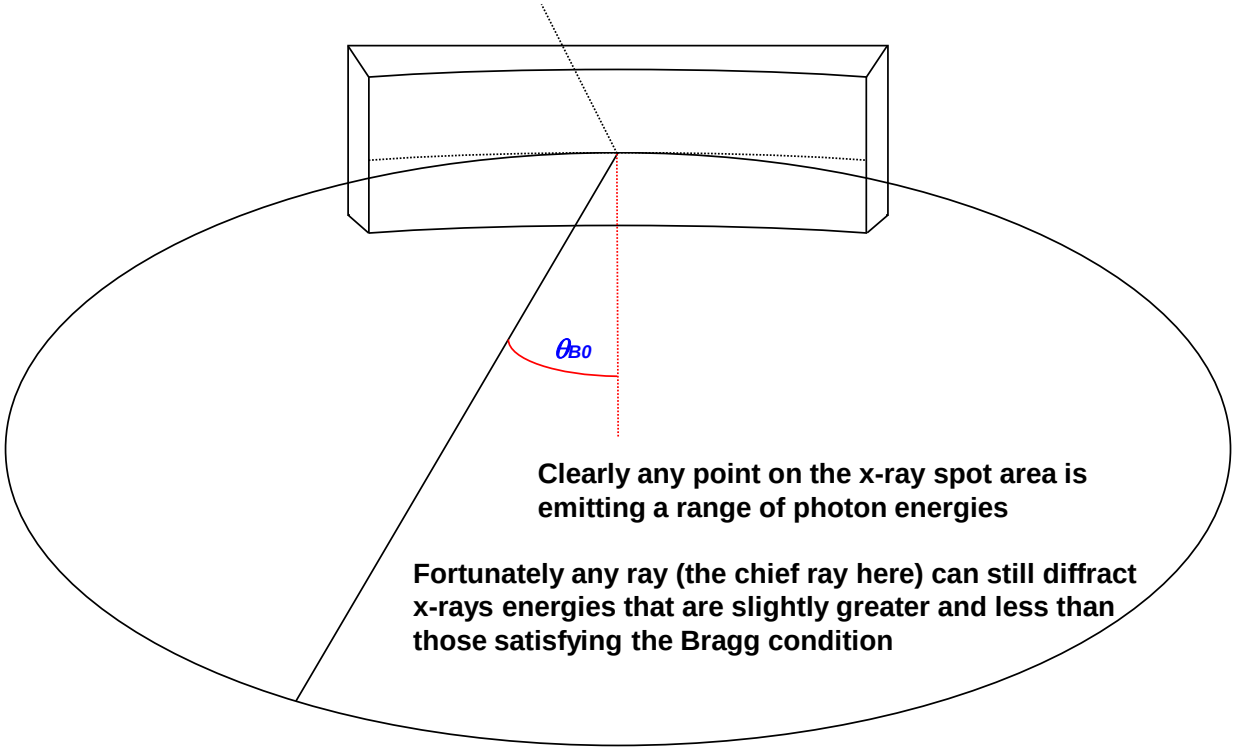

In the case of 23-μm thick Si(111), and *s*-polarized E_0 = 25271.3-eV x-rays:

$E = E_0$ diffract with 86% reflectivity
$E = E_0 + 6$ eV diffract with 7% reflectivity
$E = E_0 - 6$ eV diffract with 7% reflectivity

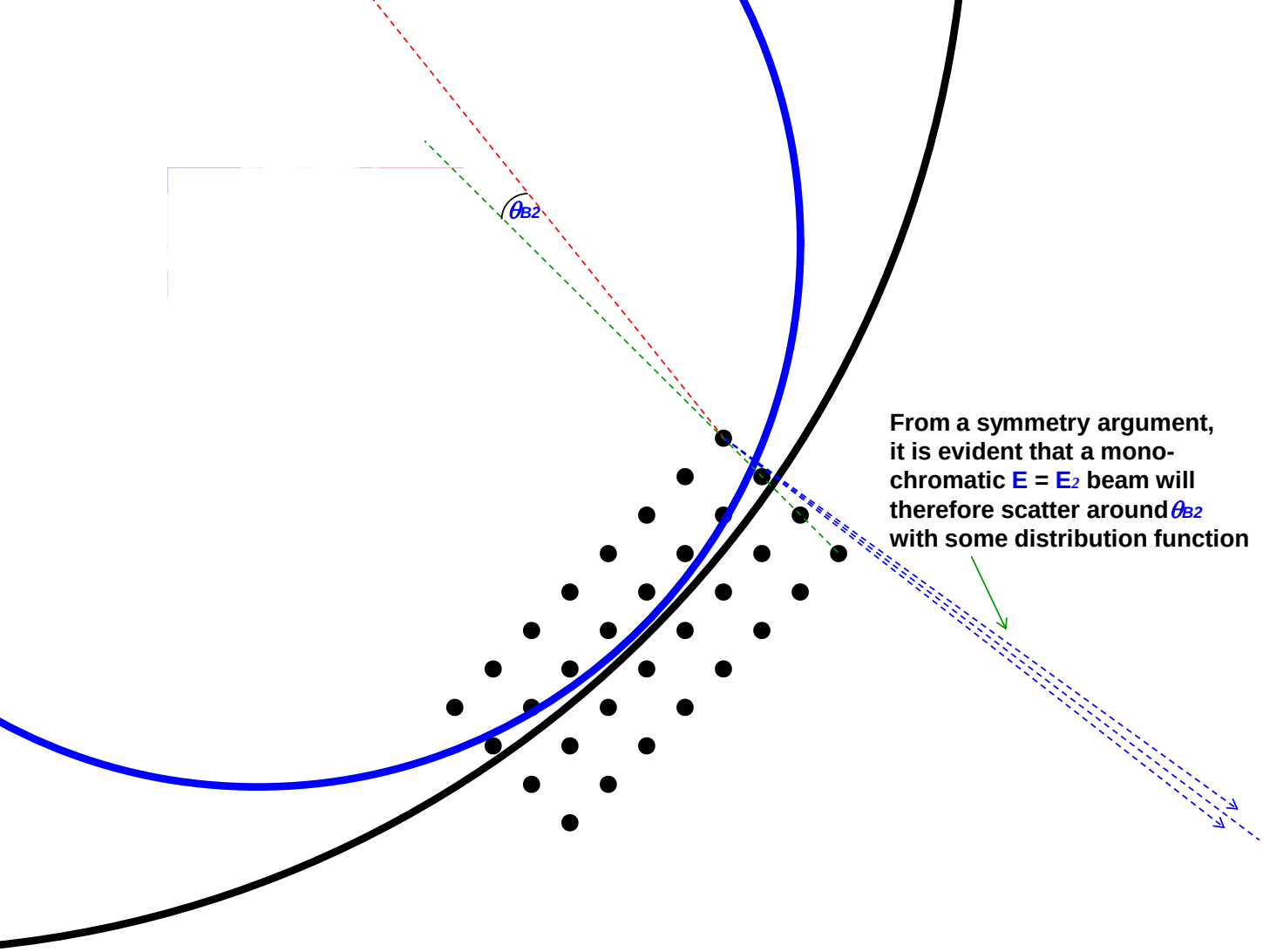
θ_{B2}
From a symmetry argument, it is evident that a mono-chromatic E = E_2 beam will therefore scatter around θ_{B2} with some distribution function

Scattering distribution for E = 25271.3-eV, *s*-polarized photons, exiting 23-μm thick Si(111) in *Laue reflection* mode

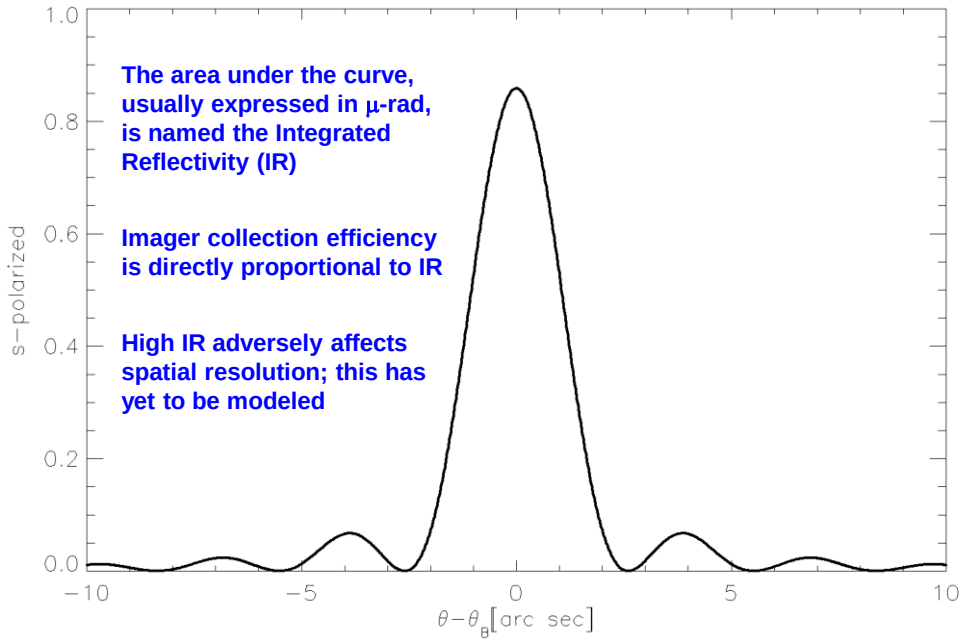

Conclusions & summary

The prototype 25-keV imager will soon be ready for testing

If it works, once can expect:

[1] Higher effective collection efficiency than a Si(12,12,12) *Bragg Reflection* system operating at a 69.8525929° Bragg angle

[2] In principle, very high spatial resolution

[3] Operation over a 22 - 28-keV range by slight change of the Bragg angle: careful crystal/line matches are not required

Believe that a thick Ge(111) crystal applied to the optic and polished down to 10 μm will yield optimum throughput: 5x reduced integrated reflectivity compared to 6.151-keV *reflection* system, but bandwidth is almost 200x larger

David Bliss (01672) may have a lead on a vendor that could perform this task; UMICORE

An alignment scheme has been developed; requires so-called object- & image-plane optics (Carlos Cox) to locate Sn target and detector

DISTRIBUTION

MS0899	Technical Library	9536 (electronic copy)
MS0359	D. Chavez, LDRD Office	1911